REPORT No. 921

THEORETICAL SYMMETRIC SPAN LOADING AT SUBSONIC SPEEDS FOR WINGS HAVING ARBITRARY PLAN FORM

By JOHN DEYOUNG and CHARLES W. HARPER

SUMMARY

A method is shown by which the symmetric span loading for a certain class of wings can be simply found. The geometry of these wings is limited only to the extent that they must have symmetry about the root chord, must have a straight quarter-chord line over the semispan, and must have no discontinuities in twist. A procedure is shown for finding the lift-curve slope, pitching moment, center of lift, and induced drag from the span load distribution. A method of accounting for the effects of Mach number and for changes in section lift-curve slope is also given.

Charts are presented which give directly the characteristics of many wings. Other charts are presented which reduce the problem of finding the symmetric loading on all wings falling within the prescribed limits to the solution of not more than four simultaneous equations.

The loadings and wing characteristics predicted by the theory are compared to those given by other theories and by experiment. It is concluded that the results given by the subject theory are satisfactory.

The theory is applied to a number of wings to exhibit the effects of such variables as sweep, aspect ratio, taper, and twist. The results are compared and conclusions drawn as to the relative effects of these variables.

INTRODUCTION

Theory predicts and experiment has shown that the effects of compressibility on wing characteristics can be delayed and diminished through the use of wing sweep and/or reduced aspect ratio. Experiment has also shown that if sufficient wing sweep or reduction in aspect ratio is used to reduce compressibility effects, then the characteristics of the wings will be different from those of conventional wings. The importance of being able to predict the characteristics of these heretofore unstudied plan forms in incompressible flow is obvious. Not only does it become possible to make a systematic study of the effects of major plan-form changes, but also a base is supplied from which the subcritical effects of compressibility can be predicted.

Lifting-line theory in the past has been so modified and extended that the characteristics of wings having no sweep, moderate to high aspect ratio, and any taper ratio can be determined readily with good accuracy. For studies requiring a higher degree of accuracy, lifting-surface theories have been used, but generally it has been found that the additional complexity of these methods has not sufficiently improved the predictions to warrant common use.

Lifting-line theory, however, proved wholly inadequate when used to predict the characteristics of wings having appreciable angles of sweep and/or very low aspect ratio. Lifting-surface theories, in contrast, made satisfactory predictions of the characteristics of these wings although the extent of the computing labor involved prevented the undertaking of any general study.

Continuing studies of the problem resulted in the theory first satisfactorily presented by Weissinger (reference 1) for the case of wings having a straight quarter-chord line across the wing semispan. It was found that this approach, which can be considered a simplified lifting-surface theory, enables rapid and satisfactory predictions to be made of the incompressible-flow characteristics of wings having swept and/or low-aspect-ratio plan forms as well as those of more conventional plan form. Further, it was found to be admirably suited for the problem of undertaking a systematic study of the effects of plan form on wing characteristics. Development of the method and procedures for its application together with the results of applying it to study the characteristics of a series of wings have been presented in references 2, 3, and 4. It is the purpose of this report to combine and extend the material contained in these three references.

NOTATION

m	number of span stations at which circulation and downwash are found
n	an integer defining a spanwise station on the wing quarter-chord line for which the value of circulation is determined
ν	an integer defining a specific point within the wing plan form for which the boundary condition of no flow through the wing is applied
η	dimensionless lateral coordinate measured perpendicular to the plane of symmetry, fraction of semispan
$\eta_{c.p.}$	spanwise location of center of pressure
$\eta_{c.p._a}$	spanwise location of center of pressure due to additional lift on the wing
ϕ	trigonometric spanwise coordinate ($\cos^{-1}\eta$), radians
ϕ_n	value of ϕ at station n $\left(\cos^{-1}\frac{n\pi}{8}\right)$

α wing angle of attack measured in a plane parallel to the plane of symmetry, degrees or radians

α_ν angle of attack at station ν, degrees or radians

α_{r_0} angle of attack at station ν for zero net lift on the wing, degrees or radians

α_{r_0} angle of attack of the wing-root section for zero net lift on the wing, degrees or radians

ϵ_ν angle of twist of the wing at station ν measured relative to the wing-root section ($\epsilon_\nu=\alpha_{r_0}-\alpha_{r_0}$), degrees or radians

G_n dimensionless circulation $\left(\frac{\Gamma}{bV}\right)$, identical to the load coefficient $\frac{c_l c}{2b}$, at spanwise station n

G_{n_0} value of G_n for zero net lift on the wing

G_{n_a} value of G_n due to additional lift on the wing

$A_{\nu n}$ coefficient dependent on wing geometry and indicating the influence of arbitrary loading at span station n on the downwash angle at span station ν

$a_{\nu n}$ coefficient dependent on wing geometry and indicating the influence of symmetric loading at span station n on the downwash angle at span station ν

b span of the wing measured perpendicular to the plane of symmetry, feet

c local chord of the wing measured parallel to the plane of symmetry, feet

c_ν local chord through point ν, feet

c_{av} average chord $\left(\frac{S}{b}\right)$, feet

$M.A.C.$ mean aerodynamic chord $\left(\frac{\int_{-1}^{1} c^2 d\eta}{\int_{-1}^{1} c d\eta}\right)$, feet

λ taper ratio $\left(\frac{\text{tip chord}}{\text{root chord}}\right)$

A aspect ratio $\left(\frac{b^2}{S}\right)$

S wing area, square feet

Λ geometric sweep angle of the wing quarter-chord line, positive when quarter-chord line is swept aft of a line normal to the plane of symmetry, degrees

Λ_β compressible sweep parameter $\left(\Lambda_\beta=\tan^{-1}\frac{\tan\Lambda}{\beta}\right)$

c_l section lift coefficient $\left(\frac{l}{qc}\right)$

c_{l_α} section lift-curve slope, per radian or per degree

c_{l_0} section lift coefficient for zero net lift on the wing

c_{l_a} section lift coefficient due to additional lift on the wing

C_L wing lift coefficient $\left(\frac{\text{lift}}{qS}\right)$

C_{L_α} lift-curve slope, per radian or per degree

C_m pitching-moment coefficient $\left(\frac{\text{moment}}{qS\,M.A.C.}\right)$

C_{m_0} pitching-moment coefficient for zero net wing lift on the wing

C_{m_a} pitching-moment coefficient due to additional lift on the wing

C_{D_i} induced-drag coefficient $\left(\frac{\text{induced drag}}{qS}\right)$

$C_{D_{i_0}}$ induced-drag coefficient due to basic loading (zero net lift on the wing)

$C_{D_{i_a}}$ induced-drag coefficient due to additional loading (net lift on the wing)

$a.c.$ longitudinal position of aerodynamic center, measured from the leading edge of the mean aerodynamic chord, in percent of the mean aerodynamic chord

Γ circulation, square feet per second

h absolute distance from a vortex to a downwash point, measured perpendicular to the vortex, feet

ρ density of air, slugs per cubic foot

w induced velocity, perpendicular to the mean chord line of the wing, positive for downwash, feet per second

V free-stream velocity, feet per second

q dynamic pressure, pounds per square foot

β compressibility parameter $(\sqrt{1-M^2})$

M Mach number

κ ratio of the experimental section lift-curve slope c_{l_α} to the theoretical value of $\frac{2\pi}{\beta}$, both taken at the same Mach number

κ_ν value of κ at spanwise station ν

H_ν wing geometric parameter $d_\nu\left(\frac{1}{\kappa_\nu}\right)\left(\frac{b}{c_\nu\beta}\right)$

d_ν scale factor

METHOD

THEORY AND LIMITATIONS

A detailed mathematical development of the method is given in the appendix to this report. However, as a preliminary to the discussion of the use of the method and the results obtained from it, an outline of the theory and its application is given here.

The wing is replaced by a plate of zero thickness but having a plan form and twist identical to that of the wing. It is assumed that the chordwise distribution of loading on the plate can be concentrated into a lifting line lying along the quarter-chord line of the wing. The method as developed here requires that the lifting line and, hence, the quarter-chord line of the wing in question, be a straight line over each semispan. At the plane of symmetry the method allows an angular discontinuity of the quarter-chord line to exist which therefore enables consideration of any degree of wing sweep.[1] The boundary condition which fixes the spanwise variation of the circulation is that the slope induced in the flow field by the downwash normal to the plate due to the lifting line and its trailing vortex sheet shall be equal to the slope of the plate with respect to the free stream at specified points (control points) within the wing boundary, or, in effect, that no flow shall occur through the plate at the control points. On the basis of two-dimensional theory, the chordwise location of these control points is chosen to

[1] It should be noted that this specifies that the angle of sweep is taken with respect to the quarter-chord line. In this report it will be understood that sweep angle refers to sweep of the quarter-chord line.

be at the three-quarter-chord line.[2] As will be shown later, this implicitly specifies that for each section the lift coefficient increases at the theoretical two-dimensional rate of 2π per radian change in true angle of attack of the section. The spanwise locations of the control points are chosen for reasons of mathematical expediency alone since only at certain fractions of the wing semispan is it convenient to solve the integral expressions for the total downwash.

The method treats the lifting line and its trailing vortex sheet as being continuous. However, explicit values for the circulation strength are found only for those spanwise points on the quarter-chord line which correspond to the spanwise location of the control points. The total number of control points m can be as great as desired. Comparison of the loadings predicted where various values of m are used shows that little change occurs where m is made greater than seven. Further, comparison with experimental results has shown that as few as seven (one at midspan and six distributed symmetrically about this point) will enable good predictions to be made of the span loading of wings without sharp discontinuities in span loading as would result from partial-span flaps. All of the material presented in this report is based on the seven-point solution with the exception of the appendix which is not restricted.

Using the vortex pattern substituted for the wing and applying the boundary condition allows a set of simultaneous equations to be formed, each of which involves (1) the slope of the flow $\left(\frac{w}{V}\right)_\nu$ (or angle of attack of the plate [3] α_ν) induced by the total downwash at each control point ν, (2) the load coefficient $\left(G_n=\frac{c_l c}{2b}\right)$ of the lifting line at each spanwise point n on the quarter-chord line, and (3) influence coefficients $A_{\nu n}$ which relate the influence of the circulation at any point n to the downwash at any point ν and are a function of wing geometry only. The method shows that for an arbitrary loading the equations have the following form:

$$\left(\frac{w}{V}\right)_\nu=\alpha_\nu=\sum_{n=1}^{m} A_{\nu n}\, G_n,\ \nu=1,2,\ \ldots\ m \qquad (1)$$

Each equation gives the downwash angle at the control point ν, the spanwise location of which is defined by

$$\eta=\cos\frac{\nu\pi}{8}$$

where the downwash results from the circulation at m points n on the wing the spanwise locations of which are defined also by

$$\eta=\cos\frac{n\pi}{8}$$

In the case of symmetrically loaded wings, each panel produces an identical equation for the corresponding semispan point. Since only one of these identical equations is of value, the total series reduces to the equations corresponding to the wing midpoint and one panel. For the seven-point solution, equation (1) is therefore written

$$\alpha_\nu=\sum_{n=1}^{4} a_{\nu n}\, G_n,\ \nu=1,2,3,4 \qquad (2)$$

where $a_{\nu n}$ represents the influence coefficients for the symmetric seven-point solution. The set of four simultaneous equations so formed can be easily solved to obtain the distribution of total load (in terms of G_n) on any wing for which the angle of attack at each spanwise station, sweep, and chord distribution are specified. The distribution of load is specified at only four spanwise stations, namely $\eta=0.924$, 0.707, 0.383, and 0 ($n=1$, 2, 3, and 4, respectively). Values of loading at additional spanwise stations can be found by means of the interpolation function given in the appendix (equation (A52)).

The simplicity of the procedure depends to a large extent on the fact that the solution can be found in terms of the coefficients $a_{\nu n}$. Even where these must be computed for each wing plan form the method offers computational advantages over other equally accurate methods. However, because these $a_{\nu n}$ coefficients are a function of geometry alone, it is possible to relate them in a simple manner such that a limited amount of computation will give the $a_{\nu n}$ coefficients for all plan forms to which the method is applicable. Details of this procedure and the results of applying it are discussed in a later section of the report.

The method assumes that the flow follows the wing surface and makes some allowance for the trailing sheet aft of the trailing edge becoming horizontal.[3] Hence, the method should apply to higher angles of attack with considerable accuracy, provided the flow remains along the wing surface. The method assumes incompressible flow but it will be shown how the effects of compressibility can be included within the limits of applicability of the Prandtl-Glauert rule. The method assumes the theoretical section lift-curve slope of 2π (or with account taken of compressibility, $2\pi/\beta$) but a procedure will be shown which accounts for the variation in section lift-curve slope from the theoretical value.

It is clear from the foregoing outline of the theory that the method can account for variations in those geometrical char-

[2] It is important for the reader to realize here that a choice has been made between a number of possible procedures. These possibilities arise from the fact that the exact location, on a tapered wing, of constant-percent-chord lines depends upon the orientation of the reference line along which the chord is measured. The orientation of the reference line is usually chosen such that an airfoil section so defined will have aerodynamic characteristics closely resembling those found two-dimensionally for the same section. This then enables an estimation of the effect of changes in section characteristics on over-all wing characteristics. For unswept wings, there is little reason to consider any orientation of the reference line other than parallel to the free-stream direction. However, when a wing is swept, the question of orientation of the reference chord cannot be so easily answered. Insufficient experimental data exists to determine the most satisfactory orientation, and strong arguments can be presented for at least two orientations, namely, parallel to the free stream and perpendicular to some swept reference line. In the present analysis the reference chord was chosen as being parallel to the free stream since it greatly simplifies the mathematical procedure and since consideration of the differences expected from use of the alternate choice indicates they will be small.

[3] The reader should note that the boundary condition is given by $w_\nu=V_\nu \sin\alpha_\nu$, from which $\left(\frac{w}{V}\right)_\nu$ is seen equal to $\sin\alpha_\nu$. The substitution of α_ν for $\sin\alpha_\nu$ has the effect of increasing the value of loading on the wing above that necessary to satisfy the boundary condition. However, the boundary condition was fixed assuming that the shed vortices moved downstream in the extended chord plane. A more realistic picture is obtained if the vortices are assumed to move downstream in a horizontal plane from the wing trailing edge. It can be readily seen that, if this occurs, the normal component of velocity induced by the trails at the three-quarter-chord line is reduced and, if the boundary condition is to continue to be satisfied, the strength of the bound vortex must increase. It follows that substitution of α_ν for $\sin\alpha_\nu$ then has the effect of accounting for the bend up of the trailing vortices. It is not known how exact the correction is, but calculations and experimental verification show it of to be the correct order.

[3] See footnote 5.

acteristics of wings, namely plan form and twist, which have the greatest influence on the spanwise distribution of lift. With the exception of variations in c_{l_α} the method cannot directly account for any effects dependent upon the geometry of the airfoil section even though these may affect the span loading. The substitution of uniformly cambered sections for uncambered sections across a wing span is assumed to change only the wing angle for zero lift and this change is assumed equal to that shown by the section. The substitution of variable camber is assumed equivalent to twisting uncambered sections.

PROCEDURE FOR DETERMINATION OF AERODYNAMIC CHARACTERISTICS FROM SPAN LOADING

The foregoing section has shown a method by which the symmetric span load distribution of any wing having a straight quarter-chord line over the semispan can be determined from a knowledge of wing geometry only. With such loading determined it becomes possible to quickly find other characteristics. It should be noted, however, that these characteristics are derived directly from the wing load distribution and that no further aerodynamic theory is involved.

It is possible to find the gross load distribution and resultant characteristics directly for a wing at any angle of attack and having any plan form and twist. Past experience, however, has shown that gross characteristics can better be studied if the basic and additional type loadings are handled separately. Since the two types of loading are additive, this procedure is permissible.

Basic loading is that existing with zero net lift on the wing and is, therefore, due to twist or effective twist [4] (e. g., spanwise change in camber) of the wing-chord plane. The basic loading and characteristics dependent on it are unchanged by the addition of load due to uniform spanwise wing angle-of-attack change and are equal at all angles of attack to that found for zero net lift on the wing.

Additional loading is that due to equal geometric angle-of-attack change at each section of the wing. The distribution of additional load is a function only of wing plan form and is thus independent of any basic load due to twist existing on the wing. The magnitude of the additional load is a function only of angle of attack of the wing and thus each equal increment of angle of attack will give the same increase and distribution of additional load irrespective of the gross load on the wing. The wing characteristics due to additional load of any given plan form are thus a function of the lift coefficient or angle of attack of the wing.

In the following sections the procedure for determining basic-type span load distribution and the characteristics associated with it (denoted by a subscript 0) is first presented and then the procedure for finding additional-type span load distribution and the associated characteristics (denoted by a subscript a). Finally, it is shown how characteristics due to gross load distribution (denoted by absence of a subscript) can be found.

[4] Hereafter reference will be made to twist only. The reader will understand that effective twist will be handled in an identical manner.

PROCEDURE FOR DETERMINATION OF AERODYNAMIC CHARACTERISTICS DUE TO BASIC LOADING

Span load distribution and angle of zero lift for arbitrary twist.—It is not possible to obtain the distribution of basic load on a twisted wing directly from equation (2) since the values of α_ν for each station are not generally known for the condition of zero net lift and thus, as written, eight unknown values appear. However, only one unknown has actually been added to the four unknowns (the individual loads of equation (2)) since, while four values of α_ν appear, they are related to one another through knowlege of the twist distribution. To form the fifth equation required for the solution in addition to the four represented by equation (2), use is made of equation (A46) of the appendix which gives the total lift in terms of the four individual loads. Thus

$$C_L=\frac{\pi A}{8}\left(G_4+2\sum_{n=1}^{3}G_n\sin\phi_n\right) \tag{3}$$

Equating this to zero (basic loading) and with equation (2), a set of five simultaneous equations is formed, the solution of which will give the values of loading at the spanwise points and the angle of zero lift of the reference station. Thus

$$\left.\begin{aligned} 0&=G_4+2\sum_{n=1}^{3}G_n\sin\phi_n \\ \epsilon_\nu+\alpha_{\mathrm{ref}_0}&=\sum_{n=1}^{4}a_{\nu n}G_n,\ \nu=1,2,3,4 \end{aligned}\right\} \tag{4}$$

Solution of the five equations will give values of the angle of zero lift of the reference section and the four individual loads. The angle of attack of sections other than the reference section is determined from the twist.

Some simplification of this process can be made, however. When equated to zero lift, equation (A46) involves only the four individual loads, and it is therefore possible to express one load in terms of the other three. Elimination of one unknown in the remaining equations enables a solution to be made for the angle of zero lift and three individual loads from a set of four simultaneous equations. Finally, since the individual section angles for zero lift are each expressed as the sum of the reference angle and a twist angle (which is zero for the reference station), one equation and one unknown (the reference angle) can be eliminated by subtracting one equation from the remaining three. Values can then be found for the three loads from solution of only three simultaneous equations, with the angle of zero lift for the reference chord and the value of the fourth load found from the previously eliminated equations.

The exact form of the equations depends on the section chosen as a reference. If, as is customary, the root is taken as a reference, then

$$\alpha_{\nu_0}=\alpha_{4_0}+\epsilon_\nu=\alpha_{r_0}+\epsilon_\nu \tag{5}$$

where ϵ_ν is the angle of twist at station ν with respect to station 4, and the set of equations required for the solution take the following form. The three simultaneous equations giving the three outboard loads are

$$\left.\begin{aligned}\epsilon_1&=[a_{11}-a_{41}-0.765(a_{14}-a_{44})]G_{1_0}+[a_{12}-a_{42}-1.414(a_{14}-a_{44})]G_{2_0}+[a_{13}-a_{43}-1.848(a_{14}-a_{44})]G_{3_0}\\ \epsilon_2&=[a_{21}-a_{41}-0.765(a_{24}-a_{44})]G_{1_0}+[a_{22}-a_{42}-1.414(a_{24}-a_{44})]G_{2_0}+[a_{23}-a_{43}-1.848(a_{24}-a_{44})]G_{3_0}\\ \epsilon_3&=[a_{31}-a_{41}-0.765(a_{34}-a_{44})]G_{1_0}+[a_{32}-a_{42}-1.414(a_{34}-a_{44})]G_{2_0}+[a_{33}-a_{43}-1.848(a_{34}-a_{44})]G_{3_0}\end{aligned}\right\} \quad (6)$$

The equation giving the root load is

$$G_{4_0}=-(0.765G_{1_0}+1.414G_{2_0}+1.848G_{3_0}) \quad (7)$$

The equation giving the angle of the root section for zero lift is

$$\alpha_{r_0}=\alpha_{4_0}=(a_{41}-0.765a_{44})G_{1_0}+(a_{42}-1.414a_{44})G_{2_0}+(a_{43}-1.848a_{44})G_{3_0} \quad (8)$$

The dimensionless circulation G_n can be related to other forms of loading coefficients by

$$G_n=\frac{1}{2A}\left(\frac{c_{l_0}c}{c_{av}}\right)_n=\left(\frac{c_{l_0}c}{2b}\right)_n$$

Conversely, if the load at each of the four span stations is known for the case of zero wing lift, it becomes a simple matter to solve equation (2) directly and determine the required wing twist.

Induced drag.—With the values of loading found at the four spanwise positions, the induced drag can be found from the following equation which is derived in the appendix. In terms of the nondimensional circulation G_n,

$$C_{D_{i_0}}=\frac{\pi A}{2}\left[G^2_{1_0}+G^2_{2_0}+G^2_{3_0}+\frac{G^2_{4_0}}{2}-G_{4_0}(0.056G_{1_0}+0.789G_{3_0})-G_{2_0}(0.733G_{1_0}+0.845G_{3_0})\right] \quad (9)$$

Through use of equation (4), the induced drag can be put in terms of only three values of G_n. Thus

$$C_{D_{i_0}}=\pi A[0.668G^2_{1_0}+G^2_{2_0}+2.082G^2_{3_0}+(0.215G_{1_0}+1.442G_{3_0})G_{2_0}+1.061G_{1_0}G_{3_0}] \quad (9a)$$

Pitching moment.—It is quite evident that, as a wing is swept, the distribution of span load will increasingly affect the wing pitching moment where this is measured about an axis normal to the plane of symmetry. Correspondingly, as the wing is swept, any changes in the chord load distribution exert relatively less effect on wing pitching moments. Further, since the possible distortion of a chord loading from the conventional is not great, the span load distribution begins to control the wing pitching moments even at small angles of sweep. Since the subject method gives, as will be shown, good predictions of span load distribution, then it is safe to assume that good estimations of pitching moments should be possible.

The moment produced by basic-type load distribution is in the form of a pure couple since zero net load exists on the wing. It follows immediately that the magnitude and sign of the moment are independent of the fore-and-aft location of any reference axis normal to the plane of symmetry. Using the expression for continuous loading (equation (A17) of the appendix) and summing the moment of each wing element about an arbitrary axis, the value of the couple due to the basic load distribution can be found. About an axis normal to the plane of symmetry and in terms of dimensionless circulation this is

$$C_{m_0}=-\frac{Ab}{M.A.C.}\tan\Lambda\,(0.138G_{1_0}+0.198G_{2_0}+0.135G_{3_0}+0.016G_{4_0}) \quad (10)$$

If equation (4) is again used to eliminate G_{4_0}, equation (10) becomes

$$C_{m_0}=-\frac{Ab}{M.A.C.}\tan\Lambda(0.126G_{1_0}+0.175G_{2_0}+0.106G_{3_0}) \quad (10a)$$

PROCEDURE FOR DETERMINATION OF AERODYNAMIC CHARACTERISTICS DUE TO ADDITIONAL LOADING

Span load distribution and lift-curve slope.—Since the additional loading distribution for wings of a given plan form is the same, regardless of twist or camber, it is necessary to consider only the case of the flat wing. Further, since the magnitude of the additional load varies directly with angle of attack, it is only necessary to consider unit angle-of-attack changes as all other loadings will be directly proportional to this. Thus, to find the additional load distribution, equation (2) is written in the following form

$$1=\sum_{n=1}^{4}a_{\nu n}\frac{G_{n_\alpha}}{\alpha},\ \nu=1,2,3,4 \quad (11)$$

Solution of the set of four simultaneous equations gives the values of circulation per radian $\frac{G_{n_\alpha}}{\alpha}$ at the four spanwise stations $\eta=0.924$, 0.707, 0.383, and 0.

Substitutions of the values of $\frac{G_{n_\alpha}}{\alpha}$ in the expression for lift coefficient gives the wing lift coefficient for one radian change in angle of attack, or in effect, lift-curve slope. Thus, with equation (3)

$$\frac{dC_L}{d\alpha}=C_{L_\alpha}=\frac{\pi A}{8}\left(\frac{G_{4_\alpha}}{\alpha}+1.848\frac{G_{3_\alpha}}{\alpha}+1.414\frac{G_{2_\alpha}}{\alpha}+0.765\frac{G_{1_\alpha}}{\alpha}\right) \quad (12)$$

The dimensionless circulation per radian $\frac{G_{n_\alpha}}{\alpha}$ can be expressed in the more usual loading-coefficient form through the relations

$$\frac{G_{n_\alpha}}{\alpha}=\frac{C_{L_\alpha}}{2A}\left(\frac{c_{l_\alpha}c}{C_Lc_{av}}\right)_n=C_{L_\alpha}\left(\frac{c_{l_\alpha}c}{2bC_L}\right)_n$$

Induced drag.—The induced drag due to additional loading can be computed at any lift coefficient exactly as was

the induced drag due to basic loading. Values of loading at the four spanwise points are found for the particular value of C_L and substituted in the appropriate form of equation (9). If the more usual expression for induced drag as a function of C_L is desired, then values of $\frac{G_{n_a}}{\alpha}$ are substituted in the following expression which differs only algebraically from equation (9):

$$\frac{C_{D_{i_a}}}{C_L^2}=\frac{\pi A}{2C_{L_\alpha}}\left[\left(\frac{G_{1_a}}{\alpha}\right)^2+\left(\frac{G_{2_a}}{\alpha}\right)^2+\left(\frac{G_{3_a}}{\alpha}\right)^2+\frac{1}{2}\left(\frac{G_{4_a}}{\alpha}\right)^2 -\frac{G_{4_a}}{\alpha}\left(0.056\,\frac{G_{1_a}}{\alpha}+0.789\,\frac{G_{3_a}}{\alpha}\right) -\frac{G_{2_a}}{\alpha}\left(0.733\,\frac{G_{1_a}}{\alpha}+0.845\,\frac{G_{3_a}}{\alpha}\right)\right] \quad (13)$$

Spanwise center of pressure.—Substitution of the values for individual loads in equation (A17) of the appendix gives an expression for the continuous distribution of additional load. Integration of the increments of bending moment about an axis lying in the plane of symmetry will give total root bending moment. Then, with knowledge of the total load, an expression giving the spanwise location of the center of load (on the quarter-chord line) can be found. In terms of the values of the dimensionless circulation, this expression is (from reference 5)

$$\eta_{c.p._a}=\frac{0.352\,\frac{G_{1_a}}{\alpha}+0.503\,\frac{G_{2_a}}{\alpha}+0.344\,\frac{G_{3_a}}{\alpha}+0.041\,\frac{G_{4_a}}{\alpha}}{0.383\,\frac{G_{1_a}}{\alpha}+0.707\,\frac{G_{2_a}}{\alpha}+0.924\,\frac{G_{3_a}}{\alpha}+0.500\,\frac{G_{4_a}}{\alpha}} \quad (14)$$

Either of the two loading coefficients can be used directly in place of the values of $\frac{G_{n_a}}{\alpha}$.

Pitching moment.—The value of the pitching moment due to additional-type load can be found exactly as was that due to basic load. However, account must be taken of the fact that the value of the moment is directly dependent on both the position of the reference axis and the amount of additional load. This can be accomplished directly by using the results of the previous section which gave the spanwise position of the center of pressure. Since the center of pressure is placed by the method on the wing quarter-chord line, it is simply a matter of geometry to locate the longitudinal position of the center of pressure with respect to any reference axis. The value of the moment-curve slope $\frac{C_{m_a}}{C_L}$ is then simply the difference between the longitudinal position of this reference axis and the longitudinal position of the center of pressure expressed as a fraction of the mean aerodynamic chord.

PROCEDURE FOR DETERMINATION OF AERODYNAMIC CHARACTERISTICS DUE TO GROSS LOADING

Gross loading must be considered when a twisted wing is carrying other than zero net lift. Since the load distribution is the sum of a constant and a variable, its shape varies with lift coefficient and thus the resulting characteristics must generally be determined at each lift coefficient. For the most part, excepting possibly the effect on the character of wing stall, the effects of twist on aerodynamic characteristics are of minor importance compared to the effects of sweep, aspect ratio, or taper ratio. However, where the twist varies with load due to the elastic properties of the wing, careful consideration must be given the gross loading if a true picture of the characteristics is to be obtained.

Span load distribution.—Since basic and additional load are additive, the gross load distribution at a given C_L is simply the sum of the two. The magnitude of the total load is equal to the value of the additional load. Thus, the gross load coefficient is given by $G_n=G_{n_0}+G_{n_a}$.

It is sometimes of importance to determine the twist required in a wing to have a given gross load distribution at a particular lift coefficient. If this distribution is chosen and the additional load distribution for the wing corresponding to the particular lift coefficient is subtracted from it, then the necessary basic load distribution is defined. As noted previously, the twist required is readily determined. For wings having pronounced sweep or very low aspect ratio, the twist required to give load distribution approaching the desired elliptical may become great even where the distribution is desired at a lift coefficient of only 0.2 or 0.3.

Lift-curve slope.—If the twist is constant, the lift-curve slope for the wing is that found for the untwisted wing. However, if the twist varies with load, then the lift coefficient must be determined for each angle of attack in order to find the lift-curve slope. The required values of the lift coefficient can be determined from equation (3) once the values of G_n are known for each angle of attack.

Induced drag.—Total induced drag can be found by substituting the values of total loading coefficient in equation (9). It is, of course, impossible to make C_{D_i} a function of C_L when twist is present since C_{D_i} is a function of load distribution and this varies with each lift coefficient. (Note: $C_{D_i}\neq C_{D_{i_0}}+C_{D_{i_a}}$.)

Pitching moment.—The gross pitching moment is found by adding directly the pitching moment due to basic lift to the pitching moment due to additional lift. This gross characteristic must be carefully examined if twist is a function of total load or dynamic pressure. In these cases a new twist and the pitching moment due to basic lift must be found for each flight condition. It is possible the resultant changing value of basic load moment can be of sufficient magnitude to seriously affect the stability of an airplane.

CORRECTION FOR SECTION LIFT-CURVE SLOPE

The development of the basic theory involves the assumption that each section on the wing maintains a lift-curve slope of 2π. This is implicit in the choice of the three-quarter-chord line as the location for the control points. It may be desirable at times, however, to consider the effects of deviation in lift-curve slope from the theoretical value of 2π. How this can be done by moving the control point from the three-quarter-chord line is shown in the following discussion.

The logic underlying the choice of the three-quarter-chord line as a location for the control points can be shown as follows. The velocity w induced at any distance h from an infinite vortex of strength Γ can be expressed as

$$w=\frac{\Gamma}{2\pi h}$$

The circulation is in turn related to the section lift coefficient c_l of a section through the expression

$$l=\rho\Gamma V=c_l\frac{1}{2}\rho V^2 c$$

From these two expressions it can be found that

$$c_l=4\pi\left(\frac{w}{V}\right)\left(\frac{h}{c}\right)$$

It can be seen that the term $\frac{w}{V}$ indicates a change in the direction of flow with respect to the free-stream direction, which change decreases with distance from the lifting line. If the lifting line is assumed to be replacing a plate insofar as lift is concerned, then simplified lifting-surface theory requires that, at some distance from the lifting line, the direction of flow must be parallel to the plate. In effect, then, the induced downwash angle becomes equal to the angle of attack of the plate. It remains to determine how far aft of the lifting line the downwash angle must be measured in order to properly relate the increase in circulation to the change in angle of attack of the plate. From the foregoing expressions and assuming small angles, the following relation can be written:

$$\frac{c_l}{\alpha}=\left(\frac{c_l}{w/V}\right)=4\pi\left(\frac{h}{c}\right)$$

Now, if a section lift-curve slope of 2π is assumed, it is evident that $\left(\frac{h}{c}\right)$ must equal $\frac{1}{2}$ or that h is equal to $\frac{1}{2}c$, thus fixing the point where no flow occurs through the plate at $\frac{1}{2}c$ aft of the lifting line or on the three-quarter-chord line.

It follows directly that, if a lift-curve slope is less than 2π, then the control point should move forward of the three-quarter-chord line, and if greater, aft. Thus, adjustment can be made for changes in section lift-curve slope at each of the four control stations. The procedure for doing this will be shown in the application of the method. It is not clear just how well this procedure will account for changes in section lift-curve slope resulting from separation of flow. Therefore, some caution should be used in interpreting results obtained from this method where large changes in lift-curve slope from the theoretical are involved.

In using this lift-curve-slope correction, it must be realized that an attempt is being made to impose considerations of section characteristics on a theory which cannot rigorously allow such considerations. The question of the applicability of the correction becomes of particular importance where the wing has large values of sweep of the quarter-chord line. As the subject theory is developed, the sections containing the control point and the point at which load is determined lie in a line parallel to the free-stream direction. Thus any considerations of section characteristics can be applied only to sections lying along these lines. However, simple sweep theory indicates that it is more correct to make the controlling airfoil section that one lying along a line normal to the wing quarter-chord line. These two sections are quite different, of course, if sweep is present. If no taper is present, their thickness distributions are the same, but their thickness ratios vary by the cosine of the angle of sweep. If taper is present, both thickness distribution and thickness ratio vary.

Study of the problem has so far indicated that neither the approach of simple sweep theory nor of the subject theory is correct insofar as choosing the controlling airfoil section, but rather that the controlling section lies somewhere between these two limits and varies with span position. In view of this, therefore, it should not be expected that true account can be taken of changes in airfoil-section characteristics. However, it is believed that use of the procedure proposed herein will indicate the trend of the changes in over-all wing characteristics to be expected from changes in section characteristics. Until such time as more detailed analytic and experimental studies of the problem are completed, it is recommended that the results of applying this correction be considered largely qualitative.

EFFECTS OF COMPRESSIBILITY

The Prandtl-Glauert rule, which accounts for the effects of compressibility, is directly applicable to the subject simplified lifting-surface theory. The approximations and limitations of the Prandtl-Glauert rule are well known and, hence, no discussion of them is given herein. However, for convenient reference, the basis for correcting the predicted span loadings and the theoretical relation of these corrections to the simplified lifting-surface theory is presented.[5]

The Prandtl-Glauert rule simply states that, as the Mach number is increased, the span load distribution of a wing distorts as though the x dimensions of the wing were increasing as the ratio of $\frac{1}{\beta}$. Thus, the effects of Mach number on a given wing can readily be considered by finding the span loading at zero Mach number of a properly distorted wing. It can be seen that increasing the x dimensions of the wing results in increasing the angle of sweep and increasing each local chord (or, in effect, a decrease in aspect ratio) while leaving the span and taper unaffected. Thus

$$A_\beta=\beta A$$

$$\Lambda_\beta=\tan^{-1}\frac{\tan\Lambda}{\beta}$$

The foregoing is applicable to any type of span-loading theory. The distorted wing is considered for the Mach number in question and the span load distribution found. This load distribution is then considered as being carried by the undistorted wing in order to find those characteristics dependent on span loading.

[5] For the limiting case of Mach number equal to 1, the reader is referred to NACA TN 1824, "Linearized Compressible-Flow Theory for Sonic Flight Speeds," by Max. A. Heaslet, Harvard Lomax, and John R. Spreiter.

In the case of the subject span-loading theory, the compressibility correction can be considered in another way. As before, the angle of sweep is effectively increased by increasing Mach number. However, the increase in local chord in the ratio $\frac{1}{\beta}$ can be regarded as an increase in the distance between the lifting vortex and the control point on the undistorted wing. From the previous section it will be recalled this corresponds to an increase in section lift-curve slope—in this case exactly in the ratio of $\frac{1}{\beta}$. Thus, the theoretical section lift-curve slope, where compressible effects are included and the control point is held at the three-quarter-chord point, implicity becomes $\frac{2\pi}{\beta}$. Any corrections for section lift-curve-slope change thus become based on the deviations of the experimental section lift-curve slope at a given Mach number from the value of $\frac{2\pi}{\beta}$ at the same Mach number. It can be seen that this increase in c_{l_α} is exactly equivalent in effect to the decrease in aspect ratio. It is obvious from this that two techniques can be used in applying the compressibility correction to the simplified lifting-surface theory. Either the wing geometry can be appropriately altered or the disposition of the original layout of the lifting vortex and control points can be altered. The choice of procedure is governed entirely by the relative simplicity in handling the computations. As will be shown under the following sections on the application of the method, both are used, the choice depending on the type of loading and wing being considered.

APPLICATION OF METHOD

LOADING CHARACTERISTICS FOR ARBITRARY WINGS

In the foregoing sections, a method for predicting the span loading on wings has been outlined and it has been shown how other characteristics can be found from the span loading. Further, it has been shown how corrections can be applied to approximately account for deviations of the section lift-curve slopes from the theoretical value of 2π and for the effects of compressibility.

With the information thus far given, it is possible to predict the span loading and resulting characteristics of an arbitrary wing from a knowledge of the wing geometry only. Application of the procedure, however, shows that the most time-consuming portion is that of computing the influence coefficients $a_{\nu n}$, sixteen of which are required for the seven-point method. Examination of the theory shows that, if the number of control stations is fixed, the influence coefficients become a function of the wing geometry only, that is, sweep and chord distribution. It becomes immediately apparent that, if the number of control stations is chosen, then the corresponding influence coefficients can be presented in graphical or tabular form as a function of wing geometry. Thus, the greater part of the computing work associated with the method can be eliminated, since the same coefficients are used to find any form of symmetric loading for a given plan form.

Further simplifications, not so immediately evident, are also possible. It can be shown (see appendix) that, if the angle of sweep is fixed, all the influence coefficients become a function of $\frac{b}{c_\nu}$ alone. Thus, if a complete set of coefficients for one taper ratio is determined throughout the aspect-ratio range, the coefficients for all other plan forms having the same sweep can be related to these coefficients by relating the values of $\frac{b}{c_\nu}$ of the wing in question to those for which the coefficients were determined. Further consideration shows that the effect of section lift-curve-slope deviation from the theoretical values can also be accounted for by a change in the value of $\frac{b}{c_\nu}$ in the ratio of experimental to theoretical section lift-curve slopes. Finally, if the compressible-sweep parameter $\left(\Lambda_\beta=\tan^{-1}\frac{\tan\Lambda}{\beta}\right)$ is used rather than the geometric sweep angle and the value of $\frac{b}{c_\nu}$ is adjusted by the factor β, then the effective plan-form change due to compressibility is accounted for.

To simplify the use of the method, therefore, the influence coefficients for symmetric loading $a_{\nu n}$ for the seven-point method have been computed and are presented in table I and figure 1 as functions of the compressible sweep parameter Λ_β and the parameter H_ν. For most wings the values of the coefficient $a_{\nu n}$ can be obtained directly from figure 1. However, for certain wings of extreme plan forms the values of H_ν will be such that the values of $a_{\nu n}$ will lie off the charts. Where linear extrapolation of the curves is not acceptable, table I provides sufficient values of $a_{\nu n}$ to enable extension of the curves. Adequate accuracy of the final results will be obtained if the value of $a_{\nu n}$ is read to two decimal places.

The parameter H_ν is defined as follows:

$$H_\nu=d_\nu\frac{1}{\kappa_\nu}\frac{b}{c_\nu/\beta}$$

where

d_ν scale factor which is given on each chart

$\kappa_\nu\frac{c_{l_{\alpha_{exp}}}}{2\pi/\beta}$, the ratio of the two-dimentional experimental lift-curve slope for the airfoil section at station ν to the theoretical value, both for the Mach number under consideration

$\beta\ \sqrt{1-M^2}$

$\frac{b}{c_\nu}$ ratio of wing span to the chord of the wing at the spanwise station corresponding to the control point ν

The application of the method to the case of the arbitrary wing plan forms can be outlined as follows:

1. Compute the value of H_ν at each spanwise station ν and the value of Λ_β, both for the Mach number in question. (Note that the effects of section lift-curve-slope change and of Mach number are completely accounted for within the limits of the method by these parameters, and the predicted results will include these effects.)

2. From figure 1 or table I and with the value of H_ν, find the values of each of the 16 $a_{\nu n}$ coefficients.

3. Insert the values of $a_{\nu n}$ in equation (6) for basic load-

ing or equation (11) for additional loading and solve the simultaneous equations[6] for the values of G_{n_0} or $\frac{G_{n_a}}{\alpha}$.

4. With the values of G_{n_0} or $\frac{G_{n_a}}{\alpha}$ known, other wing characteristics can be found by substituting these values in the appropriate equation as indicated by the following table:

	Basic loading	*Additional loading*
C_{D_i}	Equation (9)_____	Equation (9).
C_{D_i}/C_L^2	_____	Equation (13).
$\eta_{c.p.}$	_____	Equation (14).
C_m	Equation(10)_____	_____

ADDITIONAL LOADING CHARACTERISTICS OF STRAIGHT-TAPERED WINGS

The previous section has shown how to apply the method to determine aerodynamic characteristics of an arbitrary wing. For the more common case of straight-tapered wings, it is possible to prepare charts giving wing aerodynamic characteristics due to additional loading directly as a function of wing sweep, aspect ratio, and taper ratio.

The method has, therefore, been used to find the additional span loading and some of the wing characteristics for a series of wings of varying plan forms and having constant section lift-curve slope across the span. Some 200 wings (the range of plan forms, but not the total number of wings is shown in fig. 2) were included in the study, the results of which are presented in figures 3 to 6. Each of these figures is a chart giving the variation of a particular wing characteristic with wing sweep and aspect ratio for five values of taper ratio. Figure 3 gives the value of the local loading coefficient at each of the four spanwise stations. Figure 4 gives the value of wing lift-curve slope. Figure 5 gives the spanwise location of the center of pressure. Figure 6 gives the chordwise location of the center of pressure or the aerodynamic center[7] measured from the leading edge of the mean aerodynamic chord.

To find the desired characteristic for a given wing, the chart for the proper taper ratio is entered with the compressible sweep parameter $\left(\Lambda_\beta=\tan^{-1}\frac{\tan\Lambda}{\beta}\right)$, and the desired value read from the curve—or interpolated—for the proper value of the aspect-ratio parameter $\frac{\beta A}{\kappa}$. Thus, it is possible to find, with no computation, many of the characteristics for untwisted wings. It should be remembered that, since basic and additional loading are considered independent, these characteristics not only represent the gross characteristics of untwisted wings, but also the additional loading characteristics of twisted wings. They are thus applicable, to some extent, to all wings having straight-taper and constant section lift-curve slope across the span.

[6] Experience has shown that the method given in reference 6 for the solution of a set of simultaneous equations is most satisfactory.

[7] For the case of the straight-tapered wing, this chordwise location of the aerodynamic center can be simply expressed in terms of the geometry of the wing and the spanwise location of the center of pressure. Thus

$$a.c.=\frac{1}{4}+\frac{3(1+\lambda)^2}{8(1+\lambda+\lambda^2)}\left[\eta_{c.p.}-\frac{1+2\lambda}{3(1+\lambda)}\right]A\tan\Lambda$$

TABLE I.—SYMMETRIC INFLUENCE COEFFICIENTS, a_{rs}. WHICH LEAD OFF THE CHARTS OF FIGURE 1

a_{11}

H_1 \ Λ_β	−45	−40	−20	0	20	40	50	60	70	75
0.8									18.60	22.67
1.0									21.66	26.78
1.2							16.26	18.95	24.72	30.88
1.6	15.85					17.20	19.28	22.96	30.84	39.09
2.0	17.44	17.00	16.08	16.19	16.94	19.54	22.26	27.14	36.90	
2.4		18.52	17.40	17.66	18.54	21.35	25.26	31.27		
2.8			18.72	19.18	20.14	24.22	28.26			
3.2			20.04	20.72	21.74	26.56	31.26			
3.6			21.36	22.26	23.34	28.90	34.26			
4.0				23.80	24.94	31.24				

a_{12}

H_1 \ Λ_β	−45	−40	−20	0	20	40	50	60	70	75
0.6	−1.32	−2.02							−6.35	−8.00
.8	−.30	−1.52	−2.05						−8.07	−10.14
1.0	.72	−1.02	−1.55					−6.60	−9.79	−12.28
1.2	1.72	−.52	−1.05				−7.03	−7.73	−11.51	−14.42
1.6	3.76	.48	−.05				−8.29	−9.41	−14.95	−18.70
2.0	5.82	1.48	.95			−6.95	−9.55	−11.32	−18.39	
2.4		2.48	1.96			−7.71	−10.81	−13.23		
2.8			2.95			−8.47	−12.07			
3.2			3.95			−9.23	−13.23			
3.6			4.95			−9.97				
4.0										

a_{13}

H_1 \ Λ_β	−45	−40	−20	0	20	40	50	60	70	75
0.8	−1.03								3.23	4.91
1.0	−1.69	−1.26							4.37	6.55
1.2	−2.20	−1.72							5.51	8.20
1.6	−3.33	−2.64	−1.23					4.54	7.79	11.50
2.0	−4.39	−3.56	−1.71					6.04	10.07	
2.4		−4.48	−2.19				4.73	7.55		
2.8			−2.67				5.71			
3.2			−3.15			4.45	6.69			
3.6			−3.63			5.15	7.67			
4.0						6.30				

a_{14}

H_1 \ Λ_β	−45	−40	−20	0	20	40	50	60	70	75
1.0										−3.31
1.2										−4.01
1.6	1.45	1.17							−4.06	−5.61
2.0	1.93	1.59							−4.67	
2.4		2.01							−5.28	
2.8			1.06						−5.89	
3.2			1.27							

DISCUSSION

COMPARISON WITH OTHER THEORY AND WITH EXPERIMENT

The extent to which the method can be evaluated varies widely with the particular characteristic in question. In general, the accuracy of predicting the characteristics associated with basic loading can be evaluated in only a limited manner, since few swept or low-aspect-ratio wings having appreciable twist or camber have been experimentally or theoretically studied. On the other hand, many wing plan forms have been studied and from those results it is possible to assess fairly well the accuracy of the method with regard to additional loading.

Basic loading.—The prediction of the effect of twist and/or camber on load distribution can be evaluated to a degree by comparison with other theories. Such a comparison is given in figure 7 wherein the predicted loading given by the subject method is compared with those given by the method

developed by V. M. Falkner and that of reference 7. It may be assumed that the Falkner method is the most accurate of the three since it approaches a true lifting-surface theory. From the comparisons shown in figure 7, it would appear the subject theory is nearly as good as the more complex theory and considerably better than the lifting-line theory of reference 7. It must be recognized that twist introduces large induction effects even on high-aspect-ratio wings. Therefore, it follows that the deviations of the predictions of the subject theory and those of the theory of reference 7 from those of Falkner's method are indicative of the ability of the two methods to account for the induction effects.

A check on the ability to predict C_{m_0} and α_{r_0} can be had from comparison with the experimental results shown in reference 7. Here a wing having 30° of sweepback was tested without twist (wing designated 24–30–0) and with 8.5° of twist (wing designated 24–30–8.5). The force tests show that the twist shifts the angle of zero lift 2.6° while the present theory gives a value of 3.3°. The force tests indicate that twist produces a value of C_{m_0} of 0.05 which is the same as that predicted by the theory.

A further comparison of experiment and the present theory can be made using results of pressure-distribution tests of a wing having 60.8° of sweepback. The geometrical characteristics of the wing together with the experimental results and theoretical predictions are shown in figure 8. The comparisons are made for zero lift where only basic loading exists. It can be seen that the agreement is good even for this unconventional plan form.

On the basis of the foregoing comparisons, it seems justifiable to conclude that the subject method can adequately predict the effects of twist and/or camber on the characteristics of wings of arbitary plan form.

Additional loading.—Much experimental data and several theories are available for comparison with the subject theory in regard to the prediction of additional-type lift. Figure 9 shows a comparison of the predicted loadings and those obtained experimentally for six wings varying in sweep, aspect ratio, and taper ratio. Figure 10 compares the variation of lift-curve slope with aspect ratio as predicted by the subject theory, by two more rigorous theories (references 8 and 9), and by a theory directed at the limiting case of zero aspect ratio (reference 10). Figure 11 compares experimental and theoretically predicted lift-curve slopes (assuming a section lift-curve slope of 2π per radian) for two families of plan forms covering a wide range of aspect ratios (references 11 and 12). The comparison between experimental (references 12 and 13) and predicted results for a random group of wing plan forms is shown in figure 12 for lift-curve slope and figure 13 for aerodynamic-center location. All experimental values of C_{L_α} and aerodynamic-center location were measured at zero lift. It is evident that in almost every case the method gives an excellent prediction.

From all of this comparative material it seems possible to safely draw the conclusion that the subject method can satisfactorily predict the additional-type span loading on wings of arbitrary plan form. Further, it seems possible that equally good predictions can be made of those characteristics primarily dependent upon such span loading.

EFFECT OF PLAN-FORM VARIATION ON THE BASIC-LOADING CHARACTERISTICS

To study the effects of plan-form variation on the basic-loading characteristics of linearly twisted, straight-tapered wings, the characteristics of a representative group of wings (see shaded wings, fig. 2) having unit washout[8] have been computed and are presented in figures 14 to 19. The Mach number was taken as zero and the section lift-curve slope as 2π. The basic-loading characteristics considered are the loading coefficient $\frac{c_{l_0}c}{\epsilon c_{av}}$ (figs. 14 to 17), the pitching-moment coefficient due to twist $\frac{C_{m_0}}{\epsilon}$ (fig. 18), and the angle of attack of the root section for zero net lift $\frac{\alpha_{r_0}}{\epsilon}$ (fig. 19).

Magnitude and spanwise distribution of load.—Examination of figures 14 to 17 reveals that the aspect ratio influences only the magnitude of the load and is in fact the predominate influence on the magnitude of the load. Reductions in aspect ratio from 6.0 to 3.5 and 1.5 result in approximately 35-percent and 70-percent reductions, respectively, in load due to twist for either the unswept or 45° swept-back wings (fig. 15).

Sweep, either forward or back, tends to reduce the magnitude of loading, although appreciable reductions are produced only by sweep angles greater than 45° (fig. 14). Sweep also affects the load distribution such that the load on the outer section of the wing is shifted inboard by sweepforward and toward the tip by sweepback; as will be seen, this is similar to the effect of sweep on the additional-type loading. Since an increase in aspect ratio magnifies the loading, it also magnifies the effects of sweep on the loading as is shown in figure 14.

As shown in figures 16 and 17, variation in taper ratio has little effect on the magnitude of basic loading; and variations in taper ratio, for taper ratios larger than 0.5, have little effect on the load distribution. However, for taper ratios less than 0.5, the loading on the outer section of the wing shifts inboard. These effects of taper ratio on loading are magnified by increases in aspect ratio.

Pitching moment.—That the pitching moment due to twist is primarily a function of sweep and aspect ratio is shown in figure 18. The magnitude of the pitching moment increases as either aspect ratio or sweep is increased so that pitching-moment coefficients as large as 0.008, for 1° of twist,

[8] In this case, 1° was chosen, and for any larger amount of twist the effects are proportional.

exist on wings having large aspect ratios and sweep angles. The effect of taper ratio is relatively small, the greatest being evidenced at the small values of taper ratio. For example, reducing the taper ratio from 0.5 to 0 reduces the pitching moment due to twist about 30 percent.

Angle of zero lift.—Although the effects of plan form on the angle of zero lift α_{r_0} may not be very important, some of the trends indicated in figure 19 are of interest. For the range of plan forms represented in figure 19, the angle of zero lift varied only about 20 percent from the mean value. This is small compared to the effects of plan form on the magnitude and distribution of loading and on the pitching moment. In contrast to the small effect of taper noted previously, taper ratio appears to be the predominant influence on α_{r_0} particularly at large aspect ratios and large sweepback. The effect of aspect ratio and sweep are secondary but not negligible.

EFFECT OF PLAN-FORM VARIATION ON THE ADDITIONAL LOADING CHARACTERISTICS

Span load distribution.—To show directly the effects of wing plan form on the additional span loading, figure 20 has been prepared by cross-plotting the data of figure 3. It shows that increasing the angle of sweepback or the taper ratio serves to move the loading $\left(\text{as defined by } \frac{c_{l_a}c}{C_{L_{\alpha}}}\right)$ outboard.

It can be noted in figure 5 that the spanwise center of pressure is independent of aspect ratio for certain combinations of taper ratio and sweep angle. These values of taper ratio are plotted against sweep angle in figure 21. Further, for the wing geometry represented by the curve of figure 21, the loading is approximately independent of aspect ratio (fig. 3), and also is approximately elliptical. For elliptical loading, the loading coefficient at the four spanwise stations have the values 1.273, 1.176, 0.900, and 0.487. It can be seen that these values compare closely with those given in figure 3 for the plan forms specified in figure 21. The farther the wing geometry departs from the configuration represented by the curve in figure 21, the greater the change of loading with aspect ratio and the rate of distortion from an elliptical load distribution. Also, examination of figure 3 will show that elliptical loading cannot be maintained, when a wing is swept, by altering aspect ratio alone; however, all wings approach an elliptical loading as aspect ratio approaches zero.

The wings specified by the curve of figure 21 have the property that their aerodynamic characteristics can be expressed in a simple manner similar to the case of unswept wings with elliptic plan forms. Namely, the induced drag is given approximately by $\frac{C_{D_i}}{C_L^2}=\frac{1}{\pi A}$, spanwise center of pressure by $\eta_{c.p.}=\frac{4}{3\pi}$, and aerodynamic-center location with respect to the mean aerodynamic chord by

$$a.c.=\frac{1}{4}+\frac{0.342-0.567\lambda-0.908\lambda^2}{10(1+\lambda+\lambda^2)}A\tan\Lambda$$

From figure 4, it can be shown that the wings specified by the curve of figure 21 give the maximum lift-curve slope for a given aspect ratio and sweep angle. For example, see figure 22 for the case of $A=3.0$.

In summary, the curve of figure 21 defines wings having the following approximate characteristics: span loading distribution independent of aspect ratio, minimum induced drag, and maximum lift-curve slope for a given sweep and aspect ratio, a constant spanwise center of pressure, and an aerodynamic-center location that is a simple function of wing geometry only.

Lift-curve slope.—Examination of figure 4 reveals certain general trends with respect to the effect of wing plan form on wing-lift-curve slope. For wings of high aspect ratio, the angle of sweep has a marked effect on lift-curve slope, with the maximum effect occurring for wings of infinite aspect ratio when the lift-curve slope is directly a function of the angle of sweep. As the aspect ratio approaches very low values, the lift-curve slope for the unswept wing is greatly reduced and the effects of sweep become small except for very large angles of sweep. Also, it can be seen that at very large angles of sweep the effects of aspect-ratio variation on lift-curve slope become small.

To better illustrate the separate effects of aspect ratio and taper ratio, the data from figure 4 have been cross-plotted to show the variation with aspect ratio of the lift-curve slope for various values of taper ratio and sweep angle. These results are shown in figure 23. This figure shows clearly how increasing the angle of sweep decreases the variation of lift-curve slope with aspect ratio. It shows further that while taper ratio as compared to aspect ratio has only a small effect on the lift-curve slope of an unswept wing, taper ratio has a predominant effect on the lift-curve slopes of highly swept wings of moderate to high aspect ratios. For very small aspect ratios (i. e., $A<1.5$), however, the lift-curve slopes of all the wings converge and become almost a linear function of aspect ratio, being essentially independent of the effects of sweep and taper (reference 10).

Aerodynamic center.—In figure 6, variations of aerodynamic-center location from 15-percent mean aerodynamic chord to 45-percent mean aerodynamic chord are indicated for the range of plan forms studied. It will be noted that, for taper ratio $\lambda=0$, the aerodynamic center moves aft for sweepback and forward for sweepforward. At taper ratios of 1.0 and 1.5 the aerodynamic center moves forward for sweepback and aft for sweepforward. For $\lambda=0$ the effects of aspect ratio are largely confined to the swept-back wings and as taper ratio is increased the effect of aspect ratio decreases for swept-back wings and increases for swept-

forward wings. Where the effects of aspect ratio are significant, an increase in aspect ratio generally moves the aerodynamic center aft.

CONCLUDING REMARKS

The simplified lifting-surface theory presented herein enables the rapid, accurate prediction of symmetric span load distribution for wings which have symmetry about the root chord and a straight quarter-chord line over the semispan and which can have arbitrary chord distribution, sweep, aspect ratio, and continuous twist. Modifications to the method are shown by means of which approximate account can be taken of changes in section lift-curve slope and by means of which the effects of compressibility as predicted by the Prandtl-Glauert rule can be included.

With the charts presented in the report, the load distribution can be obtained directly for many wings and can be obtained with slight additional computation for all wings falling within the limitations prescribed.

From the span loadings determined by the method, it is shown how several important wing characteristics can be determined. Comparison with experimental results indicates that the wing characteristics so obtained are reliable for a wide range of plan forms.

AMES AERONAUTICAL LABORATORY,
NATIONAL ADVISORY COMMITTEE FOR AERONAUTICS,
MOFFETT FIELD, CALIF., *1947–1948*.

APPENDIX

The mathematical process of finding the loading distribution for wings evolves itself into two parts: first, the determination of the integral equation which relates the downwash at a given point to the integrated effects of the bound vortex and trailing vortex sheet; and, second, the solution of the integral equation to determine the unknown loading distribution factor.

ADDITIONAL SYMBOLS USED IN THE APPENDIX

a_{μ_1} Fourier coefficients of the loading distribution series

$b_{\nu\nu}$, $b_{\nu n}$, $B_{\nu n}$ mathematical series coefficients

e_{nk} loading interpolation factors

$f_{n\mu}$, $\bar{f}_{n\mu}$ mathematical series coefficients

$g_{\nu\nu}$, $g_{\nu n}$, $\bar{g}_{\nu\nu}$, $\bar{g}_{\nu n}$ downwash influence coefficients

k value pertaining to interpolated span station $\left(\eta=\cos\frac{k\pi}{8}\right)$

$L(\eta,\bar{\eta})$, $L_{\nu\mu}$, $L^*_{\nu\mu}$ downwash integrand functions

M number of span stations taken to numerically integrate the downwash integrand function

r absolute distance from the downwash point to an elemental vortex, feet

s distance along the load vortex, feet

x longitudinal coordinate, positive downstream, feet

$\bar{x}$ longitudinal coordinate pertaining to the load vortex, feet

y lateral coordinate, positive to the right, feet

$\bar{y}$ lateral coordinate pertaining to the load vortex, feet

α_t induced angle in the wake of the wing, radians

$\bar{\eta}$ dimensionless lateral coordinate pertaining to the load vortex $\left(\frac{\bar{y}}{b/2}\right)$

θ_1,θ_2 positive angles between a vortex line and the lines joining the ends of the vortex line and a downwash point, radians

μ integer pertaining to span station $\mu\left(\eta=\cos\frac{\mu\pi}{M+1}\right)$

μ_1 integer sequence of the Fourier series for loading distribution, also pertaining to span station μ_1 $\left(\eta=\cos\frac{\mu_1\pi}{m+1}\right)$

DETERMINATION OF THE DOWNWASH INTEGRAL EQUATION FOR SWEPT WINGS

Downwash induced by the trailing vortex sheet.—

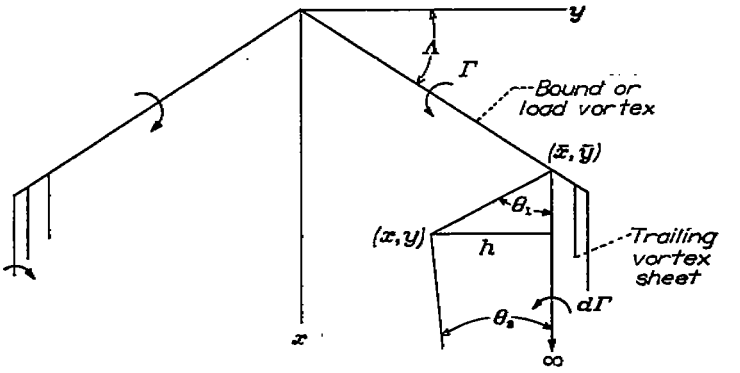

Sketch "A"

The downwash due to the trailing sheet is, for an arbitrary elemental trailing vortex, given in several references (e. g., see Glauert, reference 14). The downwash at a point in the xy plane is given by

$$dw_{xy}=\frac{d\Gamma}{4\pi h}(\cos\theta_1+\cos\theta_2) \qquad \text{(A1)}$$

where the induced velocity is positive for downwash, θ_1 and θ_2 are the inside angles between the trailing vortex line and the lines from the ends of the trailing vortex line to the downwash point, h is the perpendicular distance from the downwash point to the trailing vortex line, and $d\Gamma$ is the strength at a given span station of the trailing vortex. From the foregoing sketch it can be seen that

$$h=y-\bar{y}$$

$$\cos\theta_1=\frac{x-\bar{x}}{\sqrt{(x-\bar{x})^2+(y-\bar{y})^2}}$$

$\cos\theta_2=1$ (since $\theta_2=0$ with the trailing vortex extended to infinity)

and

$$\bar{x}=|\bar{y}|\tan\Lambda$$

Substituting these values into equation (A1) and integrating will give w_{xy} due to trailing sheet equal to

$$\frac{1}{4\pi}\int_{-b/2}^{b/2}\frac{1}{y-\bar{y}}\left[1+\frac{x-|\bar{y}|\tan\Lambda}{\sqrt{(x-|\bar{y}|\tan\Lambda)^2+(y-\bar{y})^2}}\right]\Gamma'(\bar{y})d\bar{y} \qquad \text{(A2)}$$

Downwash induced by the load vortex.—

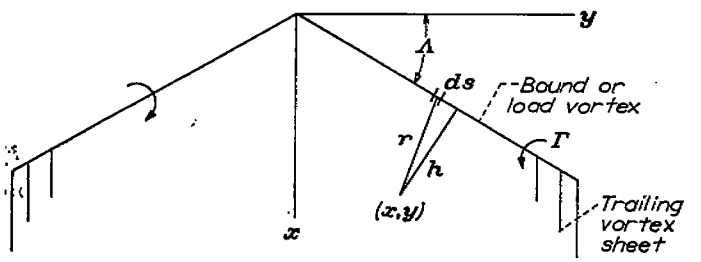

Sketch "B"

The downwash generated by the swept load vortex is the sum of the downwash generated from each semispan. Along the load vortex the circulation is continuously varying. The downwash at (x, y) due to the small element ds (see accompanying sketch) is given by (e. g., see Glauert, reference 14)

$$dw_{xy}=\frac{\Gamma h ds}{4\pi r^3} \qquad \text{(A3)}$$

For a swept load vortex, for the right semispan

$$s=\frac{\bar{y}}{\cos\Lambda}$$

$$h=x\cos\Lambda-y\sin\Lambda$$

$$r=\sqrt{(x-\bar{x})^2+(y-\bar{y})^2}$$

$$\bar{x}=|\bar{y}|\tan\Lambda$$

while for the left semispan

$$h=x\cos\Lambda+y\sin\Lambda$$

and s, r, and $\bar{x}$ are the same as for the right semispan. Substituting these values into equation (A3) and integrating will give w_{xy} due to load vortex equal to

$$\frac{1}{4\pi}\int_{-b/2}^{0}\frac{(x\cos\Lambda+y\sin\Lambda)\Gamma(\bar{y})d\bar{y}}{\cos\Lambda[(x-|\bar{y}|\tan\Lambda)^2+(y-\bar{y})^2]^{3/2}}+$$

$$\frac{1}{4\pi}\int_{0}^{b/2}\frac{(x\cos\Lambda-y\sin\Lambda)\Gamma(\bar{y})d\bar{y}}{\cos\Lambda[(x-|\bar{y}|\tan\Lambda)^2+(y-\bar{y})^2]^{3/2}} \qquad \text{(A4)}$$

Total downwash.—The total downwash due to the trailing sheet and the load vortex is equal to the sum of equations (A2) and (A4), or

$$w_{xy}=\frac{1}{4\pi}\int_{-b/2}^{b/2}\frac{1}{y-\bar{y}}\left[1+\frac{x-|\bar{y}|\tan\Lambda}{\sqrt{(x-|\bar{y}|\tan\Lambda)^2+(y-\bar{y})^2}}\right]\Gamma'(\bar{y})d\bar{y}+$$

$$\frac{1}{4\pi}\int_{-b/2}^{0}\frac{(x+y\tan\Lambda)\Gamma(\bar{y})d\bar{y}}{[(x-|\bar{y}|\tan\Lambda)^2+(y-\bar{y})^2]^{3/2}}+$$

$$\frac{1}{4\pi}\int_{0}^{b/2}\frac{(x-y\tan\Lambda)\Gamma(\bar{y})d\bar{y}}{[(x-|\bar{y}|\tan\Lambda)^2+(y-\bar{y})^2]^{3/2}} \qquad \text{(A5)}$$

The last two integrals of equation (A5) can be integrated by parts and put in the form of the first integral. With $\Gamma\left(\pm\frac{b}{2}\right)=0$, equation (A5) becomes

$$w_{xy}=\frac{1}{4\pi}\left\{\int_{-b/2}^{b/2}\frac{1}{y-\bar{y}}\left[1+\frac{x-|\bar{y}|\tan\Lambda}{\sqrt{(x-|\bar{y}|\tan\Lambda)^2+(y-\bar{y})^2}}\right]\Gamma'(\bar{y})d\bar{y}-\right.$$

$$\int_{-b/2}^{0}\frac{\left(\frac{\bar{y}}{\cos^2\Lambda}+x\tan\Lambda-y\right)\Gamma'(\bar{y})d\bar{y}}{(x+y\tan\Lambda)\sqrt{(x+\bar{y}\tan\Lambda)^2+(y-\bar{y})^2}}$$

$$\int_{0}^{b/2}\frac{\left(\frac{\bar{y}}{\cos^2\Lambda}-x\tan\Lambda-y\right)\Gamma'(\bar{y})d\bar{y}}{(x-y\tan\Lambda)\sqrt{(x-\bar{y}\tan\Lambda)^2+(y-\bar{y})^2}}+$$

$$\left.\frac{2\tan\Lambda\sqrt{x^2+y^2}}{x^2-y^2\tan^2\Lambda}\Gamma(0)\right\} \qquad \text{(A6)}$$

Equation (A6) can be simplified algebraically and rewritten into the form

$$w_{xy}=\frac{1}{4\pi}\int_{-b/2}^{b/2}\frac{\Gamma'(\bar{y})d\bar{y}}{y-\bar{y}}+$$

$$\frac{1}{4\pi}\int_{-b/2}^{0}\frac{\sqrt{(x+\bar{y}\tan\Lambda)^2+(y-\bar{y})^2}}{(x+y\tan\Lambda)(y-\bar{y})}\Gamma'(\bar{y})d\bar{y}+$$

$$\frac{1}{4\pi}\int_{0}^{b/2}\frac{\sqrt{(x-\bar{y}\tan\Lambda)^2+(y-\bar{y})^2}}{(x-y\tan\Lambda)(y-\bar{y})}\Gamma'(\bar{y})d\bar{y}+$$

$$\frac{2\tan\Lambda\sqrt{x^2+y^2}}{4\pi(x^2-y^2\tan^2\Lambda)}\Gamma(0) \qquad \text{(A7)}$$

The three integrands of equation (A7) have an infinite point at $\bar{y}=y$. The integrand in the second and third integrals can be made continuous by subtracting the function $\frac{\Gamma'(\bar{y})}{y-\bar{y}}$. Equation (A7) remains balanced if $\frac{\Gamma'(\bar{y})}{y-\bar{y}}$ is also added to the first integrand. As will be seen presently, the first integral, the integrand of which retains the infinite point, will give a finite value after integration. Equation (A7) becomes (adding the fourth term to the second integral)

$$w_{xy}=\frac{2}{4\pi}\int_{-b/2}^{b/2}\frac{\Gamma'(\bar{y})d\bar{y}}{y-\bar{y}}+\frac{1}{4\pi}\int_{-b/2}^{0}\left[\frac{\sqrt{(x+\bar{y}\tan\Lambda)^2+(y-\bar{y})^2}}{(x+y\tan\Lambda)(y-\bar{y})}-\right.$$

$$\left.\frac{1}{y-\bar{y}}+\frac{2\tan\Lambda\sqrt{x^2+y^2}}{x^2-y^2\tan^2\Lambda}\right]\Gamma'(\bar{y})d\bar{y}+$$

$$\frac{1}{4\pi}\int_{0}^{b/2}\left[\frac{\sqrt{(x-\bar{y}\tan\Lambda)^2+(y-\bar{y})^2}}{(x-y\tan\Lambda)(y-\bar{y})}-\frac{1}{y-\bar{y}}\right]\Gamma'(\bar{y})d\bar{y} \qquad \text{(A8)}$$

Equation (A8) can give the downwash at any point in the xy plane. From the discussion of the theory in the text, the downwash must be found along the three-quarter-chord line of the wing. For a given span station the x coordinate of a point on the three-quarter-chord line is given by

$$x=\frac{c}{2}+|y|\tan\Lambda$$

The nondimensional equation for downwash angle at any span station on the three-quarter-chord line can be obtained by substituting this value of x into equation (A8) and by using the following nondimensional relations:

$$\eta=\frac{y}{b/2}$$

$$\bar{\eta}=\frac{\bar{y}}{b/2}$$

$$\frac{x}{b/2}=\frac{c}{b}+|\eta| \tan \Lambda$$

$$G=\frac{\Gamma}{bV}$$

The resulting equation is

$$\left(\frac{w}{V}\right)_\eta=\frac{1}{\pi}\int_{-1}^{1}\frac{G'(\bar{\eta})d\bar{\eta}}{\eta-\bar{\eta}}+\frac{b/c}{2\pi}\int_{-1}^{1}L(\eta,\bar{\eta})G'(\bar{\eta})d\bar{\eta} \qquad \text{(A9)}$$

where the function $L(\eta,\bar{\eta})$ is given by,

for $\bar{\eta}\leq 0$,

$$\left.\begin{aligned}L(\eta,\bar{\eta})&=\frac{1}{(b/c)(\eta-\bar{\eta})}\left\{\frac{\sqrt{[1+(b/c)(|\eta|+\bar{\eta})\tan\Lambda]^2+(b/c)^2(\eta-\bar{\eta})^2}}{1+(b/c)(|\eta|+\eta)\tan\Lambda}-1\right\}+\frac{2\tan\Lambda\sqrt{[1+(b/c)|\eta|\tan\Lambda]^2+(b/c)^2\eta^2}}{[1+(b/c)(|\eta|-\eta)\tan\Lambda][1+(b/c)(|\eta|+\eta)\tan\Lambda]}\\ \text{and, for } \bar{\eta}\geq 0,\\ L(\eta,\bar{\eta})&=\frac{1}{(b/c)(\eta-\bar{\eta})}\left\{\frac{\sqrt{[1+(b/c)(|\eta|-\bar{\eta})\tan\Lambda]^2+(b/c)^2(\eta-\bar{\eta})^2}}{1+(b/c)(|\eta|-\eta)\tan\Lambda}-1\right\}\end{aligned}\right\} \qquad \text{(A10)}$$

Equation (A10) is complete for positive and negative values of the coordinate η. In the case of the unswept wing where Λ equals zero, equation (A10) simplifies considerably and the function $L(\eta,\bar{\eta})$ is given by,

for $-1\leq\bar{\eta}\leq 1$,

$$L(\eta,\bar{\eta})=\frac{1}{(b/c)(\eta-\bar{\eta})}\left[\sqrt{1+(b/c)^2(\eta-\bar{\eta})^2}-1\right] \qquad \text{(A11)}$$

MATHEMATICAL SOLUTION OF EQUATION (A9)

Arbitrary load distribution.—The solution of the integral equation (A9) to determine the unknown loading-distribution function $G(\bar{\eta})$, was obtained by Weissinger (reference 1) using a method introduced and applied by Multhopp (reference 15) to the problem of determining downwash at a straight bound vortex. Weissinger's method consists of applying the boundary conditions that the flow shall be tangent to the plate at the three-quarter-chord line at a number of span stations, then performing a numerical integration of equation (A9) at each station. The result is a set of simultaneous linear equations in which the unknowns are the values of $G(\bar{\eta})$ at the span stations chosen.

Introducing in equation (A9) the spanwise trigonometric variables ϕ_ν and ϕ defined by

$$\eta=\cos\phi_\nu$$

and

$$\bar{\eta}=\cos\phi$$

gives

$$\left(\frac{w}{V}\right)_\nu=\frac{1}{\pi}\int_0^\pi\frac{G'(\phi)d\phi}{\cos\phi-\cos\phi_\nu}-\frac{b/c_\nu}{2\pi}\int_0^\pi L(\phi_\nu,\phi)G'(\phi)d\phi \qquad \text{(A12)}$$

where b/c_ν is the value of b/c at span station ν.

In equation (A12) let $G(\phi)$ be given by the Fourier series as

$$G(\phi)=\sum_{\mu_1=1}^{m}a_{\mu_1}\sin\mu_1\phi \qquad \text{(A13)}$$

where

$$a_{\mu_1}=\frac{1}{\pi}\int_0^{2\pi}G(\phi)\sin\mu_1\phi d\phi$$

Since $G(\phi)$ is of interest only in the interval 0 to π ($-b/2\leq\bar{y}\leq b/2$) then

$$a_{\mu_1}=\frac{2}{\pi}\int_0^\pi G(\phi)\sin\mu_1\phi d\phi \qquad \text{(A14)}$$

Multhopp in reference 15 develops a quadrature formula which is a simple analogy to Gauss' (e. g., see reference 6) mechanical quadrature. This integration formula is a good choice for the functions represented by the series as given in equation (A13) since it integrates exactly functions represented by the trigonometric series to the $2m^{\text{th}}$ harmonic. The quadrature formula is given by

$$\int_{-1}^{1}f(\eta)d\eta=\frac{\pi}{m+1}\sum_{n=1}^{m}f(\eta_n)\sin\phi_n \qquad \text{(A15)}$$

where $\phi=\frac{n\pi}{m+1}$, and $f(\eta_n)$ is the value of $f(\eta)$ at $\eta=\cos\frac{n\pi}{m+1}$. Equation (A14) can be integrated by equation (A15) to give

$$a_{\mu_1}=\frac{2}{m+1}\sum_{n=1}^{m}G(\phi_n)\sin\mu_1\phi_n \qquad \text{(A16)}$$

Substitution of equation (A16) in (A13) gives the new form of the loading-distribution function as

$$G(\phi)=\frac{2}{m+1}\sum_{n=1}^{m}G_n\sum_{\mu_1=1}^{m}\sin\mu_1\phi_n\sin\mu_1\phi \qquad \text{(A17)}$$

where $G_n=G(\phi_n)$.

Then the derivative of equation (A17) is given by

$$\frac{dG(\phi)}{d\phi}=G'(\phi)=\frac{2}{m+1}\sum_{n=1}^{m}G_n\sum_{\mu_1=1}^{m}\mu_1\sin\mu_1\phi_n\cos\mu_1\phi \qquad \text{(A18)}$$

The first integral of equation (A12) containing the infinite point can be integrated directly with the series given by equation (A18). Using the following integral derived in reference 14

$$\int_0^\pi\frac{\cos n\phi}{\cos\phi-\cos\phi_0}d\phi=\frac{\pi\sin n\phi_0}{\sin\phi_0}$$

then

$$\begin{aligned}\frac{1}{\pi}\int_0^\pi\frac{G'(\phi)d\phi}{\cos\phi-\cos\phi_\nu}&=\frac{2}{\pi(m+1)}\sum_{n=1}^{m}G_n\sum_{\mu_1=1}^{m}\mu_1\sin\mu_1\phi_n\int_0^\pi\frac{\cos\mu_1\phi d\phi}{\cos\phi-\cos\phi_\nu}\\ &=\frac{2}{m+1}\sum_{n=1}^{m}G_n\sum_{\mu_1=1}^{m}\frac{\mu_1\sin\mu_1\phi_n\sin\mu_1\phi_\nu}{\sin\phi_\nu}\\ &=2b_{\nu\nu}G_\nu-\sum_{n=1}^{m}{}'2b_{\nu n}G_n\end{aligned} \qquad \text{(A19)}$$

where the prime on the summation sign indicates that the value for $n=\nu$ is not summed. Physically, equation (A19) gives the downwash angle at an infinite distance downstream for any wing geometry. This downwash angle is equal to twice the downwash angle at the quarter-chord line for the unswept wing.

The $b_{\nu n}$ coefficient of equation (A19) are given by the following equation:

$$\left.\begin{aligned}&\text{For } n=\nu\\&\qquad b_{\nu\nu}=\frac{1}{(m+1)\sin\phi_\nu}\sum_{\mu_1=1}^{m}\mu_1\sin^2\mu_1\phi_\nu\\&\text{For } n\neq\nu\\&\qquad b_{\nu n}=\frac{-1}{(m+1)\sin\phi_\nu}\sum_{\mu_1=1}^{m}\mu_1\sin\mu_1\phi_n\sin\mu_1\phi_\nu\end{aligned}\right\}\quad(A20)$$

Equation (A20) can be simplified by making the indicated summations. With the relation

$$\sum_{\mu_1=1}^{m}\mu_1\cos\mu_1 x=\text{real part of}\left(\sum_{\mu_1=1}^{m}\mu_1 e^{i\mu_1 x}\right)$$

$$=\frac{1+m\cos(m+1)x-(m+1)\cos mx}{2(-1+\cos x)}\quad(A21)$$

then for $n=\nu$

$$b_{\nu\nu}=\frac{m+1}{4\sin\phi_\nu}$$

and for $n\neq\nu$

$$b_{\nu n}=\frac{\sin\phi_n}{(\cos\phi_n-\cos\phi_\nu)^2}\frac{1-(-1)^{n-\nu}}{2(m+1)}\quad(A22)$$

The integration of the second integral of equation (A12) is done by a method similar to that used for the first integral. The integral of the product of the $L(\phi_\nu,\phi)$ function and the terms of the trigonometric series of $G'(\phi)$ is too difficult for direct integration but can be done with the aid of the integration formula. This integration can be made for an arbitrary number of points M which can differ from m.

Using a trapezoidal integration formula for the trigonometric variable gives

$$\int_0^\pi f(\phi)d\phi=\frac{\pi}{M+1}\left[\frac{f(\phi_0)+f(\phi_{M+1})}{2}+\sum_{\mu=1}^{M}f(\phi_\mu)\right]\quad(A23)$$

where $\phi_\mu=\frac{\mu\pi}{M+1}$. With the definition

$$f_n(\phi)=\frac{2}{m+1}\sum_{\mu_1=1}^{m}\mu_1\sin\mu_1\phi_n\cos\mu_1\phi\quad(A24)$$

equation (A18) can be written in shortened form as

$$G'(\phi)=\sum_{n=1}^{m}G_n f_n(\phi)\quad(A25)$$

Applying the integration formulas of equations (A23) and (A25) to the second integral of equation (A12) gives

$$\frac{-b/c_\nu}{2\pi}\int_0^\pi L(\phi_\nu,\phi)G'(\phi)d\phi=\sum_{n=1}^{m}\left(-\frac{b/c_\nu}{2\pi}\right)\int_0^\pi L(\phi_\nu,\phi)G_n f_n(\phi)d\phi$$

$$=\frac{b}{c_\nu}\sum_{n=1}^{m}G_n\left\{\frac{-1}{2(M+1)}\left[\frac{L(\phi_\nu,\phi_0)f_n(\phi_0)+L(\phi_\nu,\phi_{M+1})f_n(\phi_{M+1})}{2}+\sum_{\mu=1}^{M}L(\phi_\nu,\phi_\mu)f_n(\phi_\mu)\right]\right\}\quad(A26)$$

Equation (A26) can be simplified as follows: Let $f_{n\mu}=f_n(\phi_\mu)$ where $f_n(\phi_\mu)$ is given by equation (A24) for $\phi=\phi_\mu=\frac{\mu\pi}{M+1}$ and let $L_{\nu\mu}=L(\phi_\nu,\phi_\mu)$.

Then define

$$g_{\nu n}=-\frac{1}{2(M+1)}\left(\frac{L_{\nu 0}f_{n0}+L_{\nu,M+1}f_{n,M+1}}{2}+\sum_{\mu=1}^{M}L_{\nu\mu}f_{n\mu}\right)\quad(A27)$$

Then equation (A26) can be written

$$-\frac{b/c_\nu}{2\pi}\int_0^\pi L(\phi_\nu,\phi)G'(\phi)d\phi=\frac{b}{c_\nu}\sum_{n=1}^{m}g_{\nu n}G_n\quad(A28)$$

Equation (A12) can now be put in a form which allows solution by simultaneous equations by substituting in it the equalities given by equations (A19) and (A28). Making this substitution equation (A12) becomes

$$\left(\frac{w}{V}\right)_\nu=2b_{\nu\nu}G_\nu-\sum_{n=1}^{m}{}'2b_{\nu n}G_n+\frac{b}{c_\nu}\sum_{n=1}^{m}g_{\nu n}G_n$$

$$=\left(2b_{\nu\nu}+\frac{b}{c_\nu}g_{\nu\nu}\right)G_\nu-\sum_{n=1}^{m}{}'\left(2b_{\nu n}-\frac{b}{c_\nu}g_{\nu n}\right)G_n,$$

$$\nu=1,2,3,\ldots m\quad(A29)$$

where the prime on the summation sign indicates that the value for $n=\nu$ should not be summed.

Summarizing the development for the computation of spanwise loading over the whole wing span, the loading at m span stations is found from the simultaneous solution of m equations,

$$\alpha_\nu=\sum_{n=1}^{m}A_{\nu n}G_n$$

$$\nu=1,2,3,\ldots m\quad(A30)$$

where

$$\alpha_\nu=\left(\frac{w}{V}\right)_\nu=\text{angle of attack at span station }\nu$$

$$A_{\nu n}=2b_{\nu\nu}+\frac{b}{c_\nu}g_{\nu\nu}\text{ for }n=\nu$$

$$=-2b_{\nu n}+\frac{b}{c_\nu}g_{\nu n}\text{ for }n\neq\nu$$

$b_{\nu\nu}$ and $b_{\nu n}$ are from equation (A22)

$g_{\nu\nu}=g_{\nu n}$ for $n=\nu$

$g_{\nu n}$ is from equation (A27)

$$\frac{b}{c_\nu}=\frac{\text{wing span}}{\text{chord at span station }\nu}$$

$L_{\nu\mu}$ is obtained from equation (A10) for the swept wing, and from equation (A11) for the unswept wing, with $\eta=\cos\frac{\nu\pi}{m+1}$ and $\bar{\eta}=\cos\frac{\mu\pi}{M+1}$ and where $f_{n\mu}$ is from equation (A24) with $\phi=\phi_\mu=\frac{\mu\pi}{M+1}$.

Symmetric load distribution.—The computations for the symmetrically loaded wing can be considerably reduced by altering the preceding equations and coefficients. For a symmetrically loaded wing the distribution of local angle of attack is symmetrical about the plane of symmetry, then

$$\left.\begin{aligned}\alpha_\nu&=\alpha_{m+1-\nu}\\ G_\nu&=G_{m+1-\nu}\end{aligned}\right\} \tag{A31}$$

With symmetric loading, only the odd values of μ_1 in equation (A13) contribute to the loading, then equation (A24) becomes

$$f_{n\mu}=\frac{2}{m+1}\sum_{\mu_1=1,3,5\ldots\text{odd}}^{m}\mu_1\sin\mu_1\phi_n\cos\mu_1\phi_\mu \tag{A32}$$

Since the change of symmetric loading distribution with span is opposite in sign from one side of the span to the other, then

$$f_{n\mu}=f_{n,M+1-\mu},\text{ and }f_{n,\frac{M+1}{2}}=0$$

Furthermore, examination of equation (A32) indicates that

$$f_{n\mu}=f_{m+1-n,\mu}$$

Then for symmetric loading equation (A27) becomes

$$\bar{g}_{\nu n}=\frac{-1}{2(M+1)}\sum_{\mu=0}^{\frac{M-1}{2}}\bar{f}_{n\mu}(L_{\nu\mu}-L_{\nu,M+1-\mu}) \tag{A33}$$

where

$$n=1\ \ldots\ \frac{m+1}{2}$$

$$\left.\begin{aligned}\bar{f}_{n\mu}&=2f_{n\mu}\text{ for }n\neq\frac{m+1}{2}\\ &=f_{n\mu}\text{ for }n=\frac{m+1}{2}\\ &=f_{n\mu}\text{ for }n\neq\frac{m+1}{2}\text{ and }\mu=0\\ &=\frac{f_{n\mu}}{2}\text{ for }n=\frac{m+1}{2}\text{ and }\mu=0\end{aligned}\right\} \tag{A34}$$

Equation (A32) gives the values of $f_{n\mu}$.

For symmetric loading, with the relations given by equation (A31), equation (A29) becomes

$$\left(\frac{w}{V}\right)_\nu=\left(2b_{\nu\nu}+\frac{b}{c_\nu}\bar{g}_{\nu\nu}\right)G_\nu-\sum_{n=1}^{\frac{m+1}{2}}{}'\left(2B_{\nu n}-\frac{b}{c_\nu}\bar{g}_{\nu n}\right)G_n,$$

$$\nu=1,2,3,\ \ldots\ \frac{m+1}{2} \tag{A35}$$

(The prime on the summation sign indicates that the value for $n=\nu$ is not summed.)

where

$$\begin{aligned}B_{\nu n}&=b_{\nu n}+b_{\nu,m+1-n}\text{ for }n\neq\frac{m+1}{2}\\ &=b_{\nu n}\qquad\text{for }n=\frac{m+1}{2}\end{aligned}$$

It should be noted that the equation for $L_{\nu n}$ simplifies somewhat for the symmetrically loaded wing since, for symmetric loading, it is necessary to consider only positive values of η. Further, equation (A10) can be written using only positive values of $\bar{\eta}$ through the following relation:

$$L^*_{\nu\mu}=L(\eta,\bar{\eta})-L(\eta,-\bar{\eta})=L_{\nu\mu}-L_{\nu,M+1-\mu}$$

In summary, the foregoing analysis for the case of the symmetrically loaded wing gives

$$\alpha_\nu=\sum_{n=1}^{\frac{m+1}{2}}a_{\nu n}G_n$$

$$\nu=1,2,3,\ldots\frac{m+1}{2} \tag{A36}$$

where

$$\left.\begin{aligned}a_{\nu n}&=2b_{\nu\nu}+\frac{b}{c_\nu}\bar{g}_{\nu\nu}\text{ for }n=\nu\\ &=-2B_{\nu\mu}+\frac{b}{c_\nu}\bar{g}_{\nu n}\text{ for }n\neq\nu\end{aligned}\right\} \tag{A37}$$

$$\bar{g}_{\nu\nu}=\bar{g}_{\nu n}\text{ for }n=\nu$$

$$\bar{g}_{\nu n}=\frac{-1}{2(M+1)}\sum_{\mu=0}^{\frac{M-1}{2}}\bar{f}_{n\mu}L^*_{\nu\mu}$$

$$\bar{f}_{n\mu}=2f_{n\mu}\text{ for }n\neq\frac{m+1}{2},\ \mu\neq0$$

$$=f_{n\mu}\text{ for }n=\frac{m+1}{2},\ \mu\neq0$$

$$=f_{n\mu}\text{ for }n\neq\frac{m+1}{2},\ \mu=0$$

$$=\frac{f_{n\mu}}{2}\text{ for }n=\frac{m+1}{2},\ \mu=0$$

$$f_{n\mu}=\frac{2}{m+1}\sum_{\mu_1=1,3,5\ldots\text{odd}}^{m}\mu_1\sin\mu_1\phi_n\cos\mu_1\phi_\mu$$

$$b_{\nu\nu}=\frac{m+1}{4\sin\phi_\nu}$$

$$B_{\nu n}=b_{\nu n}+b_{\nu,m+1-n}\text{ for }n\neq\frac{m+1}{2}$$

$$=b_{\nu n}\text{ for }n=\frac{m+1}{2}$$

$$b_{\nu n}=\frac{\sin\phi_n}{(\cos\phi_n-\cos\phi_\nu)^2}\left[\frac{1-(-1)^{n-\nu}}{2(m+1)}\right]$$

$$L^*_{\nu\mu}=\frac{1}{\frac{b}{c_\nu}(\eta_\nu-\bar{\eta}_\mu)}\left\{\sqrt{\left[1+\frac{b}{c_\nu}(\eta_\nu-\bar{\eta}_\mu)\tan\Lambda\right]^2+\left(\frac{b}{c_\nu}\right)^2(\eta_\nu-\bar{\eta}_\mu)^2}-1\right\}-$$

$$\frac{1}{\frac{b}{c_\nu}(\eta_\nu+\bar{\eta}_\mu)}$$

$$\left\{\frac{\sqrt{\left[1+\frac{b}{c_\nu}(\eta_\nu-\bar{\eta}_\mu)\tan\Lambda\right]^2+\left(\frac{b}{c_\nu}\right)^2(\eta_\nu+\bar{\eta}_\mu)^2}}{1+2\frac{b}{c_\nu}\eta_\nu\tan\Lambda}-1\right\}-$$

$$\frac{2\tan\Lambda\sqrt{\left(1+\frac{b}{c_\nu}\eta_\nu\tan\Lambda\right)^2+\left(\frac{b}{c_\nu}\right)^2\eta_\nu^2}}{1+2\frac{b}{c_\nu}\eta_\nu\tan\Lambda}$$

$$\eta_\nu=\cos\frac{\nu\pi}{m+1}$$

$$\bar{\eta}_\mu=\cos\frac{\mu\pi}{M+1}$$

$$\phi_n=\frac{n\pi}{m+1}$$

$$\phi_\nu=\frac{\nu\pi}{m+1}$$

$$\phi_\mu=\frac{\mu\pi}{M+1}$$

DEVELOPMENT OF THE PARAMETERS USED IN THE SIMULTANEOUS SOLUTION FOR SYMMETRIC LOADING

The $\frac{m+1}{2}$ linear simultaneous equations of equation (A36) provide means for the solution for symmetric loading for any given symmetrical distribution of α_ν. The coefficients $a_{\nu n}$, which are $\left(\frac{m+1}{2}\right)^2$ in number, are functions of the wing geometric parameters of sweep angle Λ and the ratio $\frac{b}{c}$. The principal work in a study of spanwise loading is to compute the $a_{\nu n}$ coefficients. For a study of a range of plan forms, these $a_{\nu n}$ coefficients can be plotted as functions of sweep angle and the ratio $\frac{b}{c}$; however, $\frac{b}{c}$ will vary spanwise due to the taper of a wing and plots of $a_{\nu n}$ as a function of $\frac{b}{c}$ become unwieldy for a range of plan forms. A scale factor can be applied to $\frac{b}{c}$ such that the spanwise variation will be effectively nullified for a range of tapered wings.

For a range of aspect ratio, the values of $\frac{b}{c}$ for the outboard half of the wing semispan, $\eta>0.5$, has maximum values for zero tapered wings (provided the plan-form edges are not concave) and for the inboard half of the wing semispan, $\eta<0.5$, $\frac{b}{c}$ has maximum values for the inverse tapered wings. The ratio of $\frac{b}{c}$ in the general case to these maximum values of $\frac{b}{c}$ provides a geometric parameter that varies approximately as the aspect ratio.

The inverse chord distribution for straight-tapered wings is given by

$$\frac{b}{c}=\frac{A(1+\lambda)}{2[1-|\eta|(1-\lambda)]} \tag{A38}$$

For $\lambda=0$

$$\frac{b}{Ac}=\frac{1}{2(1-|\eta|)} \tag{A39}$$

For $\lambda=1.5$

$$\frac{b}{Ac}=\frac{5}{2(2+|\eta|)} \tag{A40}$$

The ratio of $\frac{b}{c}$ to equations (A39) and (A40) gives, respectively, the new geometric parameter as

$$\left.\begin{aligned}\frac{b/c}{\left(\frac{b}{Ac}\right)_{\lambda=0}}&=2(1-\eta)\frac{b}{c}\text{ for }0.5\leq\eta<1\\ \frac{b/c}{\left(\frac{b}{Ac}\right)_{\lambda=1.5}}&=\frac{2(2+\eta)}{5}\frac{b}{c}\text{ for }0\leq\eta\leq0.5\end{aligned}\right\} \tag{A41}$$

Let H be defined as 2/5 times the values of equation (A41). The factor 2/5 is introduced to give H the approximate values of $a_{\nu n}$ to simplify plotting procedures. Then equation (A41) becomes,

$$\left.\begin{aligned}H&=\frac{4(1-\eta)}{5}\frac{b}{c},0.5\leq\eta<1\\ &=\frac{4(2+\eta)}{25}\frac{b}{c},0\leq\eta\leq0.5\end{aligned}\right\} \tag{A42}$$

Introducing the effects of compressibility and section lift-curve slope as discussed in the text, equation (A42) becomes at the span station ν,

$$H_\nu=d_\nu\left(\frac{1}{\kappa_\nu}\right)\left(\frac{b}{c_\nu/\beta}\right) \tag{A43}$$

where d_ν is a scale factor given by

$$d_\nu=\frac{4(1-\eta_\nu)}{5}\text{ for }0.5\leq\eta_\nu<1$$

$$=\frac{4(2+\eta_\nu)}{25}\text{ for }0\leq\eta_\nu\leq0.5$$

For straight-tapered wings, equation (A43) simplifies to

$$\left.\begin{aligned}H_\nu&=\frac{2(1-\eta_\nu)(1+\lambda)}{5[1-\eta_\nu(1-\lambda)]}\left(\frac{1}{\kappa_\nu}\right)\beta A,0.5\leq\eta_\nu<1\\ &=\frac{2(2+\eta_\nu)(1+\lambda)}{25[1-\eta_\nu(1-\lambda)]}\left(\frac{1}{\kappa_\nu}\right)\beta A,0\leq\eta_\nu\leq0.5\end{aligned}\right\} \tag{A44}$$

Plots of $a_{\nu n}$ against H_ν in the range $H_\nu=0$ to 4, will give $a_{\nu n}$ coefficients for wings of any chord distribution with aspect ratios from 0 to 10 or 12.

AERODYNAMIC CHARACTERISTICS FROM INTEGRATED SPANWISE LOADING

Lift coefficient.—The wing lift coefficient is given by

$$C_L=A\int_{-1}^{+1}G(\bar{\eta})d\bar{\eta}=A\int_0^{\pi}G(\phi)\sin\phi d\phi$$

or using the quadrature formula of equation (A15),

$$C_L=\frac{\pi A}{m+1}\sum_{n=1}^{m}G_n\sin\phi_n \tag{A45}$$

For symmetric loading equation (A45) simplifies to

$$C_L=\frac{\pi A}{m+1}\left(G_{\frac{m+1}{2}}+2\sum_{n=1}^{\frac{m-1}{2}}G_n\sin\phi_n\right) \tag{A46}$$

Induced drag.—The induced drag is given by

$$C_{D_i}=A\int_{-1}^{1}G(\bar{\eta})\alpha_i(\bar{\eta})d\bar{\eta}=A\int_0^{\pi}G(\phi)\alpha_i(\phi)\sin\phi d\phi$$

or using the quadrature formula of equation (A15),

$$C_{D_i}=\frac{\pi A}{m+1}\sum_{\nu=1}^{m}G_\nu\alpha_{i_\nu}\sin\phi_\nu \tag{A47}$$

For the straight wing, α_i is the induced angle at the one-quarter-chord load vortex and the local-induced-drag distribution can be found. For the swept load vortex with the break at midspan it is not apparent how the correct induced angle at the load vortex can be found to determine local induced drag; however, the total induced drag of the wing can be found by considering the downwash in the wake of the wing.

With the use of Munk's stagger theorem (reference 16) the wing induced drag is given by considering the induced angle as one-half the value of the downwash at an infinite distance downstream. Then $\alpha_i(\phi)$ is given by one-half the value of equation (A19). Equation (A47) becomes

$$C_{D_i}=\frac{\pi A}{m+1}\sum_{\nu=1}^{m}G_\nu\left(b_{\nu\nu}G_\nu-\sum_{n=1}^{m}{}'\,b_{\nu n}G_n\right)\sin\phi_\nu \tag{A48}$$

For symmetrically loaded wings, equation (A48) reduces to

$$C_{D_i}=\frac{\pi A}{m+1}\left[G_{\frac{m+1}{2}}\left(b_{\frac{m+1}{2},\frac{m+1}{2}}G_{\frac{m+1}{2}}-\sum_{n=1}^{\frac{m+1}{2}}{}'\,B_{\frac{m+1}{2},n}G_n\right)+2\sum_{\nu=1}^{\frac{m-1}{2}}G_\nu\left(b_{\nu\nu}G_\nu-\sum_{n=1}^{\frac{m+1}{2}}{}'\,B_{\nu n}G_n\right)\sin\phi_\nu\right] \tag{A49}$$

where $\frac{m+1}{2}$ are subscripts, and the prime on the summation sign indicates that the value for $n=\nu$ is not summed.

INTERPOLATION FUNCTION FOR SPANWISE LOADING

The simultaneous solutions of the linear equations given by equation (A36) give the spanwise loading at $\frac{m+1}{2}$ wing semispan stations. The spanwise loading function is given by equation (A17) in terms of the known loading at $\frac{m+1}{2}$ points. An interpolation function can be determined to give values of loading between the known values and facilitate plotting of spanwise loading distribution.

The spanwise loading given by equation (A13) and the a_{μ_1} coefficients given by equation (A16) can be arranged into the form

$$\begin{aligned}G(\phi)=\frac{2}{m+1}\,[&(\sin\phi_1\sin\phi+\sin 2\phi_1\sin 2\phi+\ \ldots\ +\sin m\phi_1\sin m\phi)G_1+\\&(\sin\phi_2\sin\phi+\sin 2\phi_2\sin 2\phi+\ \ldots\ +\sin m\phi_2\sin m\phi)G_2+\\&\vdots\qquad\qquad\vdots\qquad\qquad\qquad\vdots\\&(\sin\phi_m\sin\phi+\sin 2\phi_m\sin 2\phi+\ \ldots\ +\sin m\phi_m\sin m\phi)G_m]\end{aligned} \tag{A50}$$

The values within the brackets can be tabulated for a given ϕ and the loading at ϕ will be the sum of the products of the tabulated constants and the known values of G_n.

For symmetric loading where only odd values of μ_1 are needed equation (A50) becomes with $m=7$

$$\begin{aligned}G(\phi)=\frac{1}{2}\,&(0.383\sin\phi+0.924\sin 3\phi+0.924\sin 5\phi+\\&0.383\sin 7\phi)G_1+\frac{1}{2}\,(0.707\sin\phi+0.707\sin 3\phi-\\&0.707\sin 5\phi-0.707\sin 7\phi)G_2+\frac{1}{2}\,(0.924\sin\phi-\\&0.383\sin 3\phi-0.383\sin 5\phi+0.924\sin 7\phi)G_3+\\&\frac{1}{4}\,(\sin\phi-\sin 3\phi+\sin 5\phi-\sin 7\phi)G_4\end{aligned} \tag{A51}$$

Letting $\phi=\phi_k=\frac{k\pi}{8}$ for $k=\frac{1}{2}, \frac{3}{2}, \frac{5}{2}$, and $\frac{7}{2}$, the factors of G_n of equation (A51) can be tabulated.

The interpolation factor, e_{nk}, with $m=7$ for symmetric loading is shown by the following table:

η	0.981	0.831	0.556	0.195
n \ k	$\frac{1}{2}$	$\frac{3}{2}$	$\frac{5}{2}$	$\frac{7}{2}$
1	0.866	0.490	−0.068	0.023
2	−.375	.768	.513	−.075
3	.278	−.352	.791	.416
4	.128	.150	−.226	.641

For symmetric loading

$$G_k=\sum_{n=1}^{4}e_{nk}G_n \tag{A52}$$

Any type of loading coefficient other than G can be used in equation (A52), such as $\frac{c_l c}{C_L c_{av}}$.

For basic loading ($C_L=0$), equation (A46) gives

$$G_4=-2(0.383\ G_1+0.707\ G_2+0.924\ G_3) \qquad \text{(A53)}$$

With equation (A53), G_4 can be eliminated in equation (A51) and a shortened interpolation table for basic loading obtained.

The interpolation factor, e_{nk}, with $m=7$ for symmetric basic loading is shown by the following table:

η	0.981	0.831	0.556	0.195
n \ k	$\frac{1}{2}$	$\frac{3}{2}$	$\frac{5}{2}$	$\frac{7}{2}$
1	0.963	0.375	0.075	−0.468
2	−.195	.556	.831	−.981
3	.513	−.630	1.207	−.768

For symmetric basic loading

$$G_k=\sum_{n=1}^{3} e_{nk}G_n \qquad \text{(A54)}$$

REFERENCES

1. Weissinger, J.: The Lift Distribution of Swept-Back Wings. NACA TM 1120, 1947.
2. Van Dorn, Nicholas H., and DeYoung, John: A Comparison of Three Theoretical Methods of Calculating Span Load Distribution on Swept Wings. NACA TN 1476, 1947.
3. DeYoung, John: Theoretical Additional Span Loading Characteristics of Wings With Arbitrary Sweep, Aspect Ratio, and Taper Ratio. NACA TN 1491, 1947.
4. Stevens, Victor I.: Theoretical Basic Span Loading Characteristics of Wings With Arbitrary Sweep, Aspect Ratio, and Taper Ratio. NACA TN 1772, 1948.
5. Multhopp, H.: Die Anwendung der Tragflügeltheorie auf Fragen der Flugmechanik. Bericht S2 der Lilienthal—Ges. f. Luftf.-Forschg., Preisausschreiben, 1938–39, pp. 53–64.
6. Margenau, H., and Murphy, G. M.: The Mathematics of Physics and Chemistry, D. Van Nostrand Co., Inc., New York, 1943.
7. Anderson, Raymond F.: Determination of the Characteristics of Tapered Wings. NACA Rep. 572, 1936.
8. Krienes, Klaus: The Elliptic Wing Based on the Potential Theory. NACA TM 971, 1941.
9. Swanson, R. S., and Priddy, E. L.: Lifting-Surface-Theory Values of the Damping in Roll and of the Parameter Used in Estimating Aileron Stick Forces. NACA ARR L5F23, 1945.
10. Jones, R. T.: Properties of Low-Aspect-Ratio Pointed Wings at Speeds Below and Above the Speed of Sound. NACA Rep. 835, 1946.
11. Zimmerman, C. H.: Characteristics of Clark Y Airfoils of Small Aspect Ratios. NACA Rep. 431, 1932.
12. Lange and Wacke: Test Report on Three and Six-Component Measurements on a Series of Tapered Wings of Small Aspect Ratio (Partial report: Triangular Wing). NACA TM 1176, 1948.
13. Shortal, J. A., and Maggin, B.: Effect of Sweepback and Aspect Ratio on Longitudinal Stability Characteristics of Wings at Low Speeds. NACA TN 1093, 1946.
14. Glauert, H.: The Elements of Aerofoil and Airscrew Theory. The MacMillan Co., New York, 1943.
15. Multhopp, H.: Die Berechnung der Auftriebsverteilung von Tragflügeln. Luftf.-Forschg., Bd. 15, 1938.
16. Munk, Max M.: The Minimum Induced Drag of Aerofoils. NACA Rep. 121, 1921.

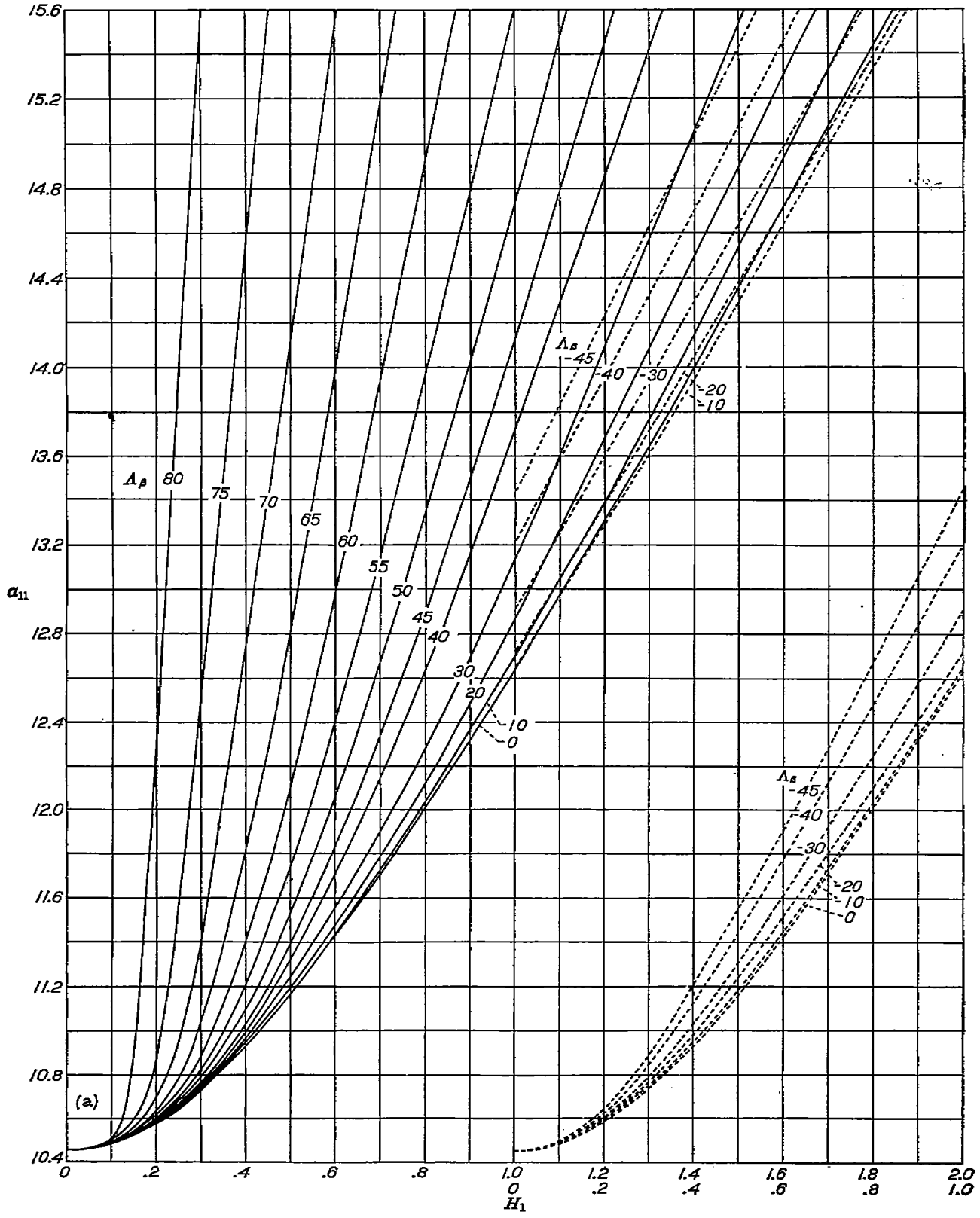

(a) $r=1$, $n=1$, $d_1=0.061$

FIGURE 1.—Influence coefficients, a_{rs}, for symmetric spanwise loading plotted as a function of the wing geometric parameter H_r for values of the compressible sweep parameter A_β, degrees.

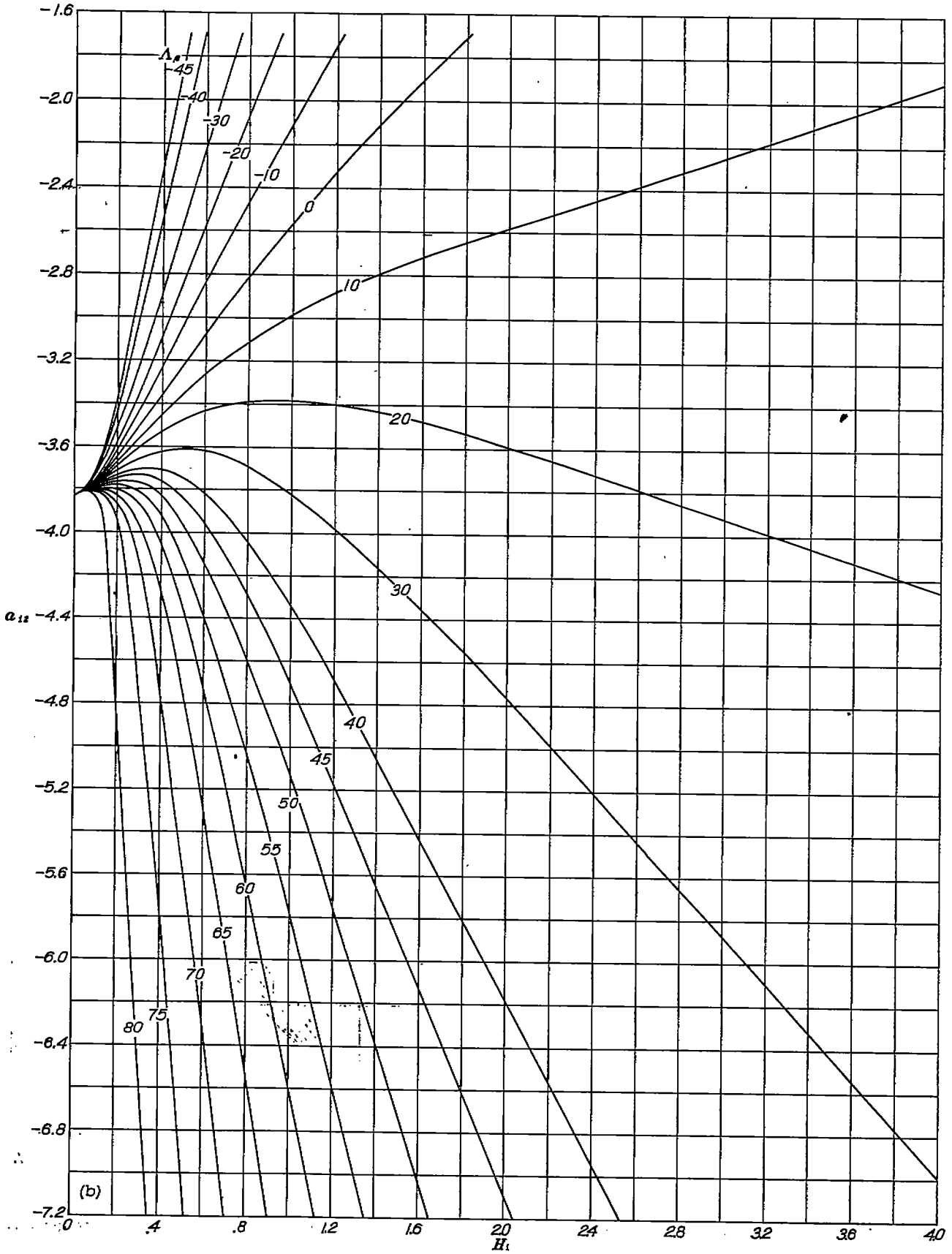

(b) $\nu=1$, $n=2$, $d_1=0.061$.

FIGURE 1.—Continued.

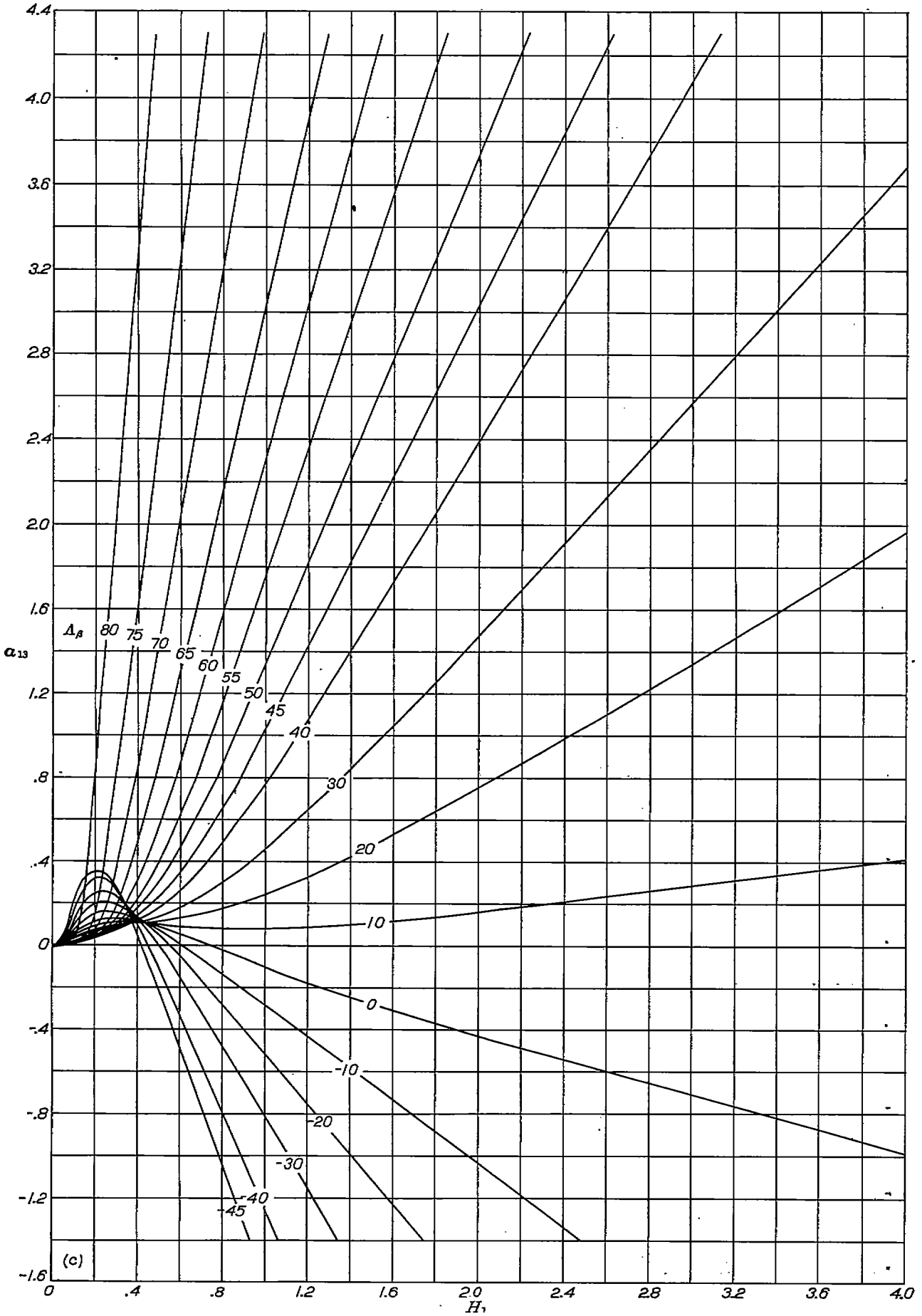

(c) $\nu=1$, $n=3$, $d_1=0.061$.

FIGURE 1.—Continued.

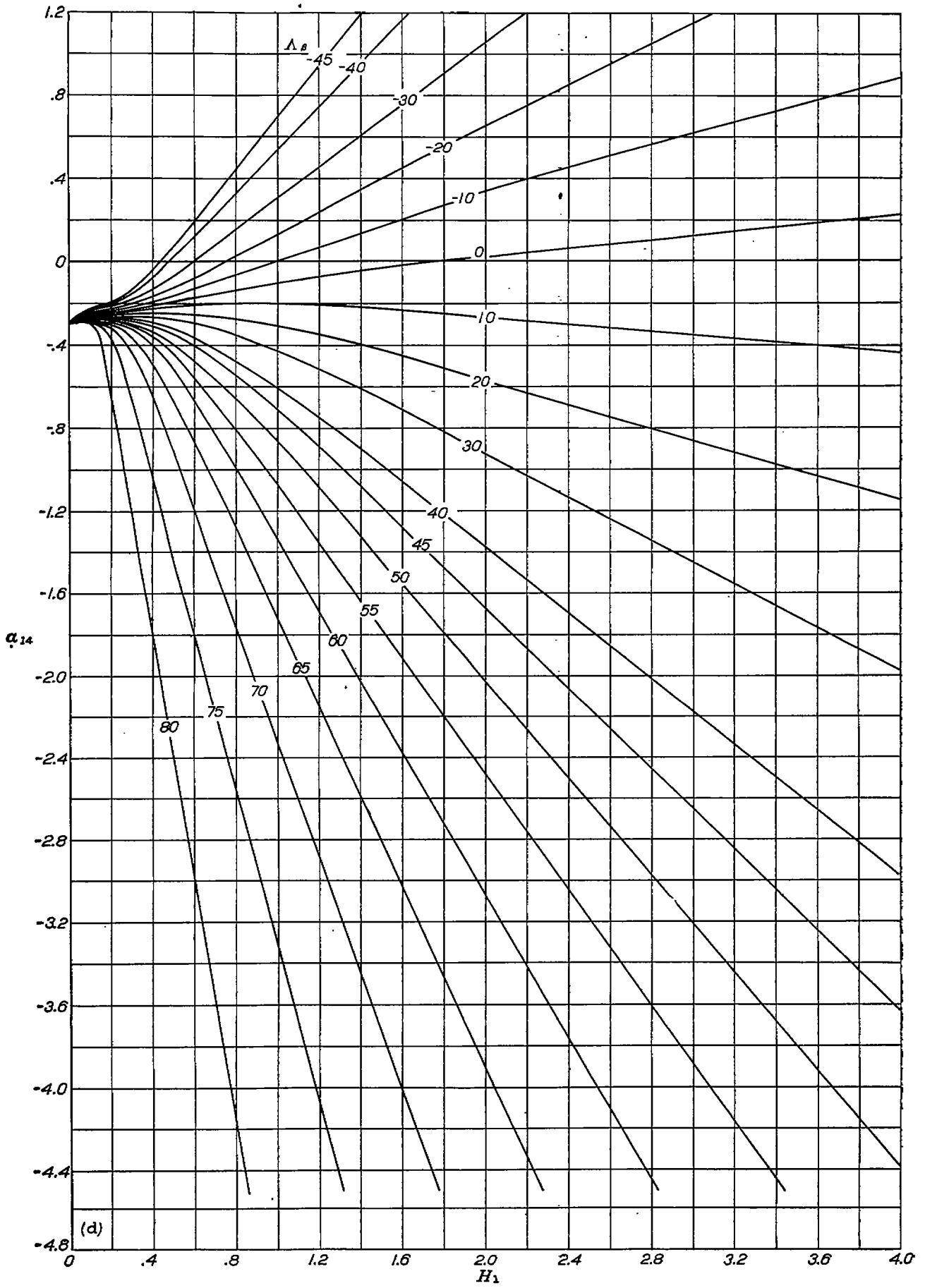

(d) $\nu=1$, $n=4$, $d_1=0.061$.

FIGURE 1.—Continued.

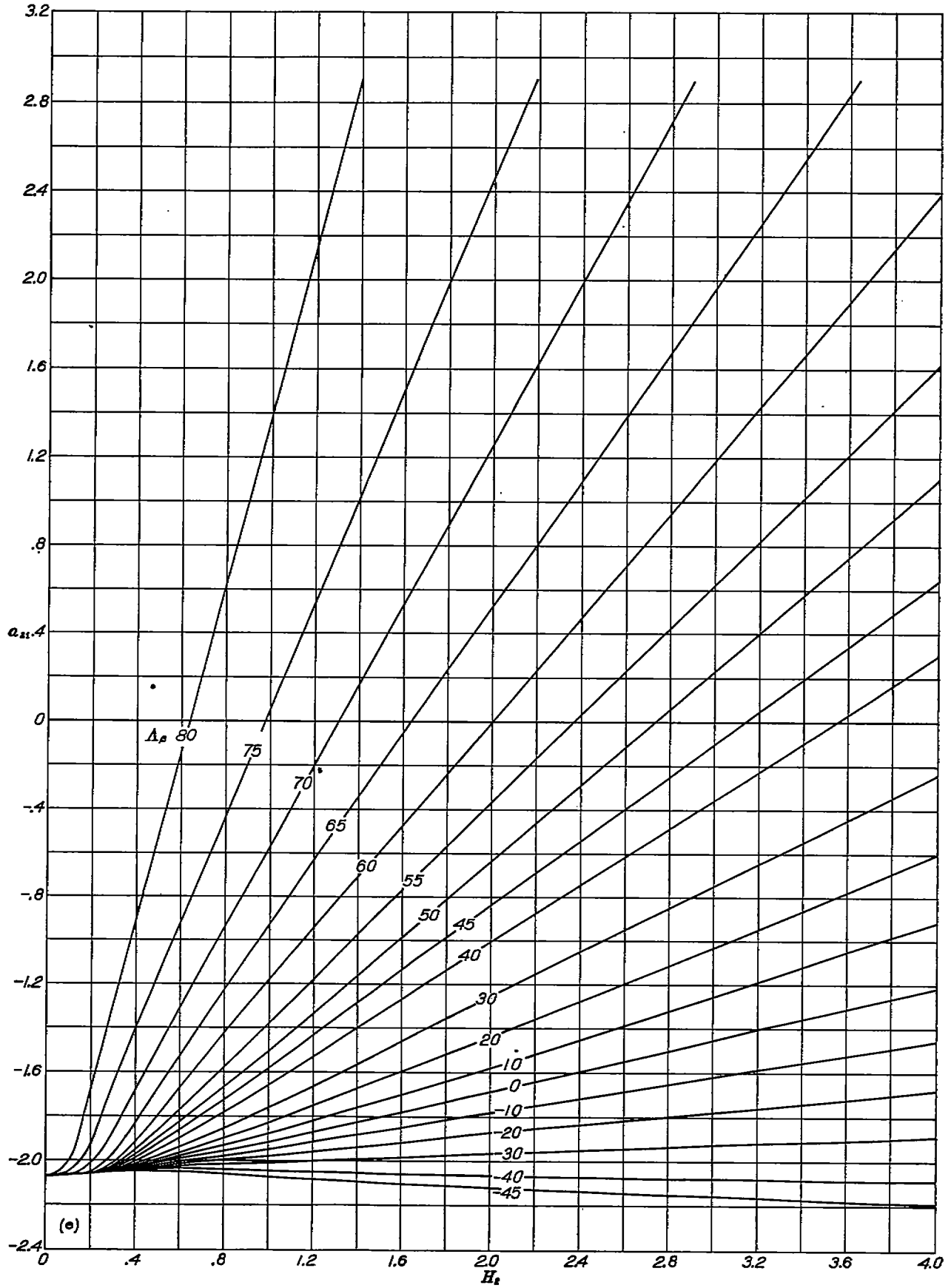

(e) $\nu=2$, $n=1$, $d_1=0.234$.

FIGURE 1.—Continued.

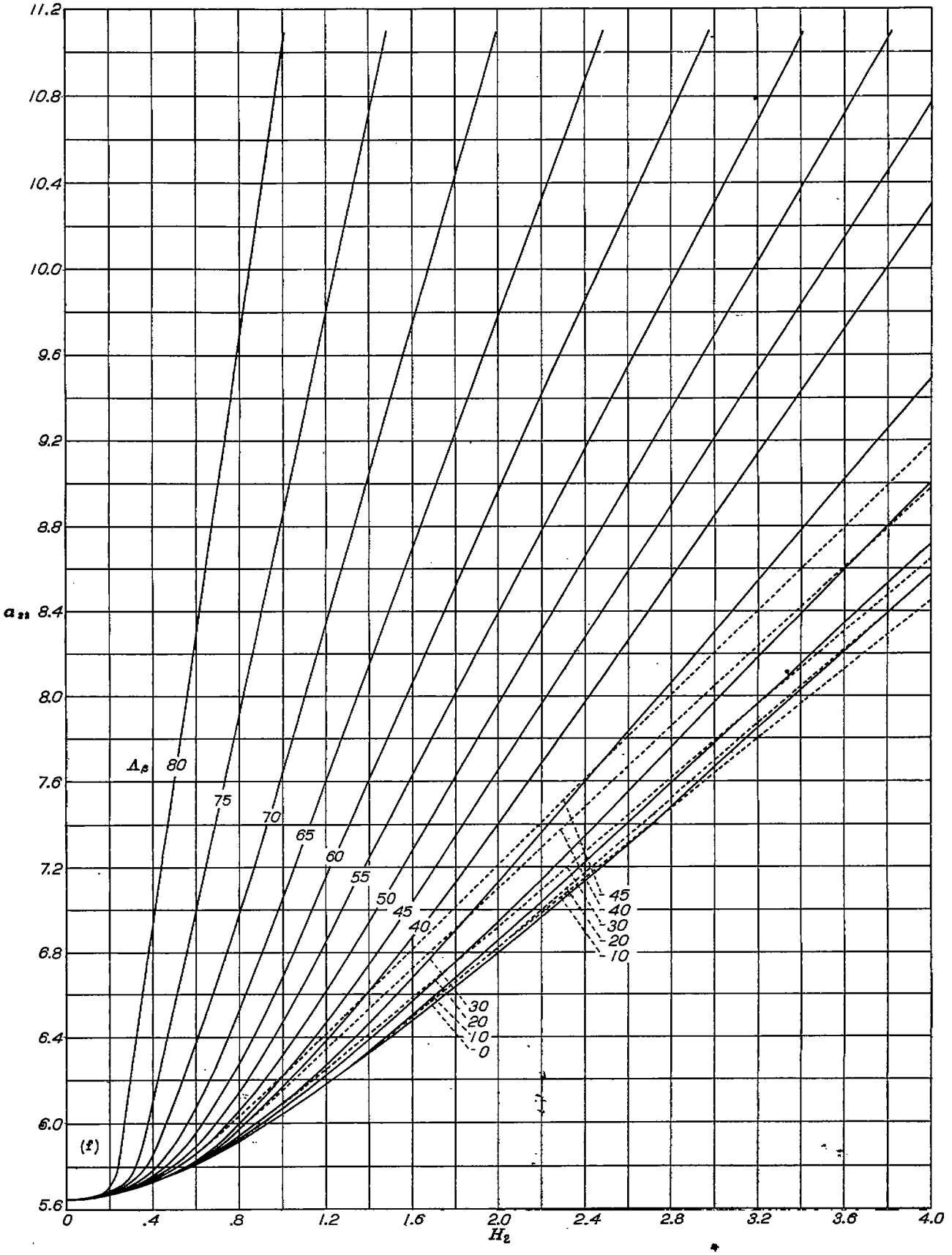

(f) $\nu=2$, $n=2$, $d_1=0.234$.

FIGURE 1.—Continued.

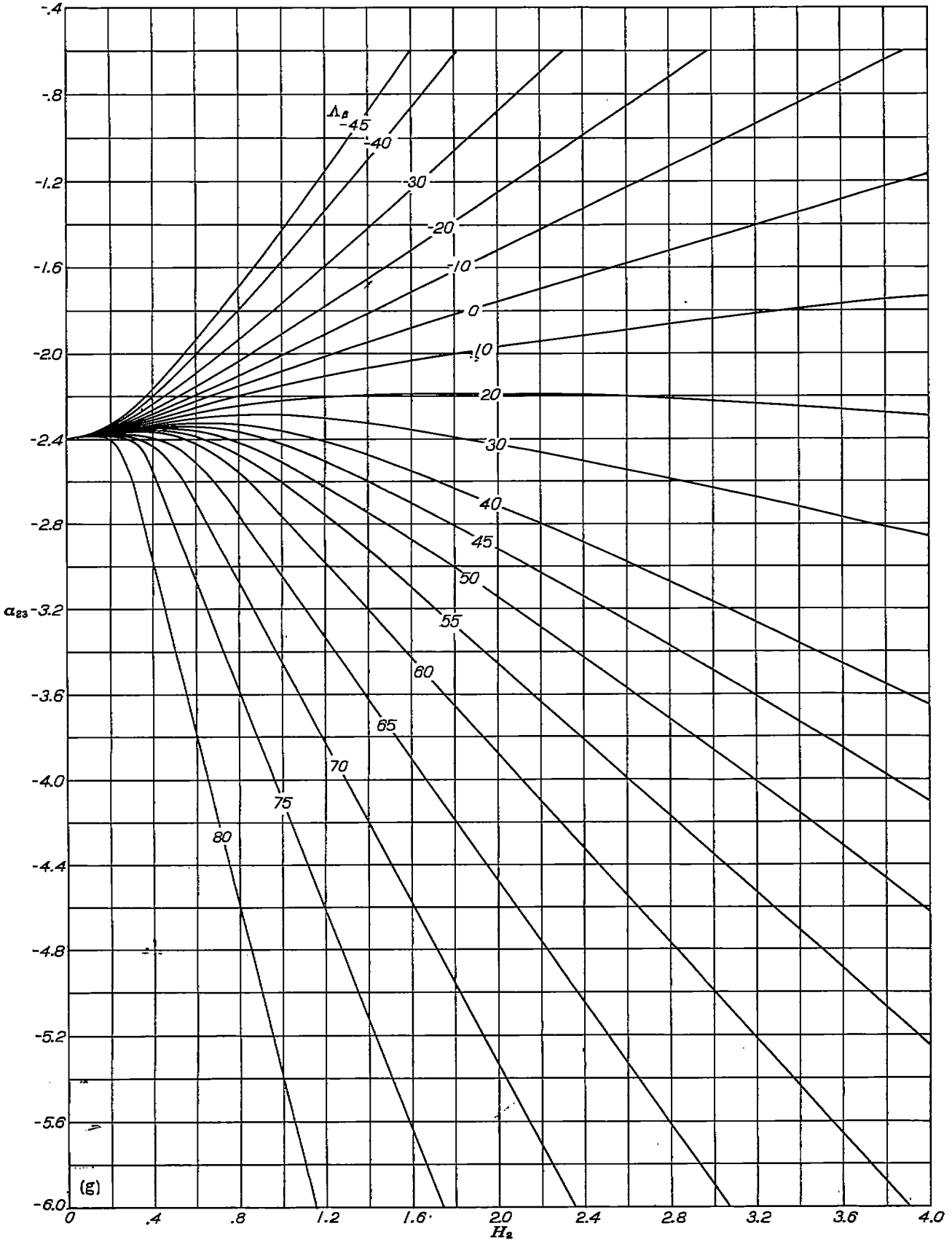

(g) $\nu=2$, $n=3$, $d_1=0.234$.

FIGURE 1.—Continued

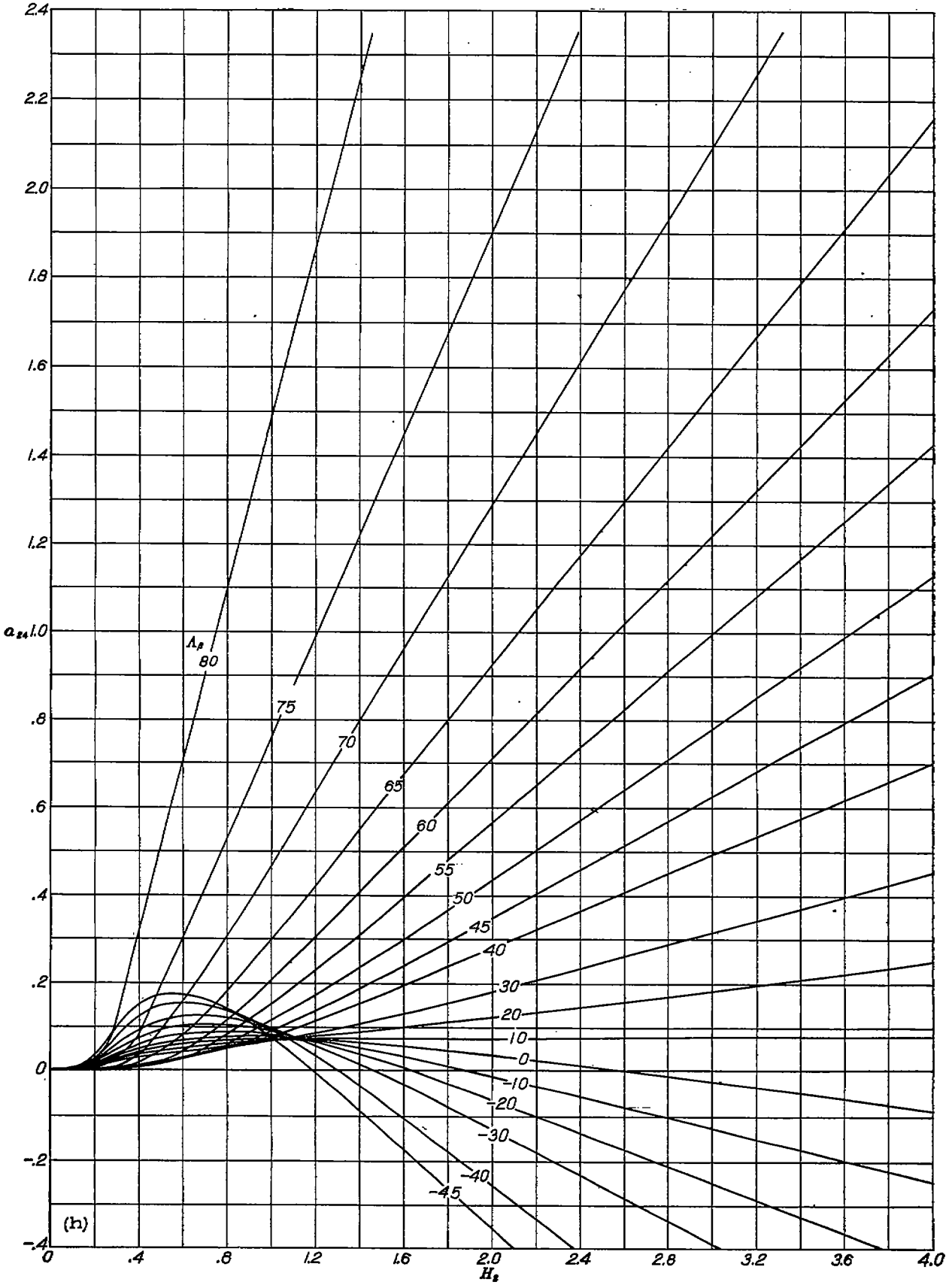

(h) $\nu=2$, $n=4$, $d_1=0.234$.

FIGURE 1.—Continued.

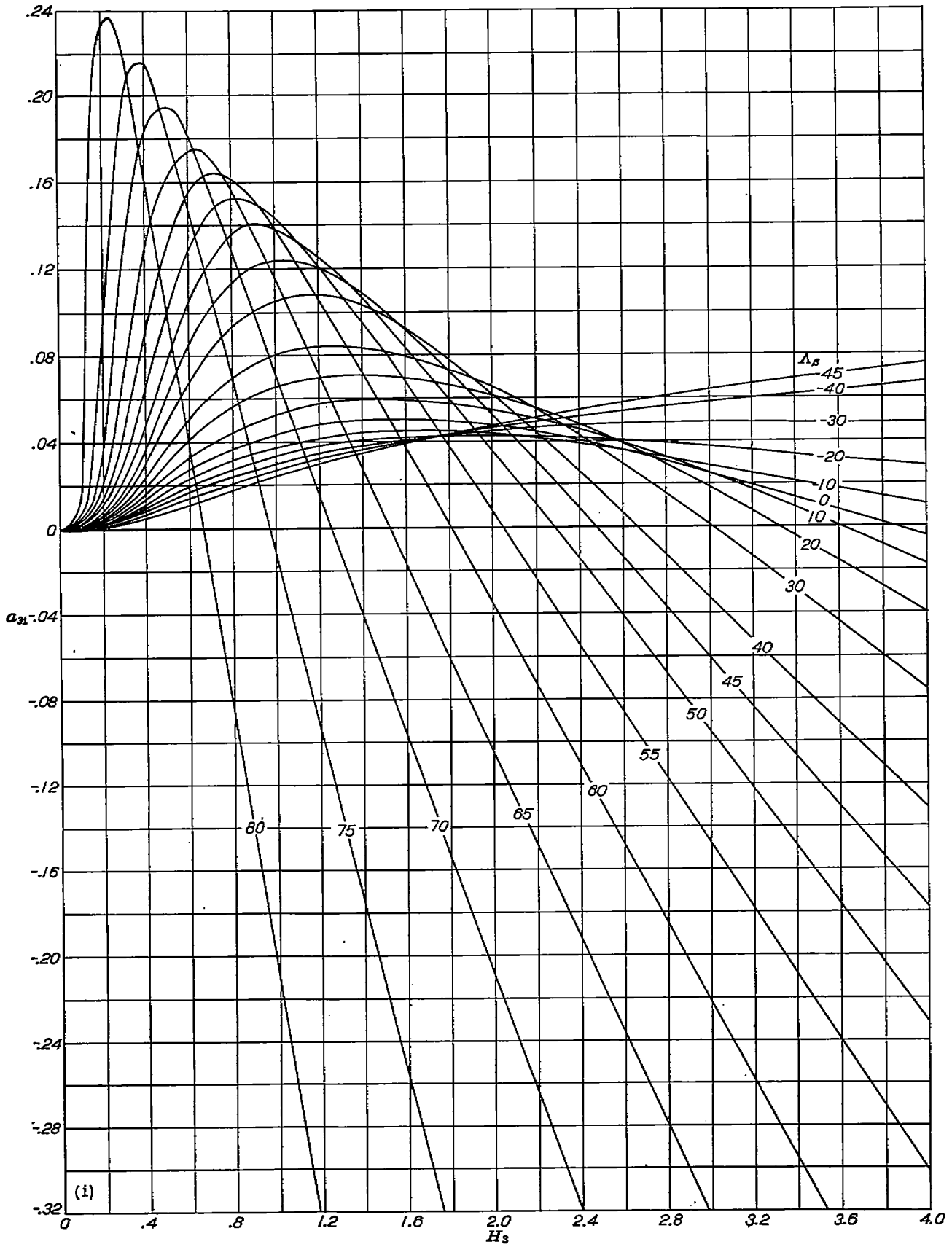

(i) $\nu=3$, $n=1$, $d_4=0.381$.

FIGURE 1.—Continued

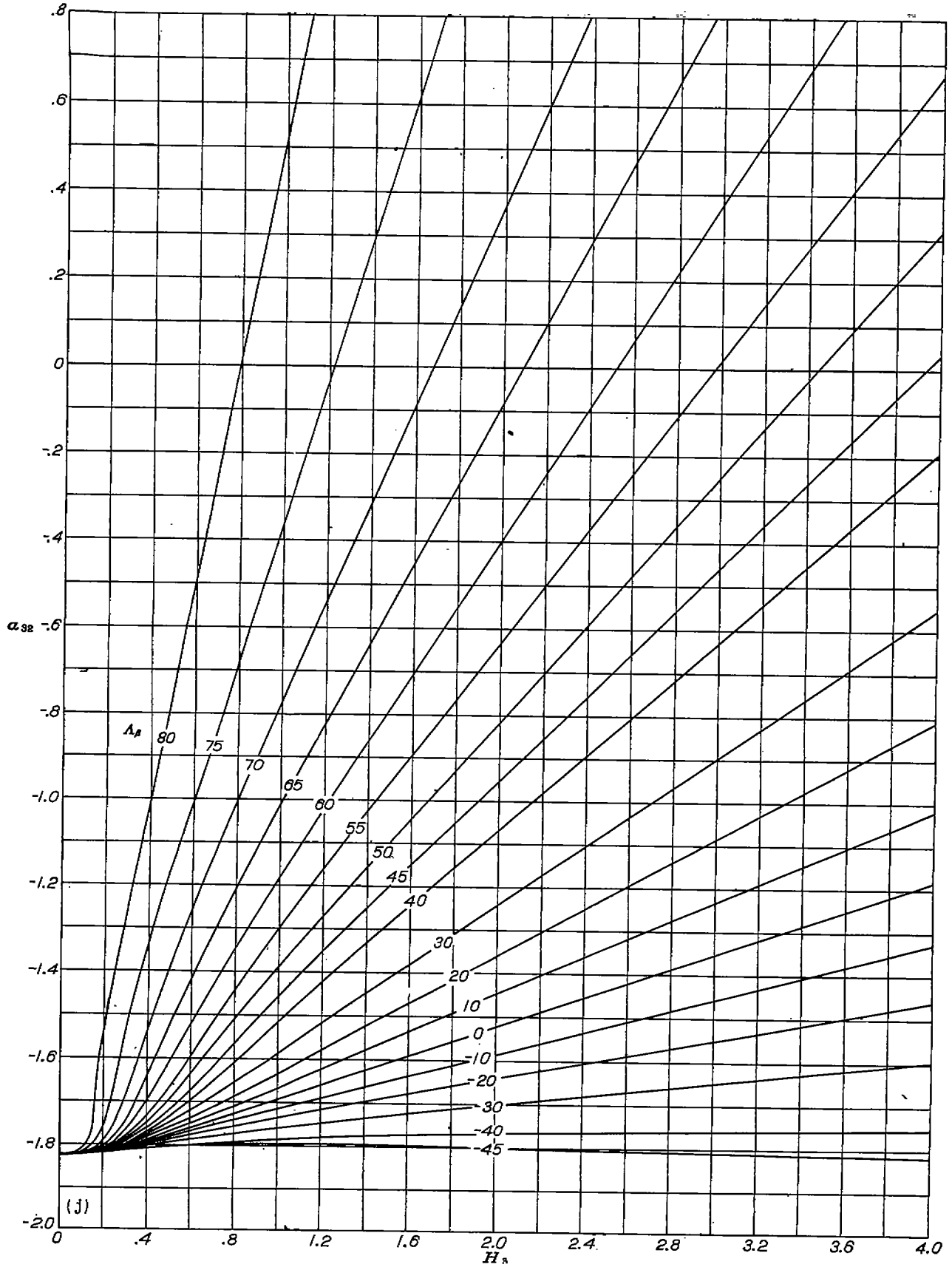

(j) $\nu=8$, $n=2$, $d_1=0.381$.

FIGURE 1.—Continued.

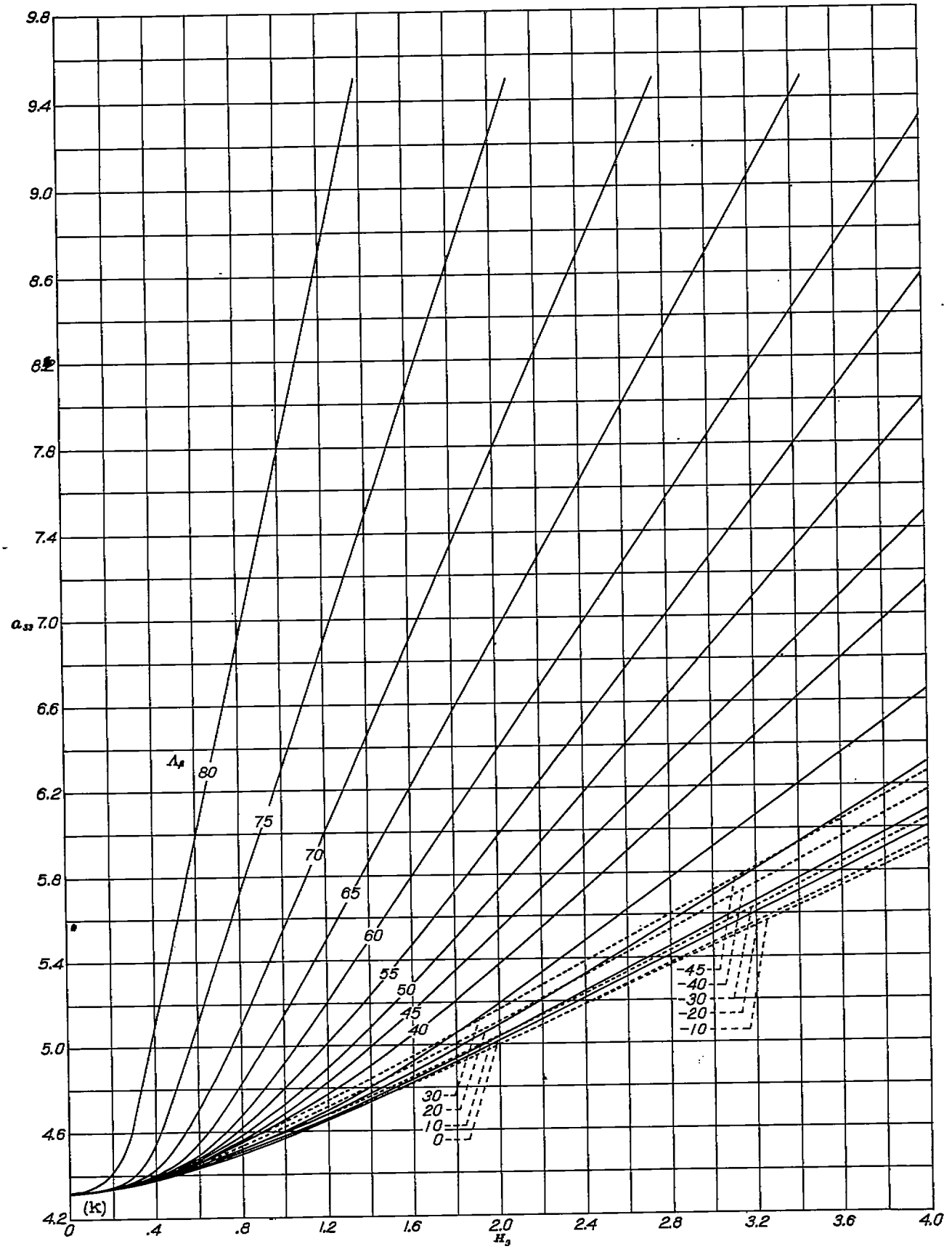

(k) $\nu=3$, $n=3$, $d_3=0.381$.

FIGURE 1.—Continued.

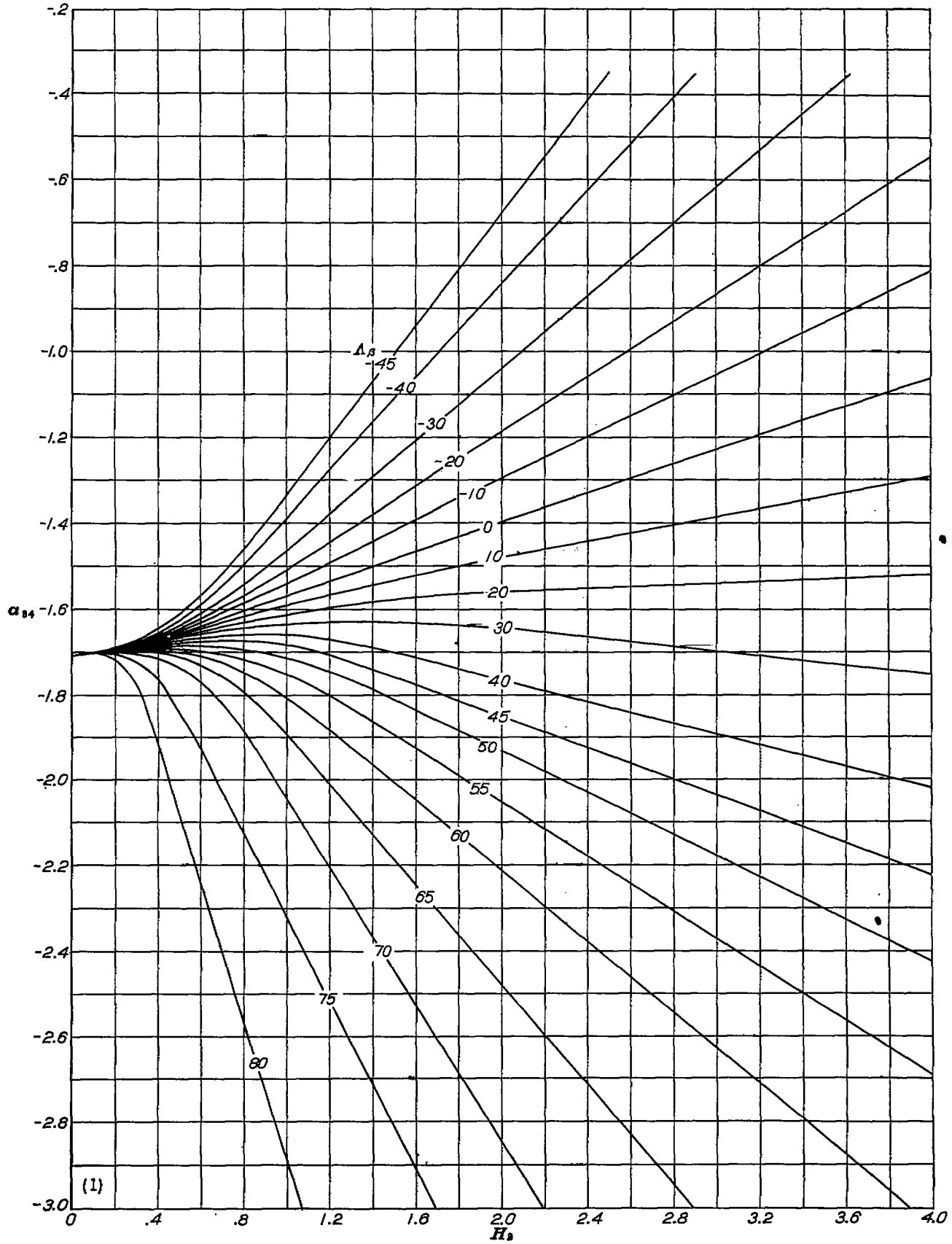

(1) $\nu=3$, $n=4$, $d_1=0.381$.

FIGURE 1.—Continued.

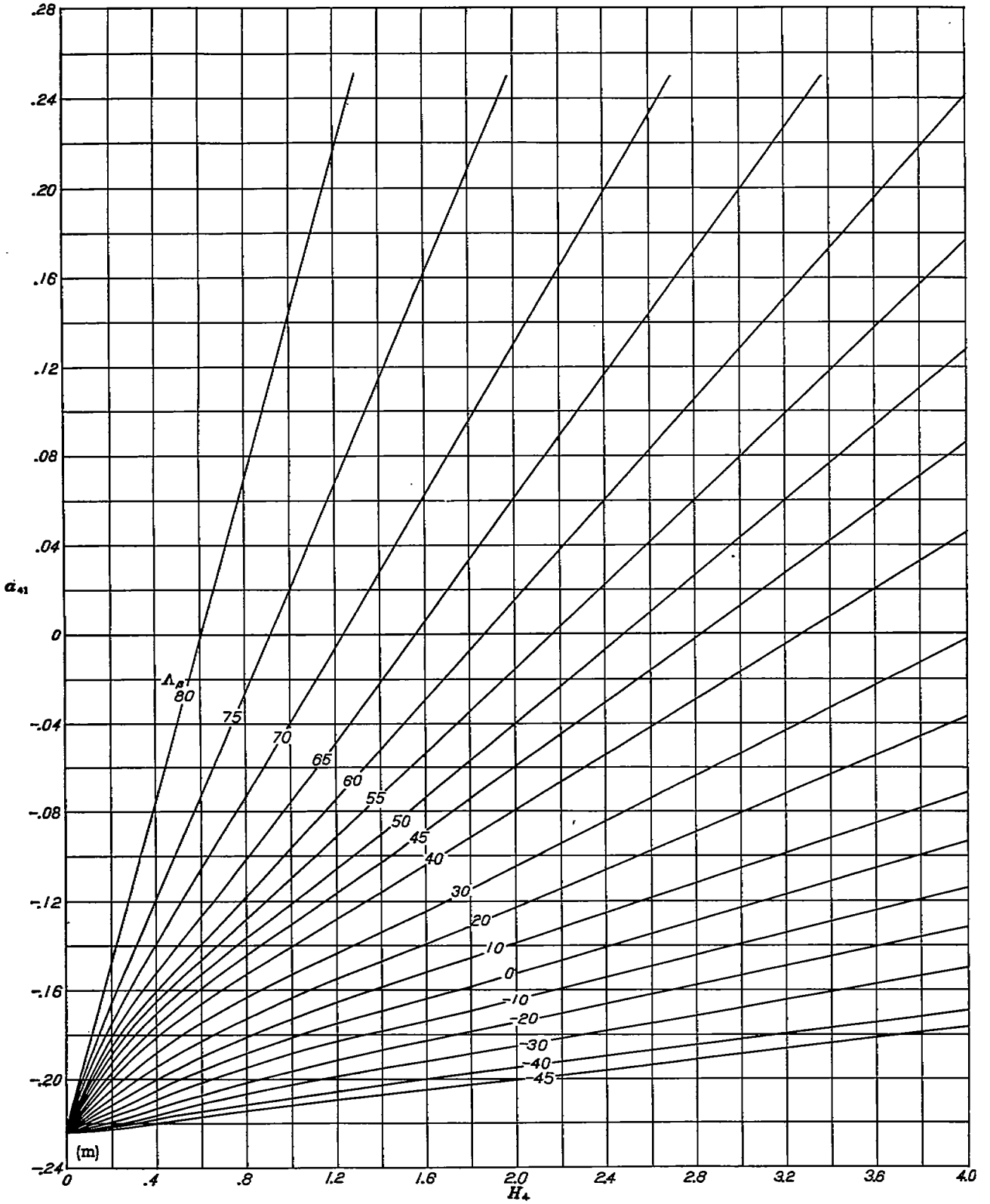

(m) $\nu=4$, $n=1$, $d_1=0.320$.

FIGURE 1.—Continued.

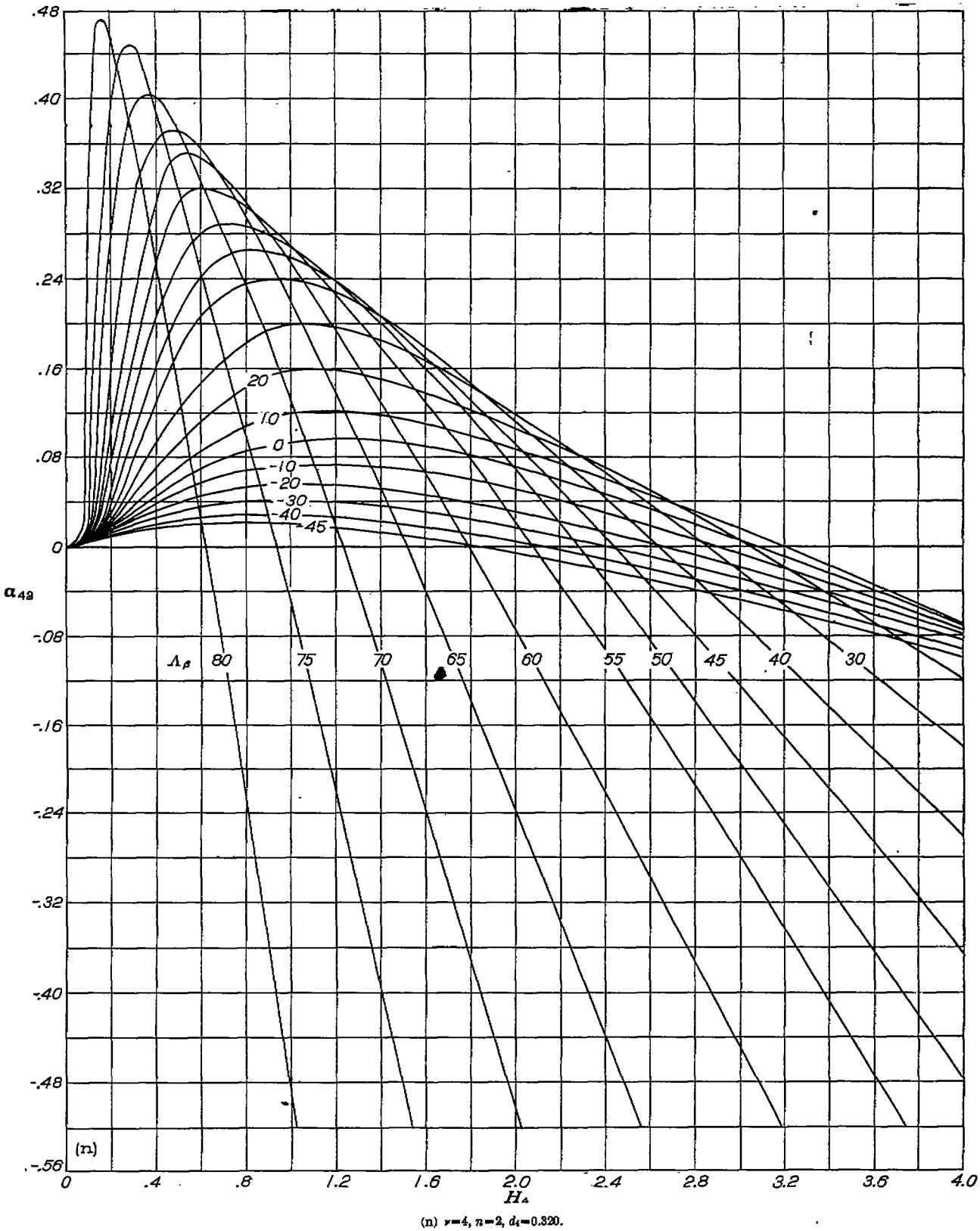

(n) $\nu=4$, $n=2$, $d_4=0.320$.

FIGURE 1.—Continued.

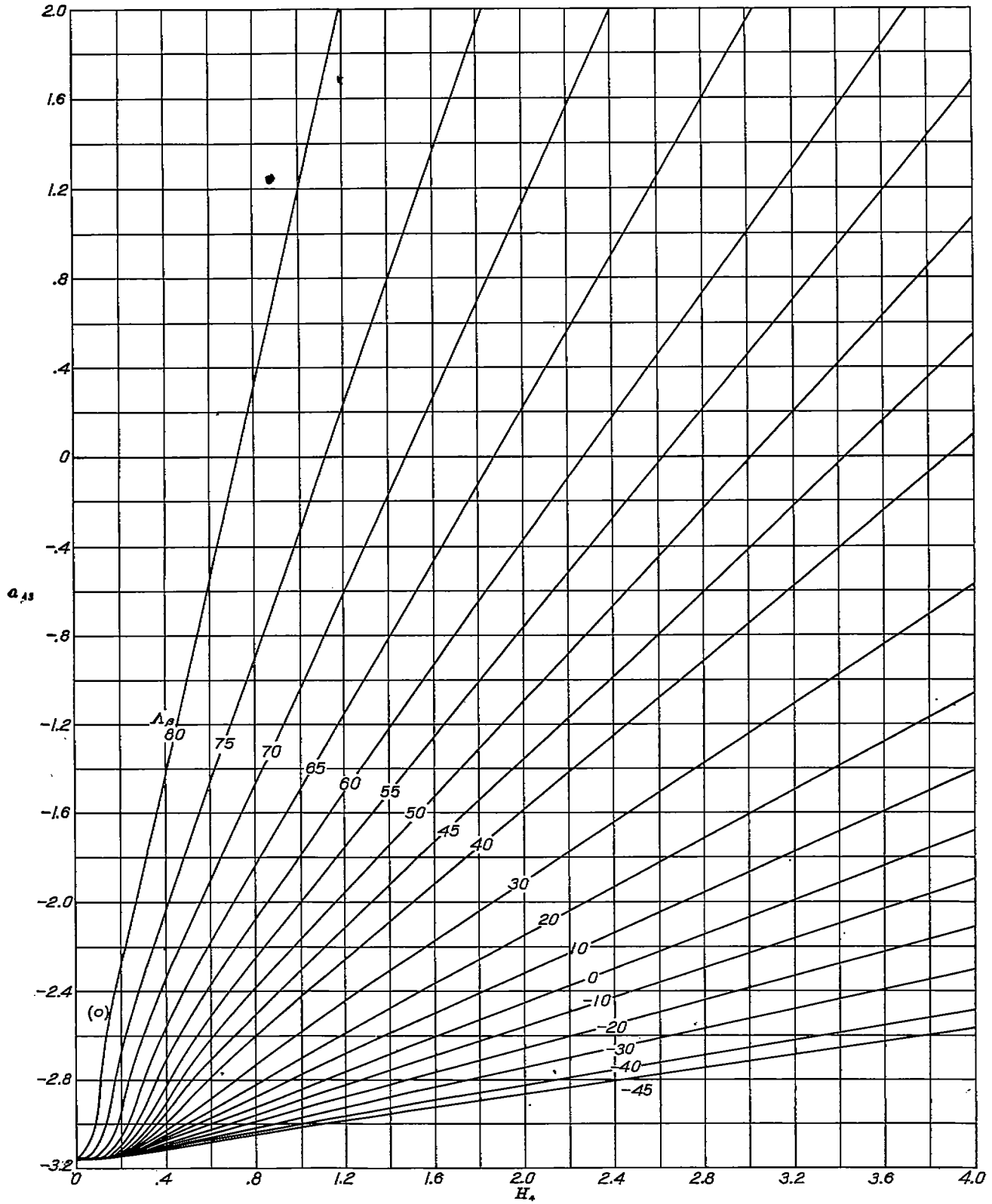

(o) $r=4$, $n=3$, $d_1=0.320$.

FIGURE 1.—Continued.

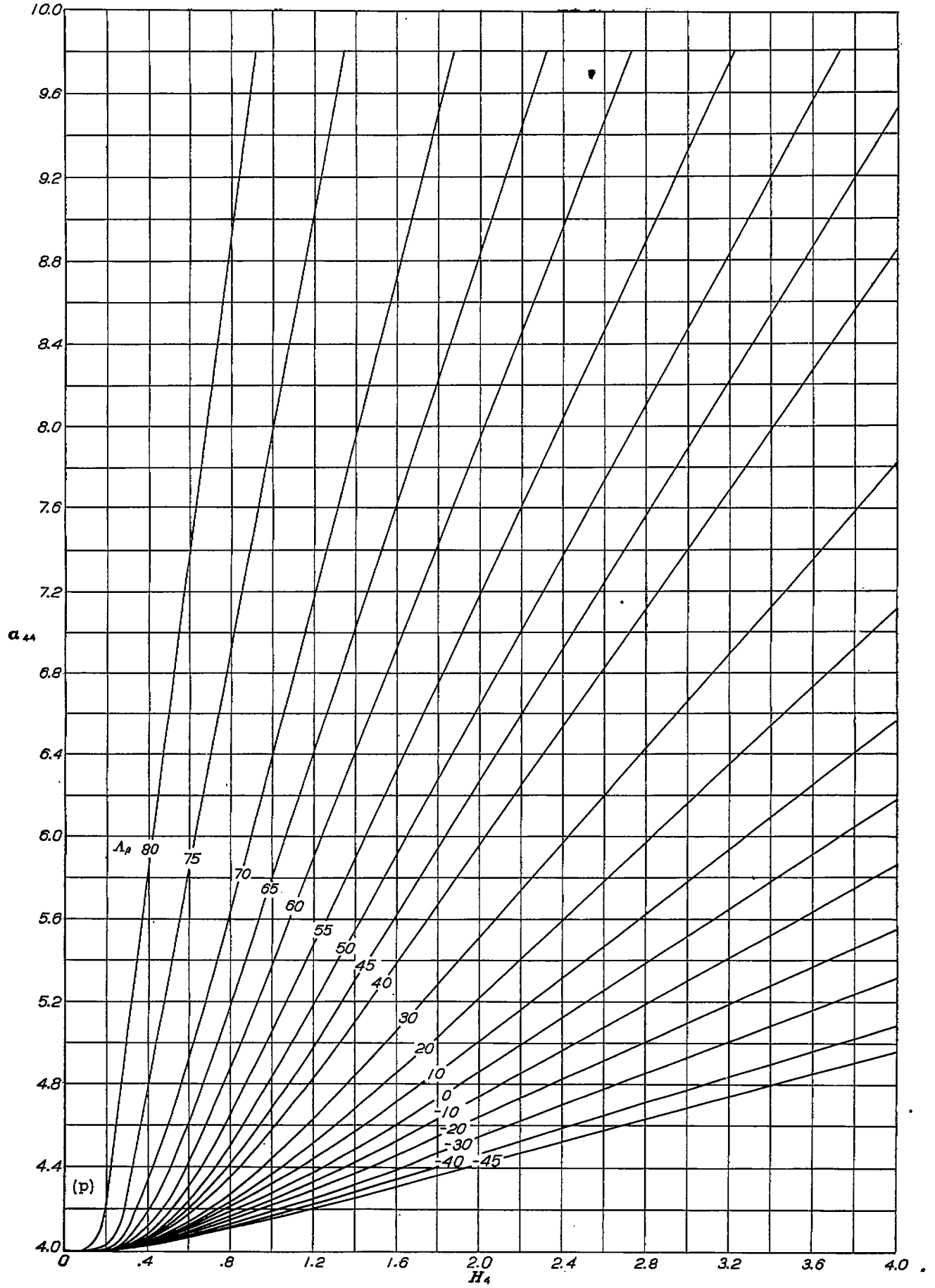

(p) $r=4$, $n=4$, $d_4=0.320$.

FIGURE 1.—Concluded.

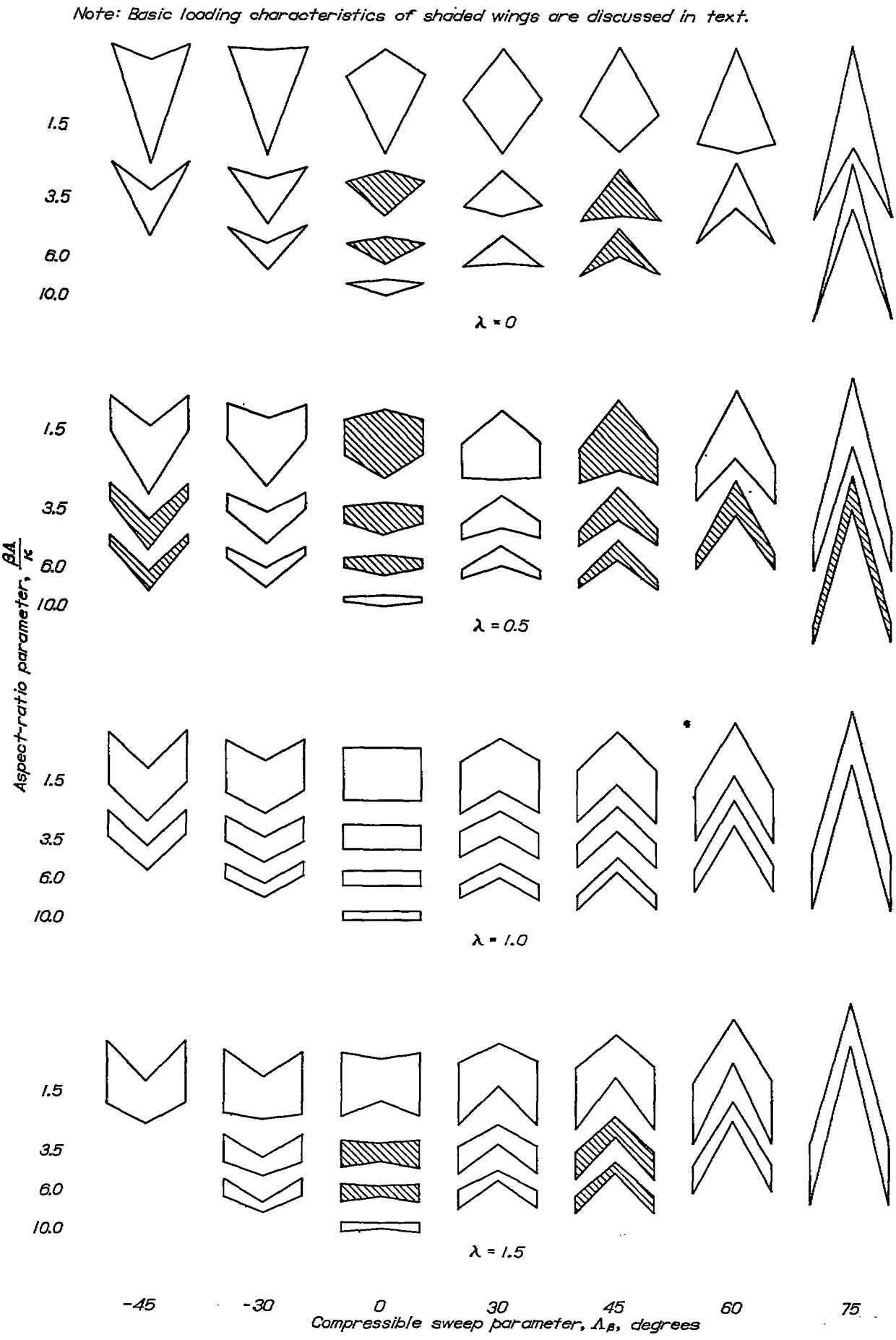

FIGURE 2.—Range of plan forms included in the study of the characteristics of straight-tapered wings.

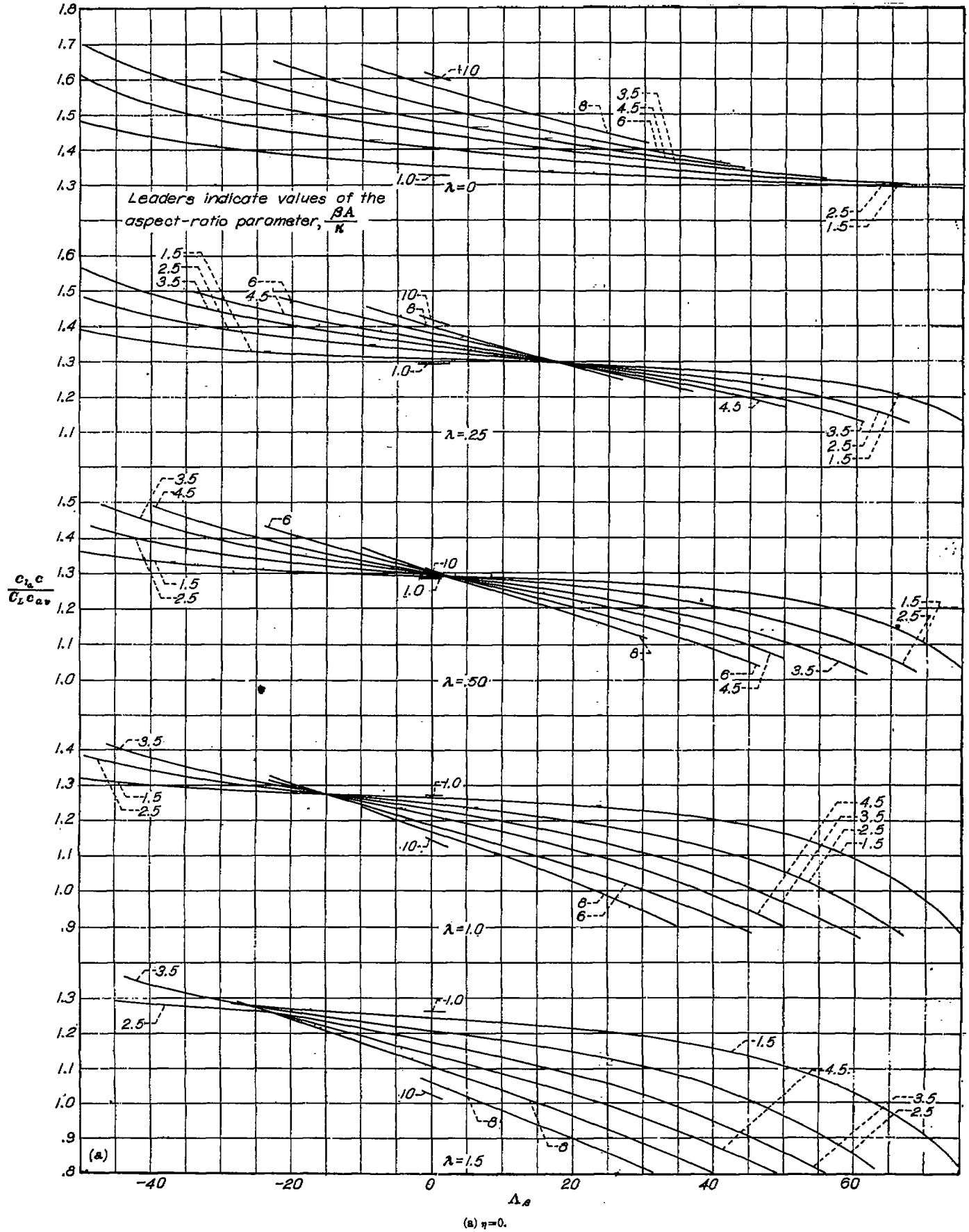

(a) $\eta=0$.

FIGURE 3.—Variation of the spanwise loading coefficient $\frac{c_{l_e} c}{C_L c_{av}}$ with the compressible sweep parameter Λ_β, degrees, for various values of the aspect-ratio parameter $\frac{\beta A}{\kappa}$ and taper ratio λ.

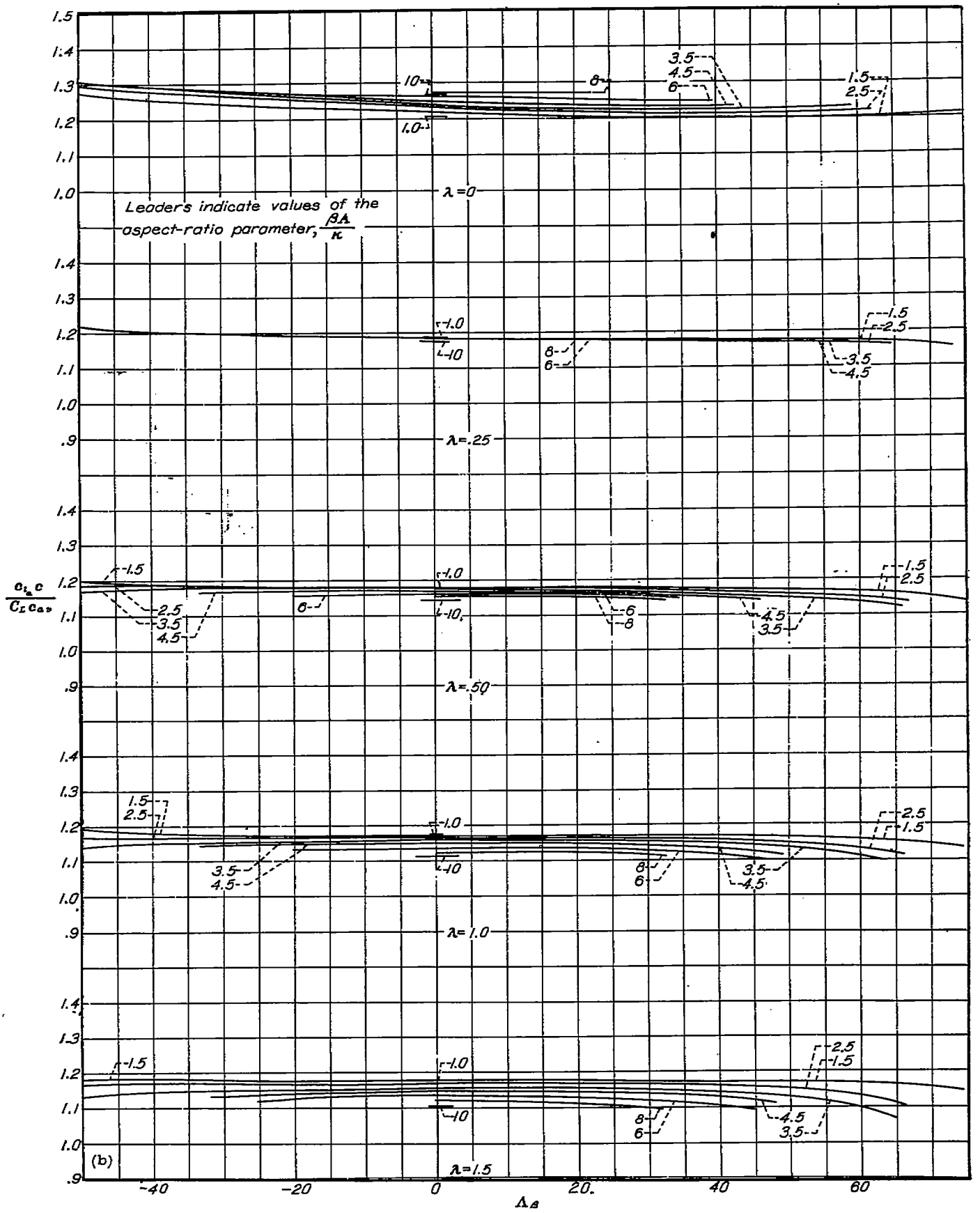

(b) $\eta = 0.383$.

FIGURE 3.—Continued.

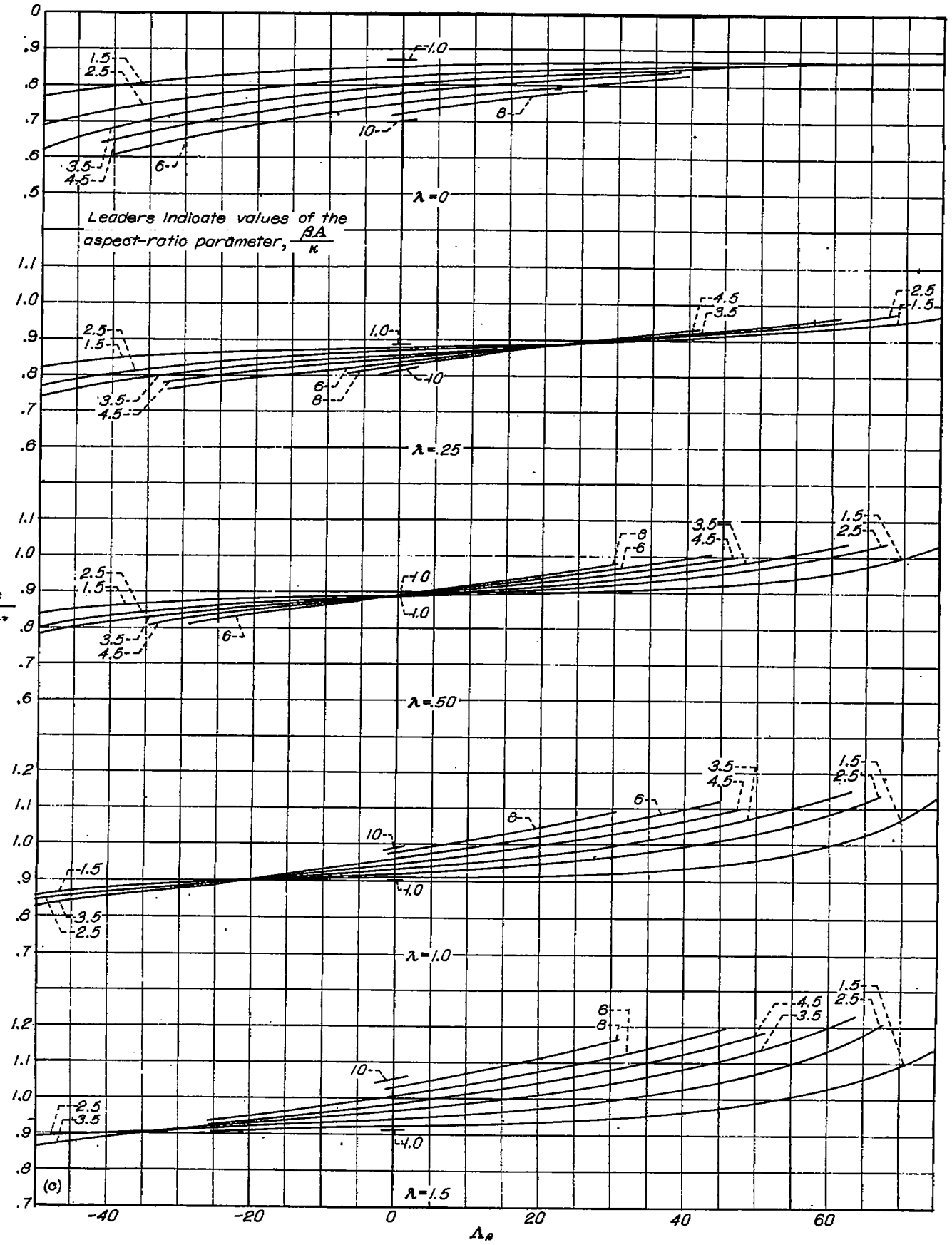

(c) η=0.707.

FIGURE 3.—Continued.

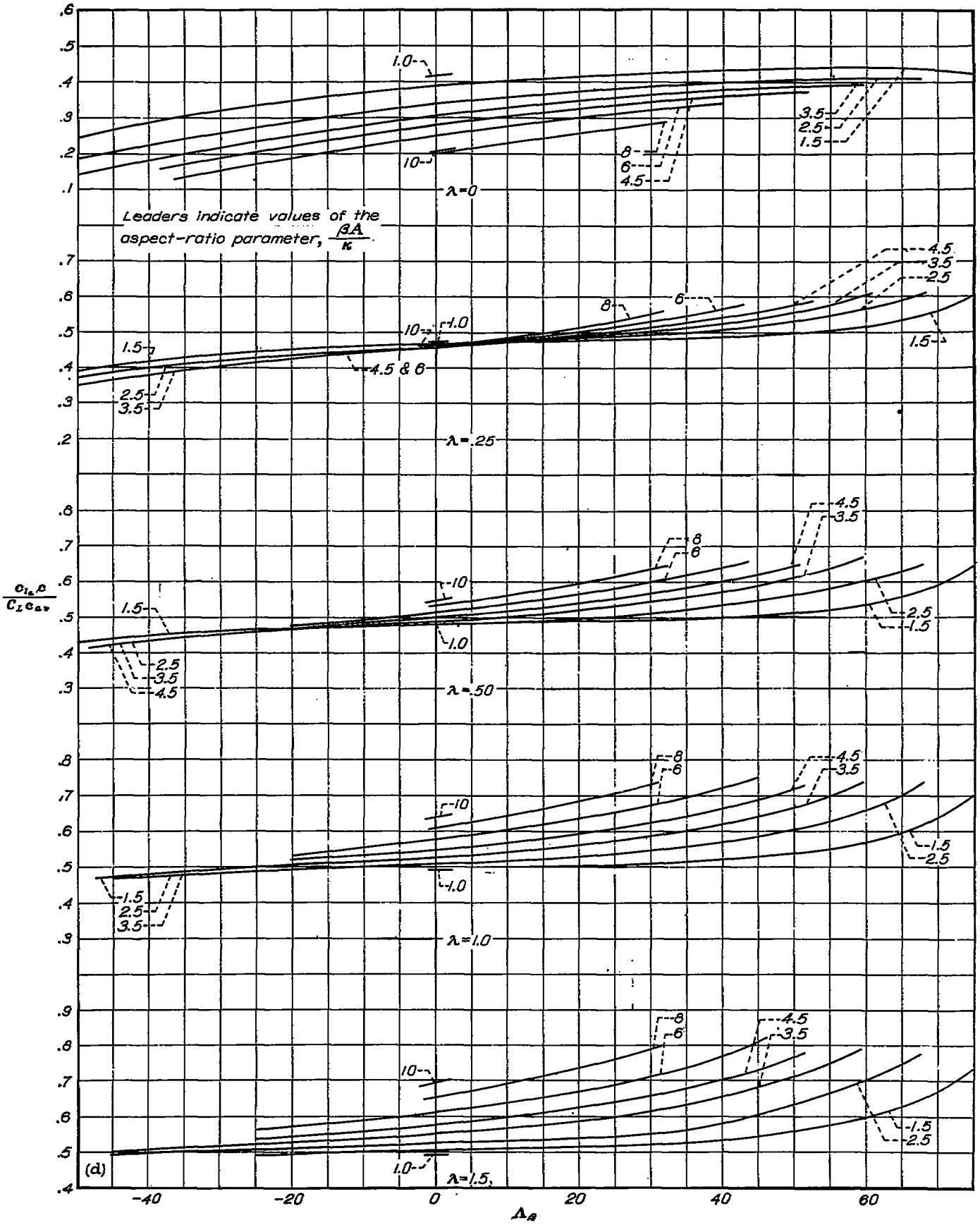

(d) $\eta=0.924$.

FIGURE 3.—Concluded.

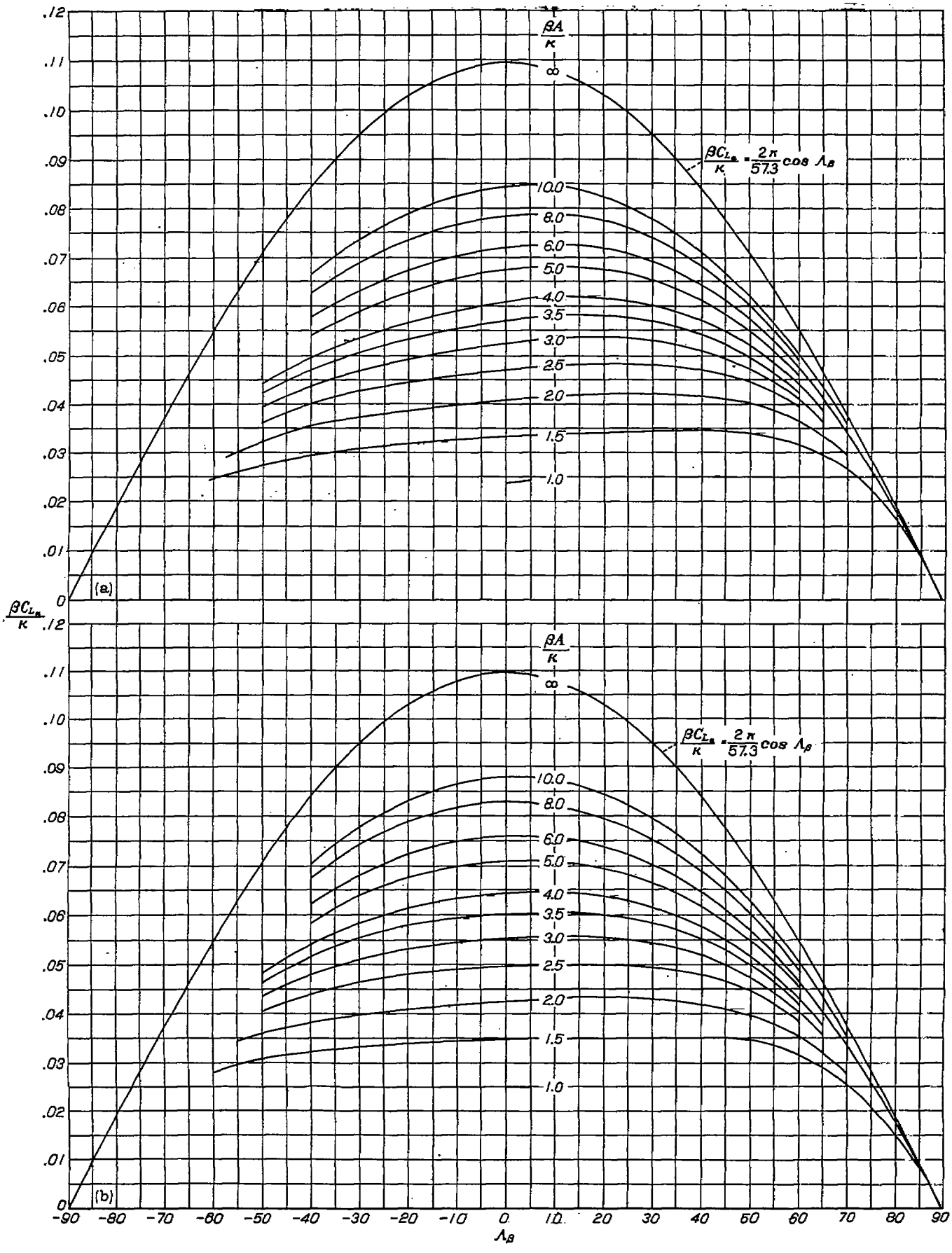

(a) λ=0.

(b) λ=0.25.

FIGURE 4.—Variation of the lift-curve-slope parameter $\frac{\beta C_{L_\alpha}}{\kappa}$ per degree, with the compressible sweep parameter Λ_β degrees, for various values of the aspect-ratio parameter $\frac{\beta A}{\kappa}$.

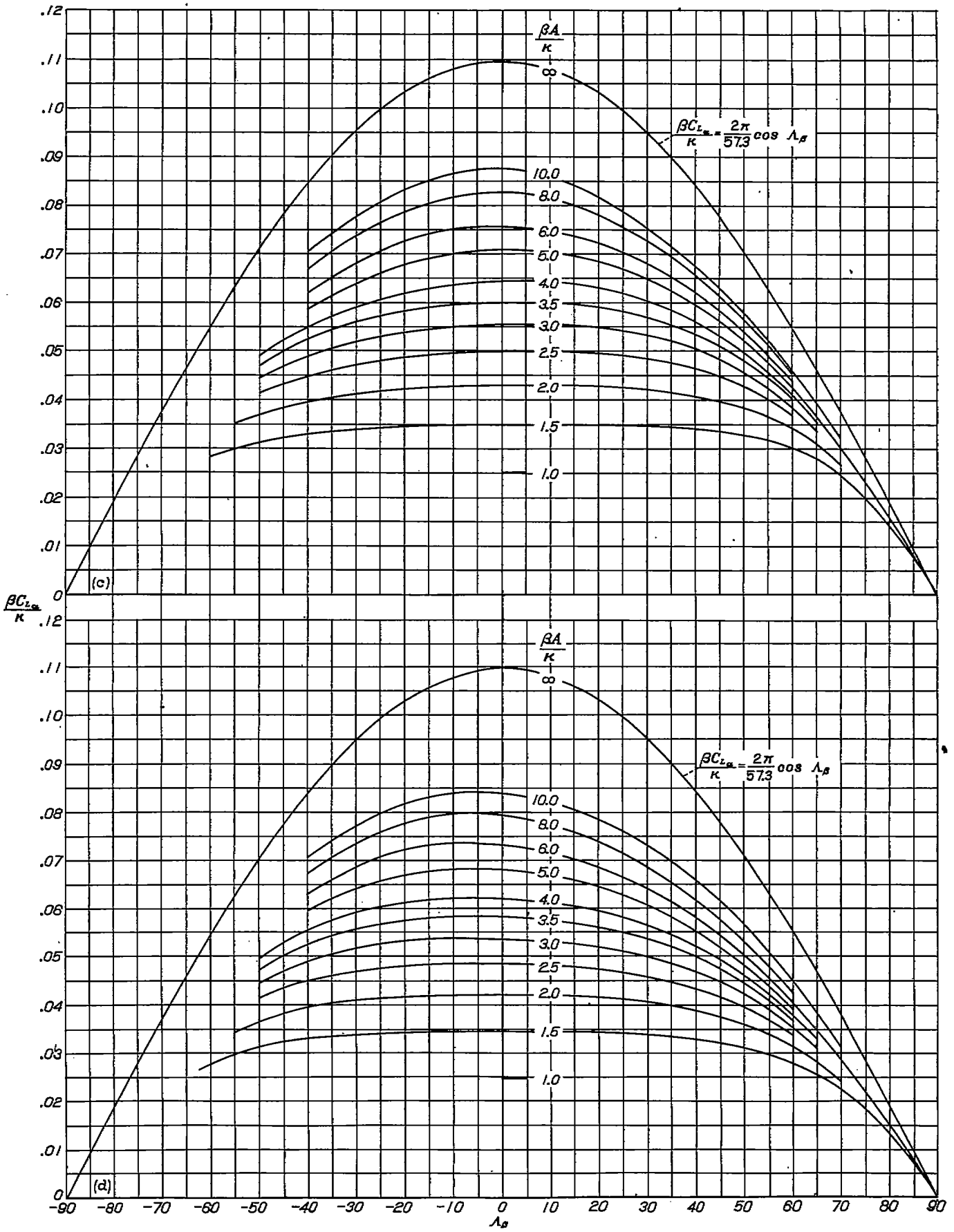

(c) λ=0.50.

(d) λ=1.0.

FIGURE 4.—Continued.

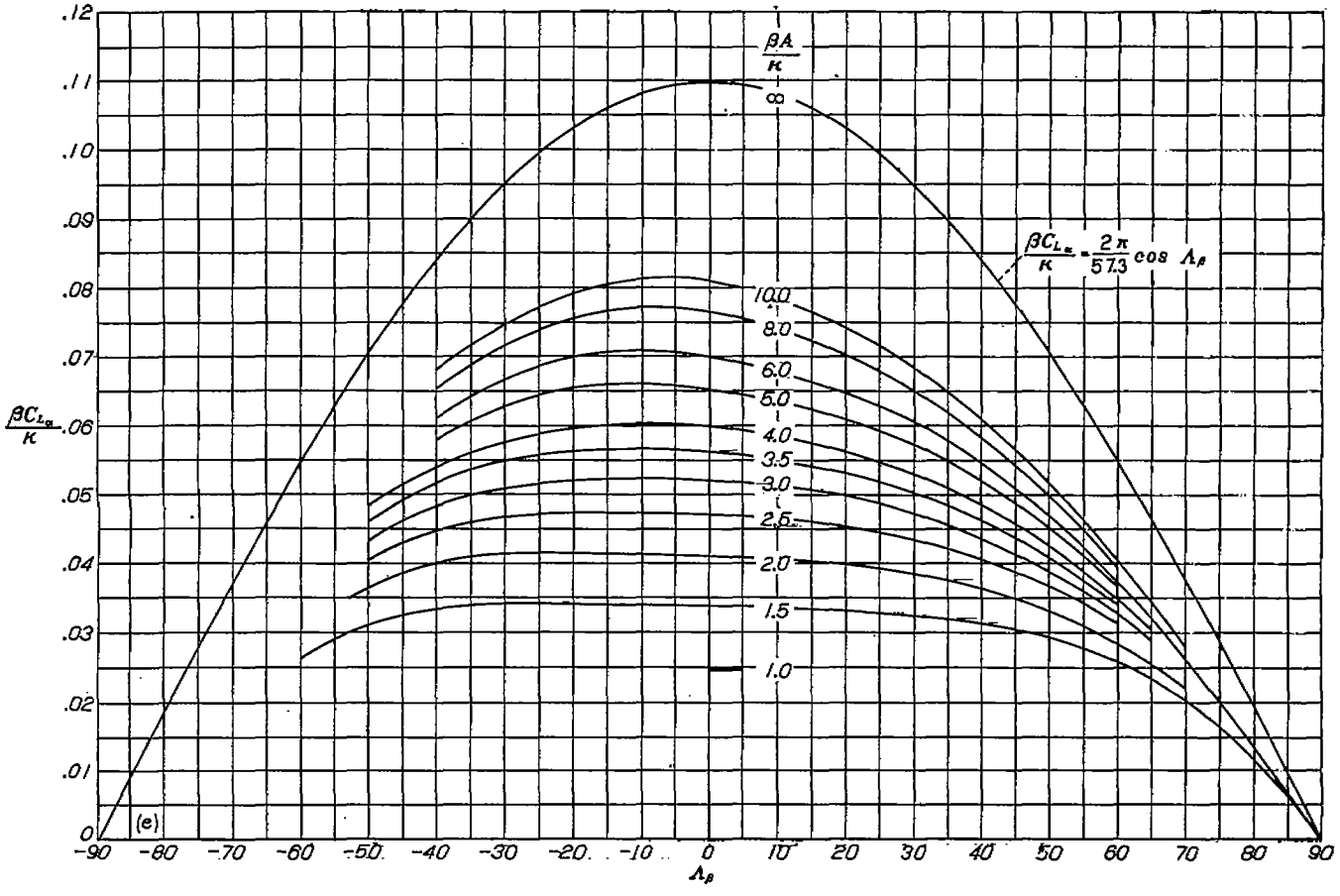

(e) λ=1.5.

FIGURE 4.—Concluded

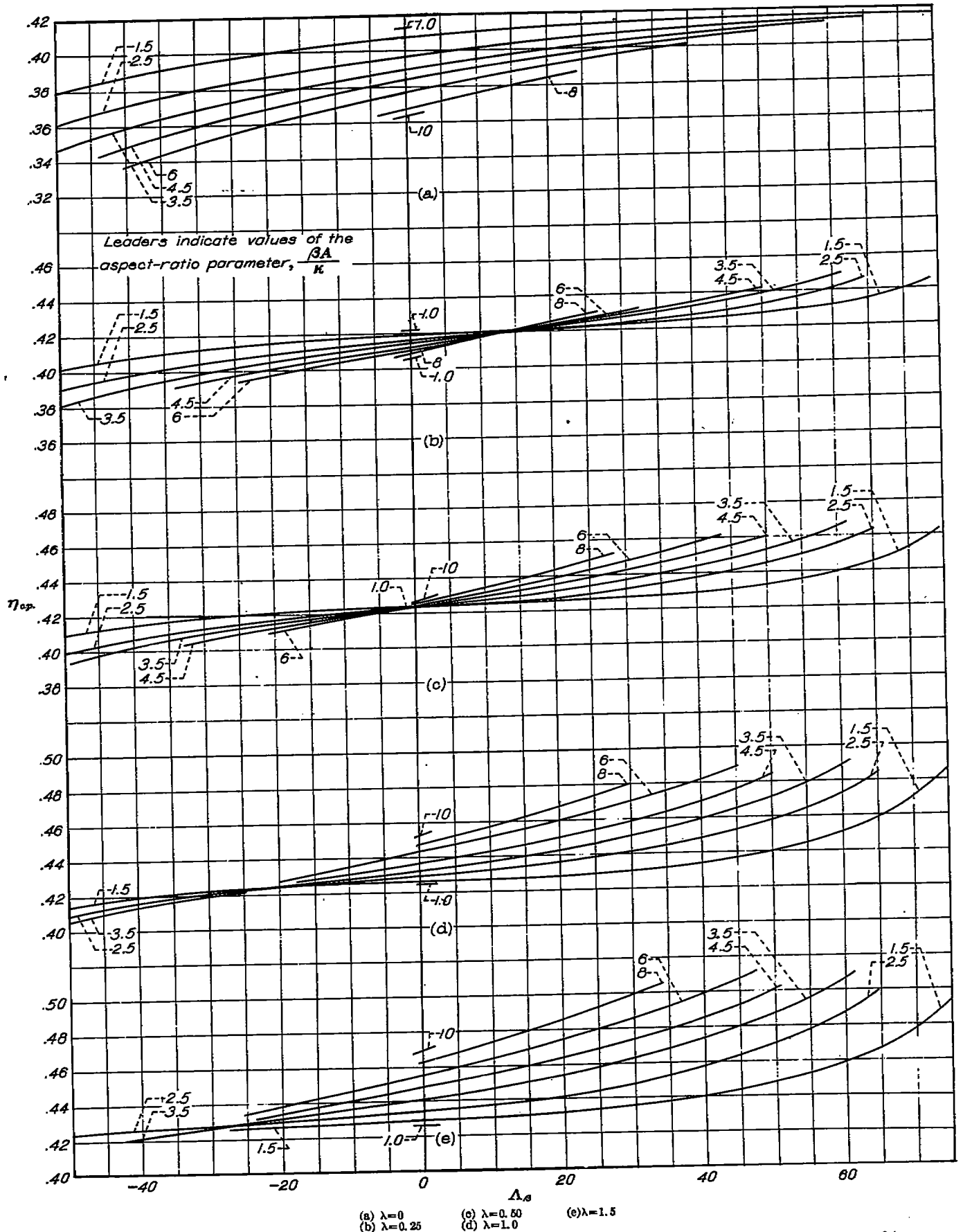

(a) $\lambda=0$ (b) $\lambda=0.25$ (c) $\lambda=0.50$ (d) $\lambda=1.0$ (e) $\lambda=1.5$

FIGURE 5.—Variation of the spanwise center of pressure $\eta_{c.p.}$ with the compressible sweep parameter Λ_{β}, degrees, for various values of the aspect-ratio parameter $\frac{\beta A}{\kappa}$ and taper ratio λ.

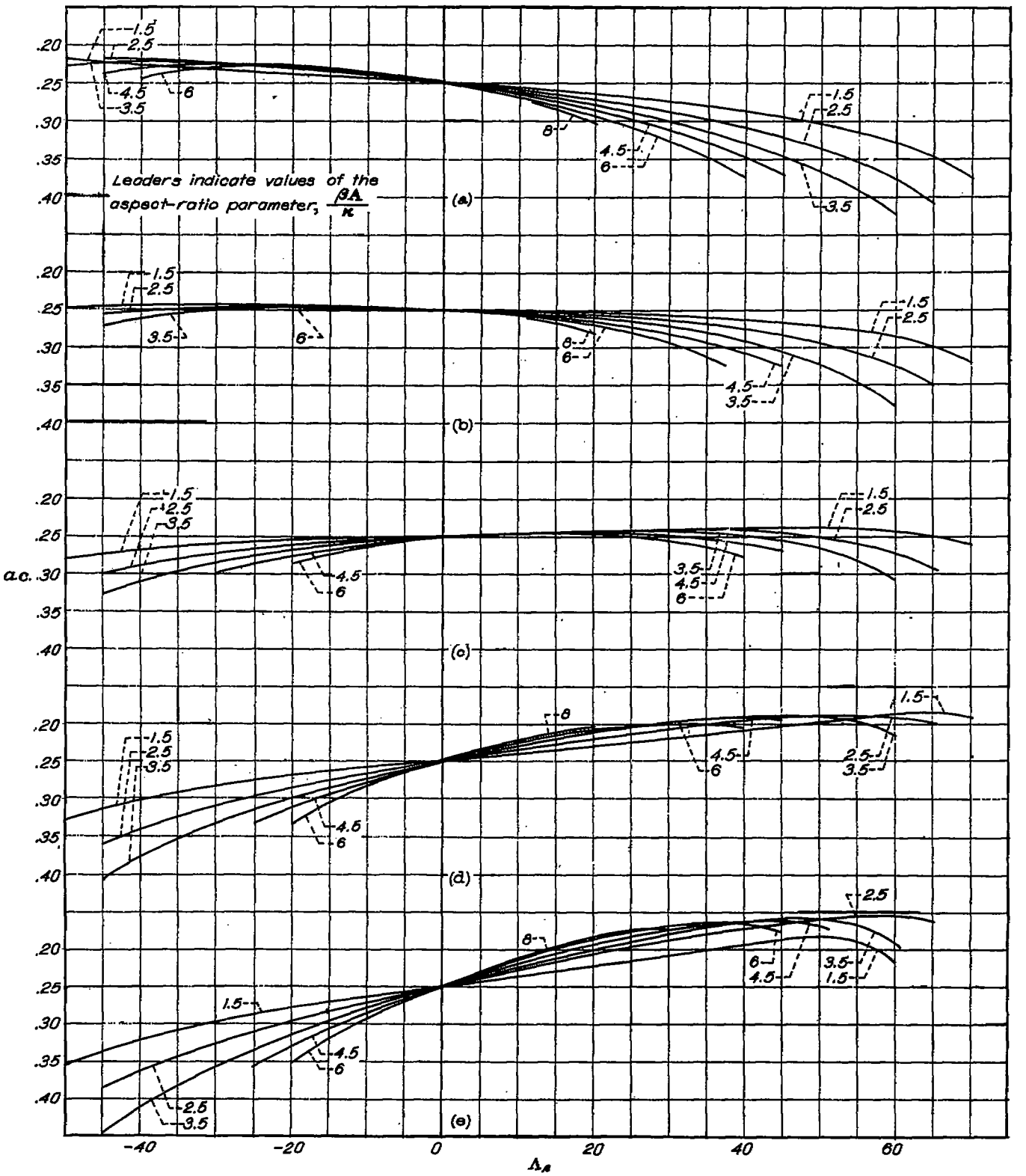

(a) λ=0 (c) λ=0.50 (e) λ=1.0
(b) λ=0.25 (d) λ=1.0

FIGURE 6.—Variation of the aerodynamic-center location, fraction of mean aerodynamic chord, with the compressible sweep parameter Λ_β, degrees, for various values of the aspect-ratio parameter $\frac{\beta A}{\kappa}$ and taper ratio λ.

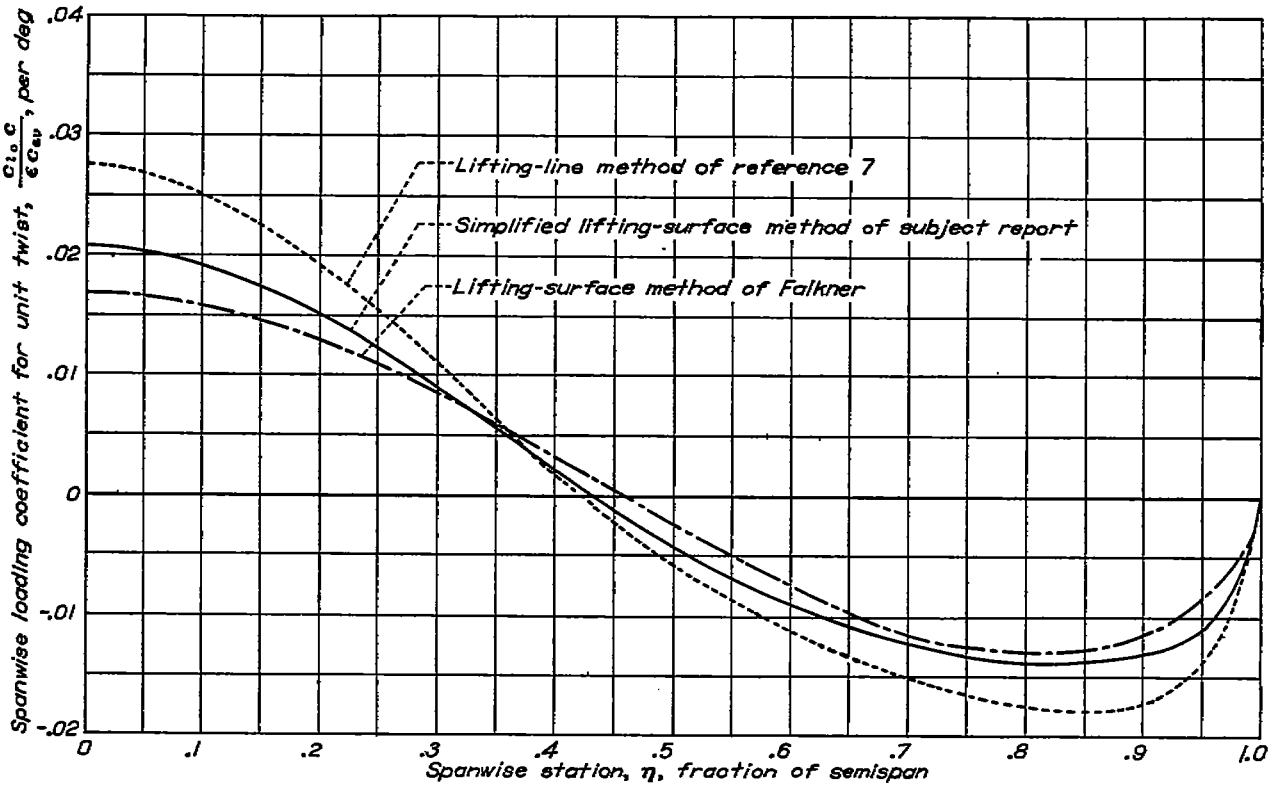

FIGURE 7.—A comparison of the basic loadings predicted by three theoretical methods for an unswept wing having an aspect ratio of 6.0 and taper ratio of 0.5.

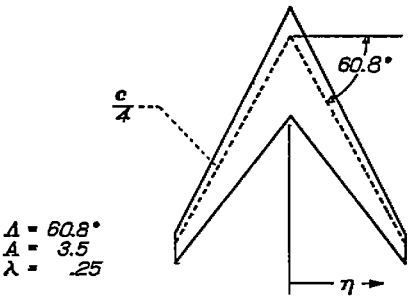

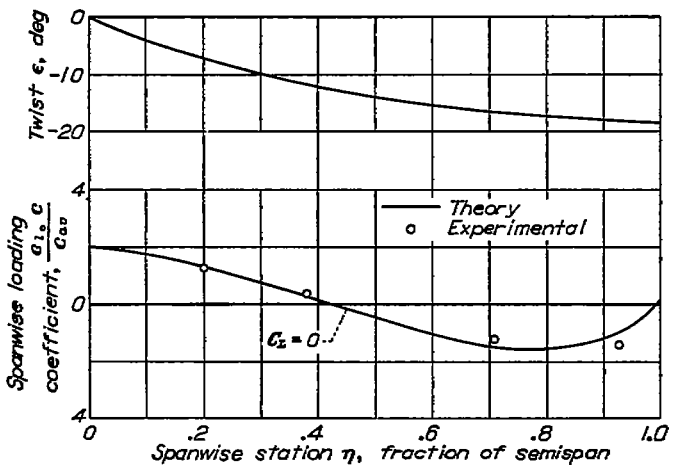

FIGURE 8.—Comparison of theoretical and experimental basic loading distribution.

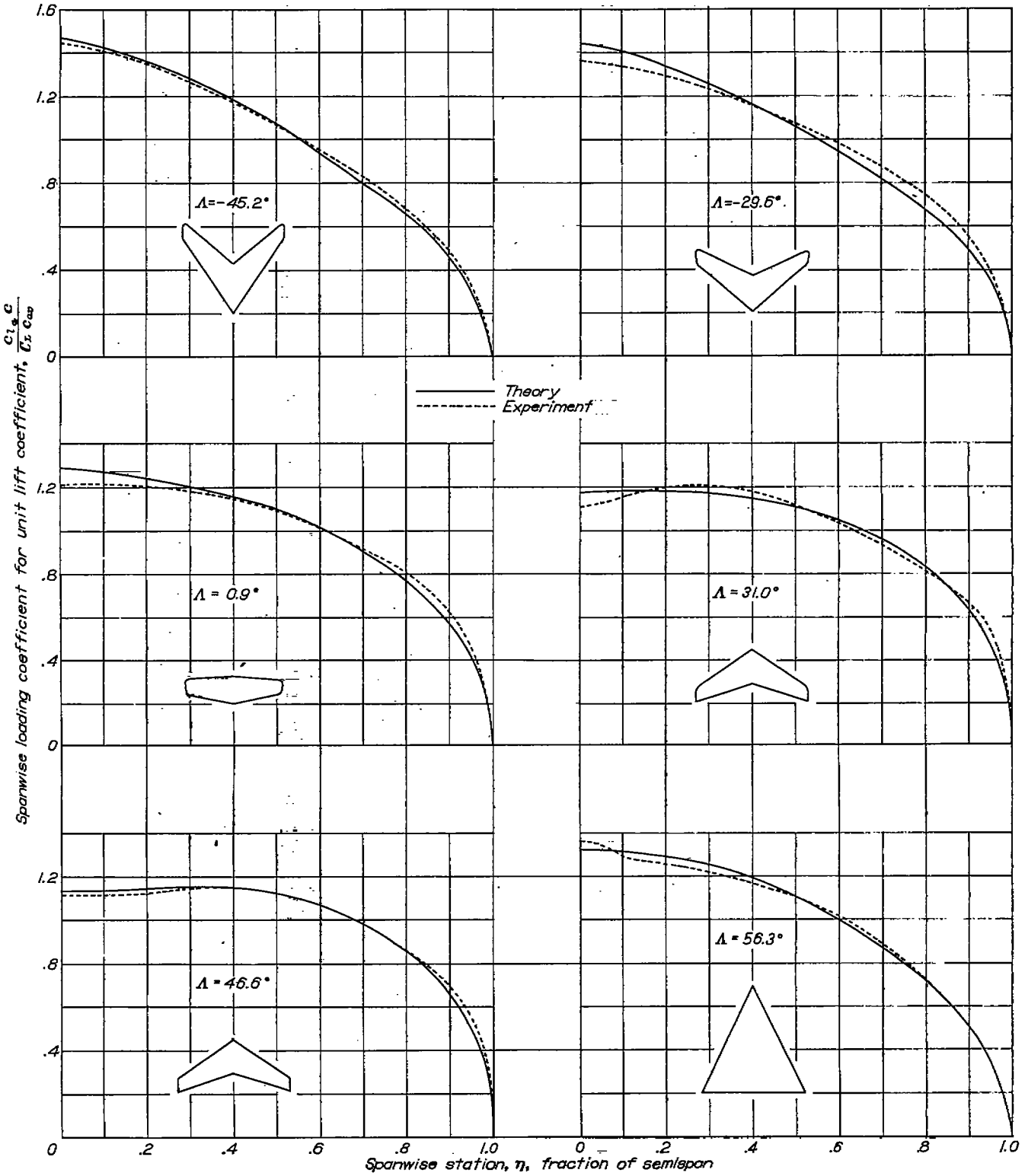

FIGURE 9.—Comparison of theoretical and experimental additional-loading distribution.

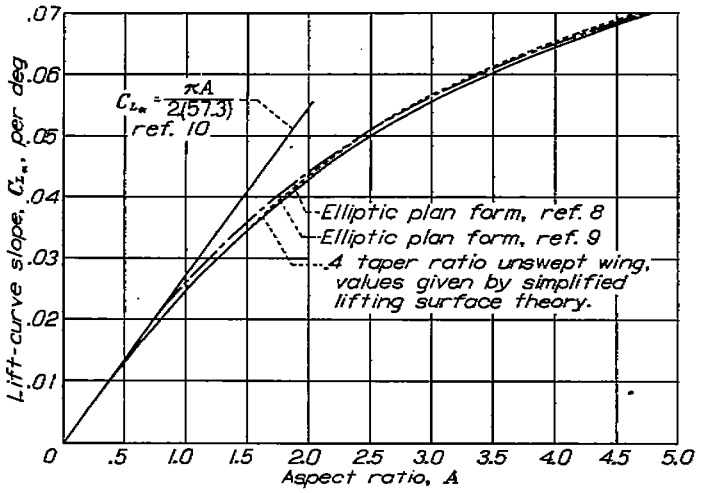

FIGURE 10.—Comparison of lift-curve slopes as obtained by the simplified lifting-surface method of the subject report with those obtained by two lifting-surface methods and by a theory for wings of zero aspect ratio.

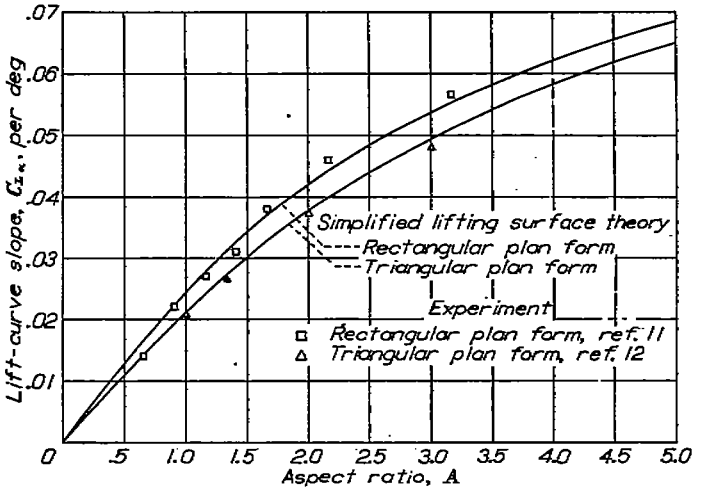

FIGURE 11.—Comparison of lift-curve slopes obtained experimentally for triangular and rectangular wings of various aspect ratios with those given by simplified lifting-surface theory of subject report.

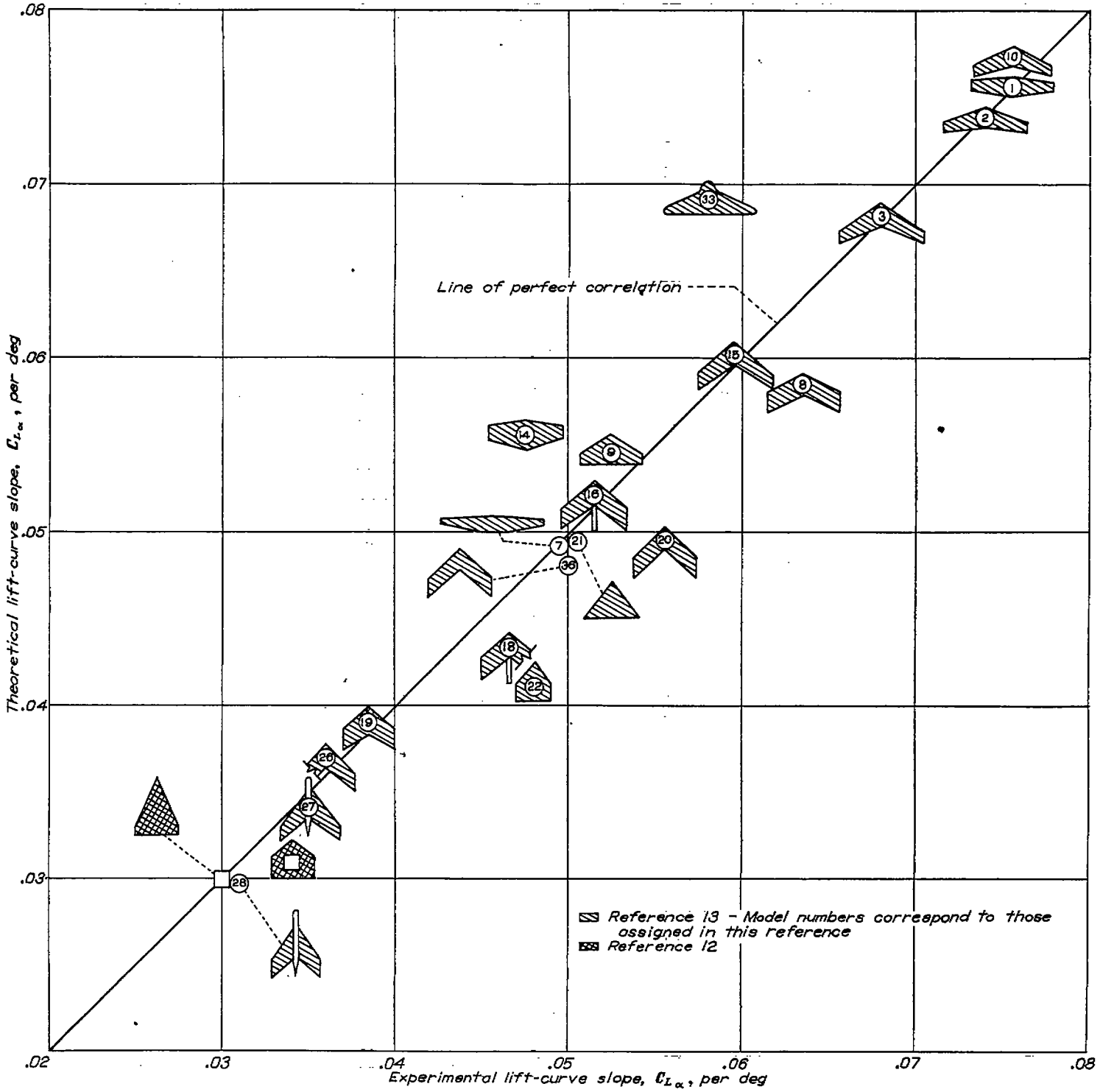

FIGURE 12.—Comparison of lift-curve slopes obtained experimentally for a random group of wing plan forms with those given by the simplified lifting-surface theory.

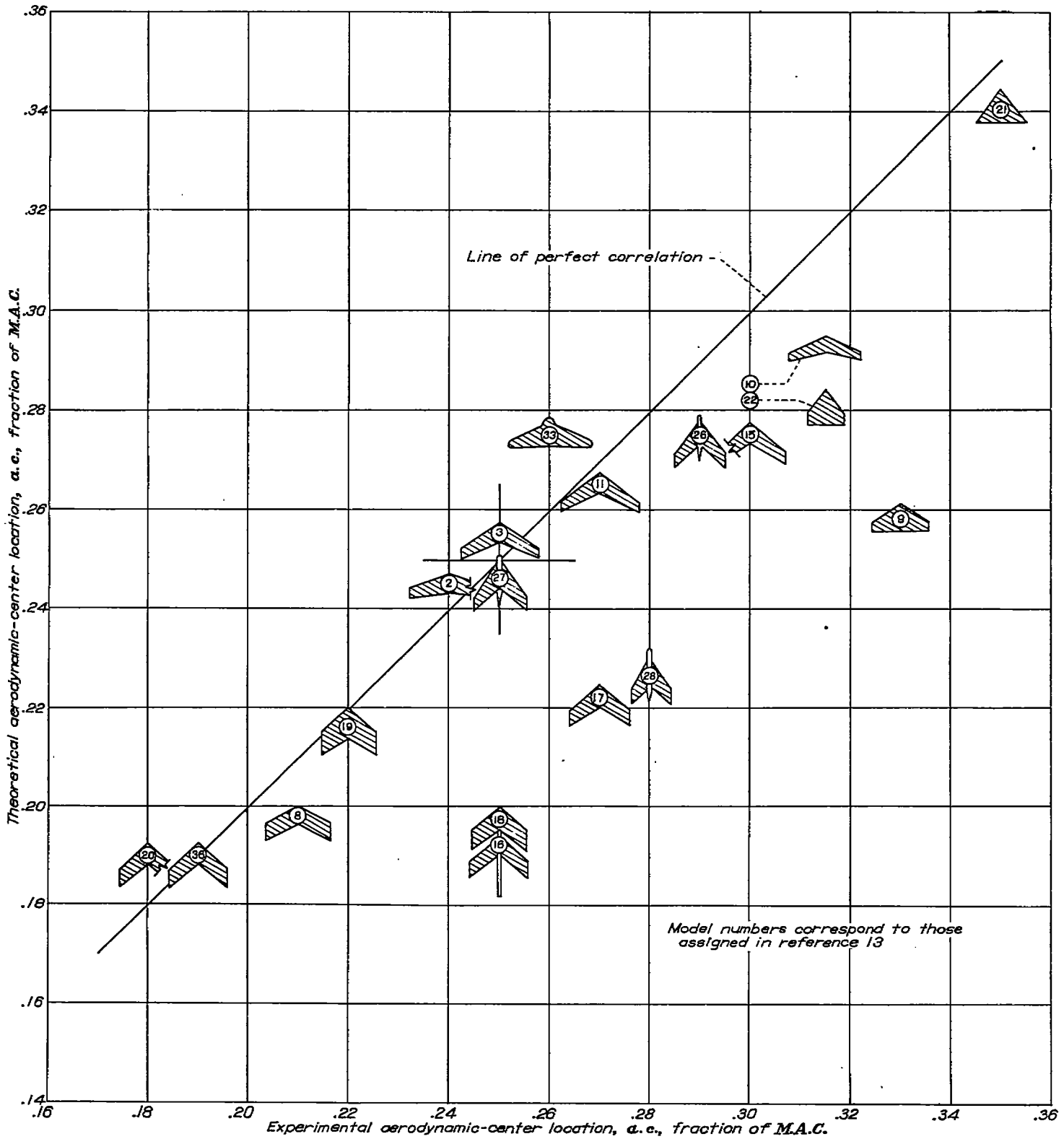

FIGURE 13.—Comparison of aerodynamic-center locations obtained experimentally for a random group of wing plan forms with those given by the simplified lifting-surface theory.

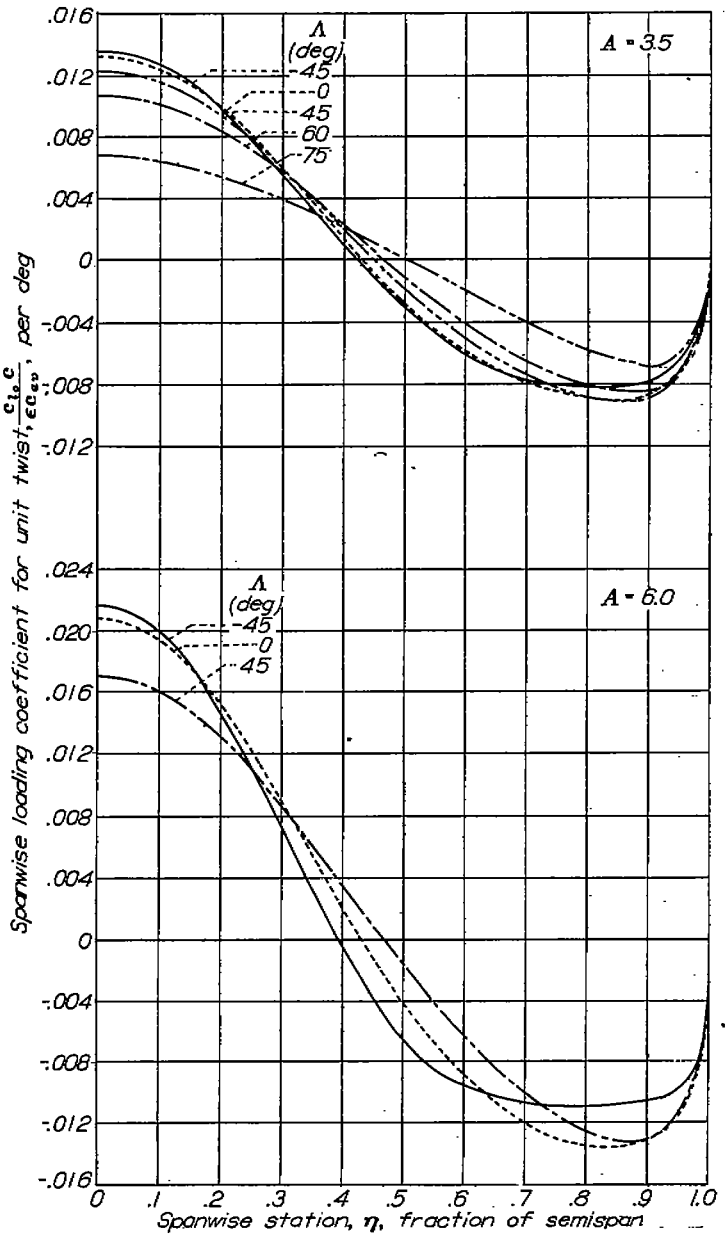

FIGURE 14.—The effect of sweep on the basic loading of wings having a taper ratio of 0.5.

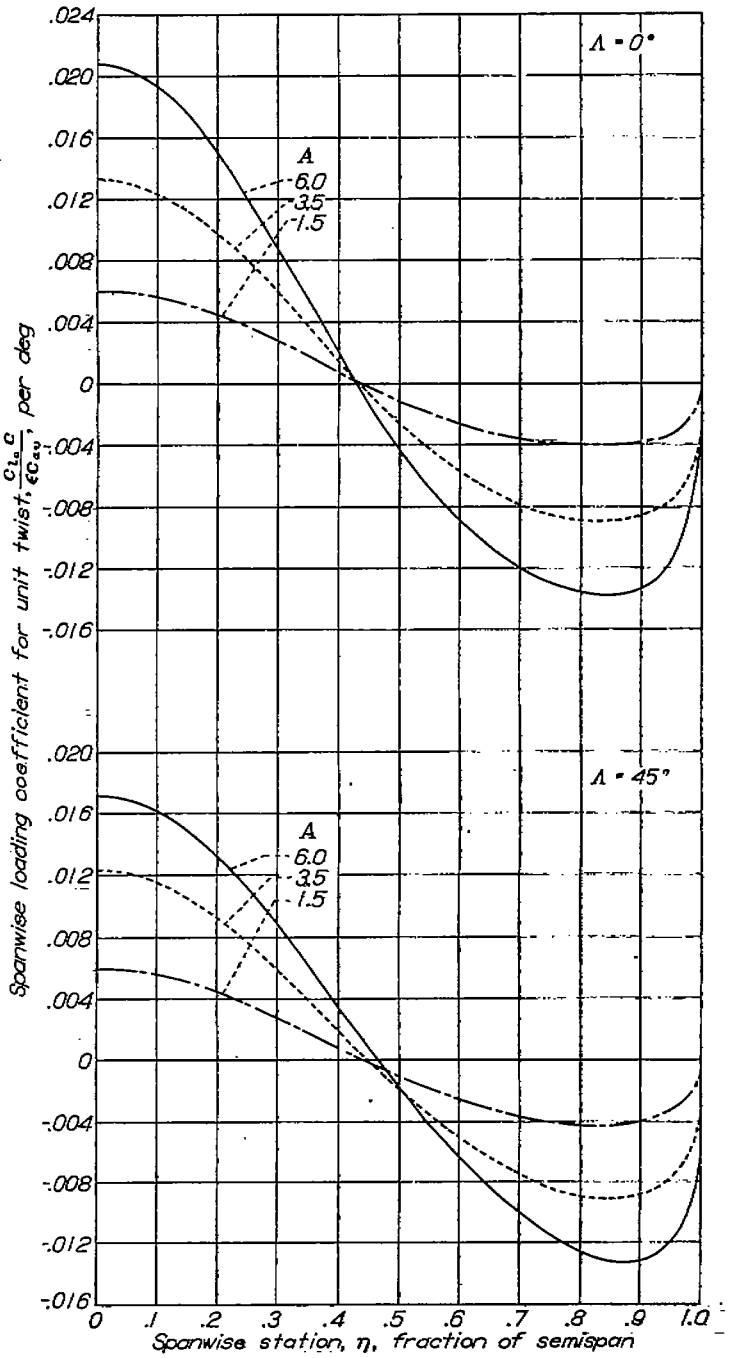

FIGURE 15.—The effect of aspect ratio on the basic loading of wings having a taper ratio of 0.5

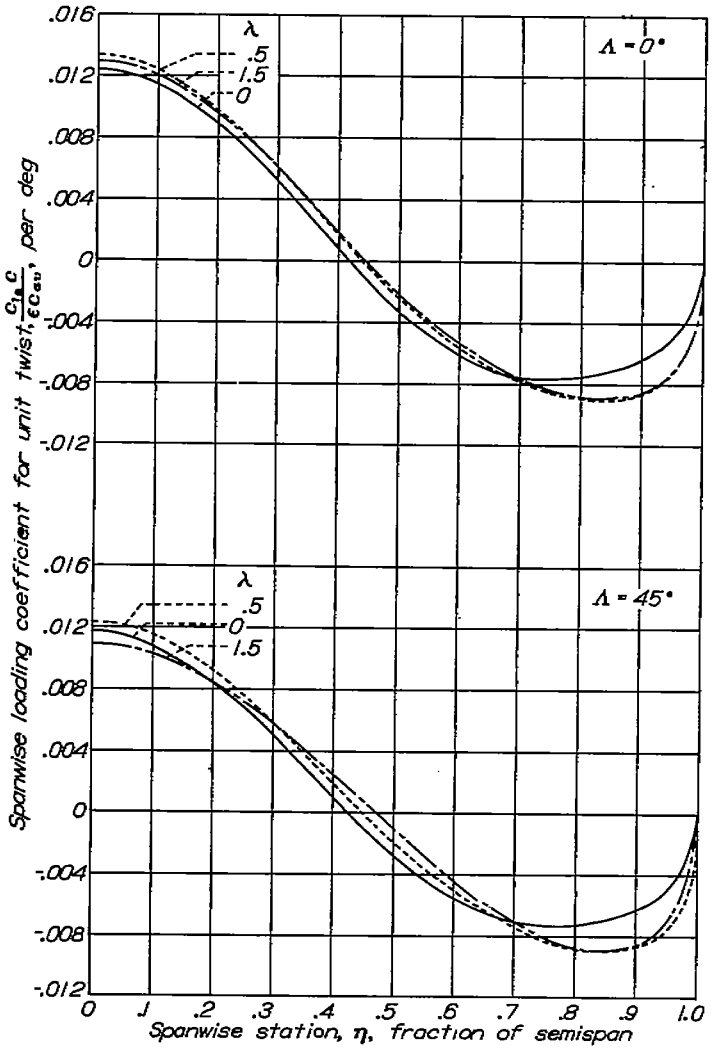

FIGURE 16.—The effect of taper ratio on the basic loading of wings having an aspect ratio of 3.5.

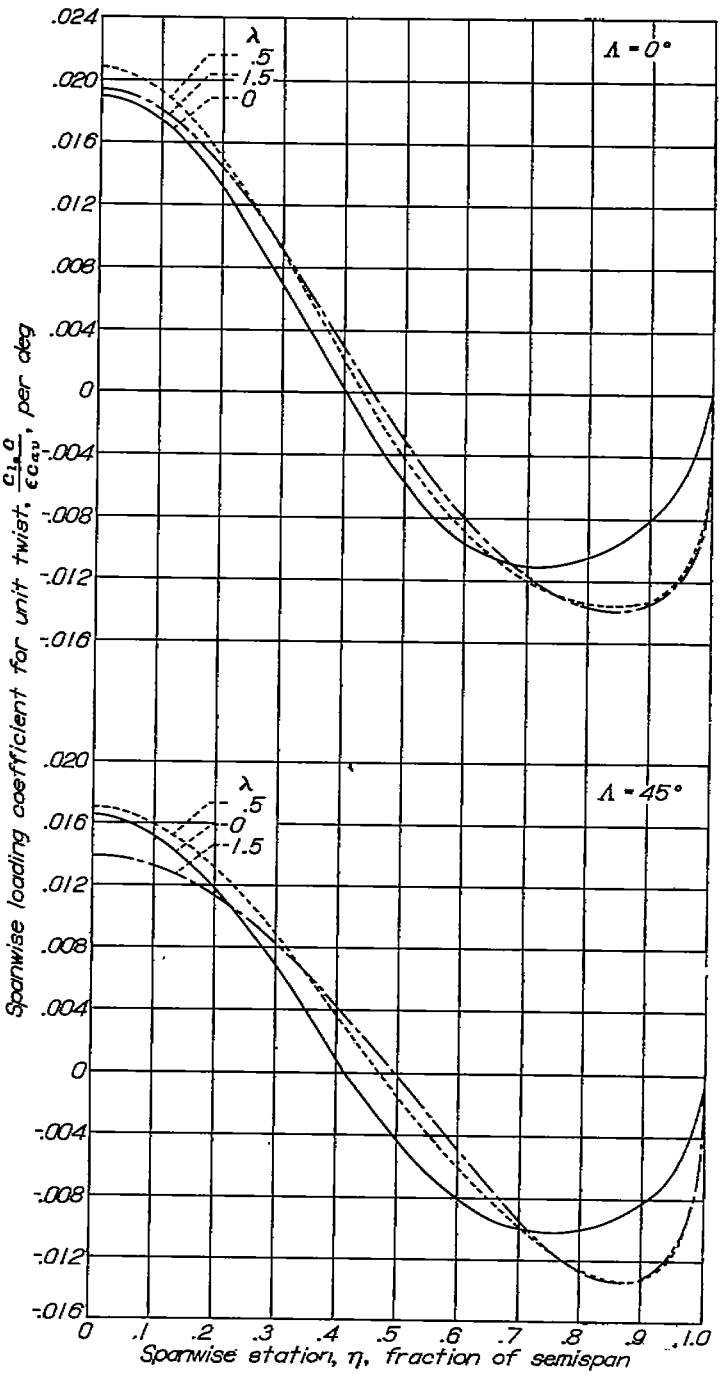

FIGURE 17.—The effect of taper ratio on the basic loading of wings having an aspect ratio of 6.0.

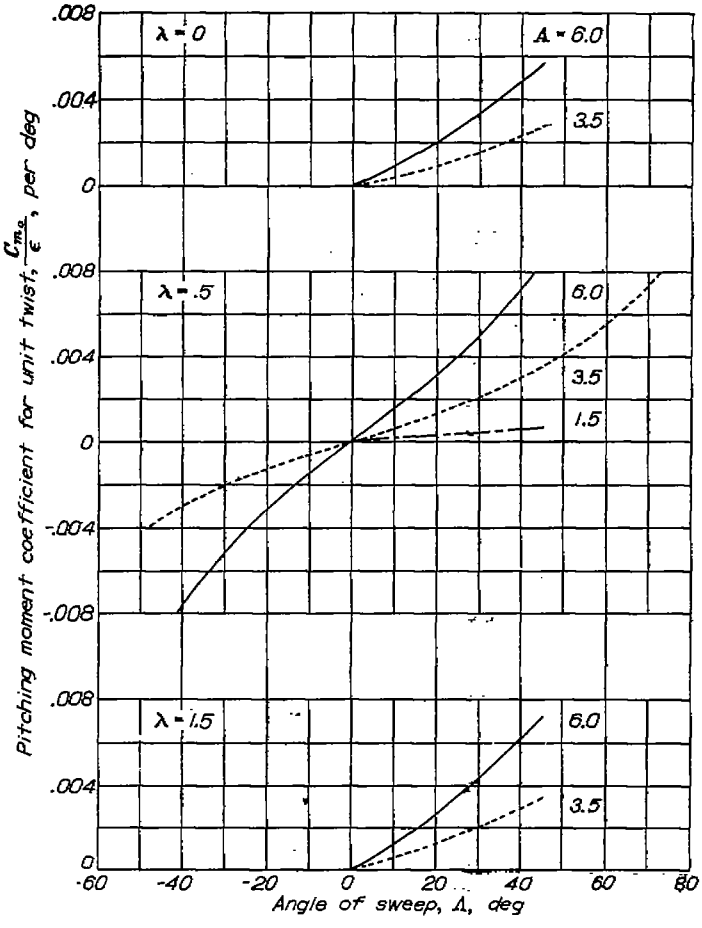

FIGURE 18.—The effect of plan form on the pitching moment due to twist.

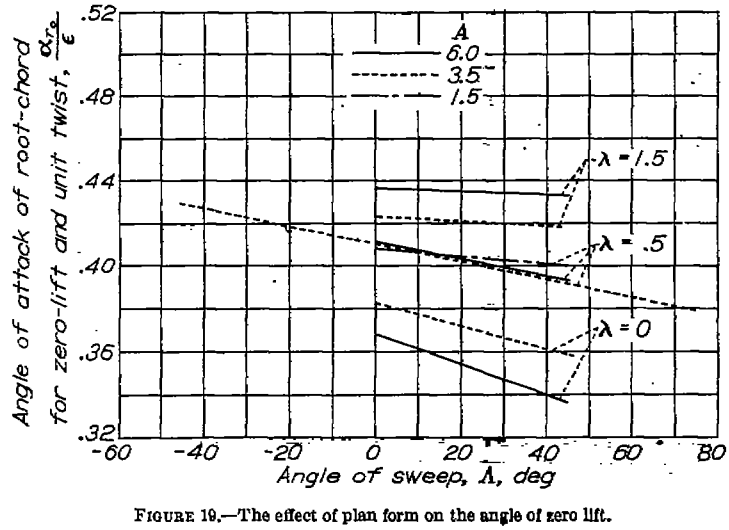

FIGURE 19.—The effect of plan form on the angle of zero lift.

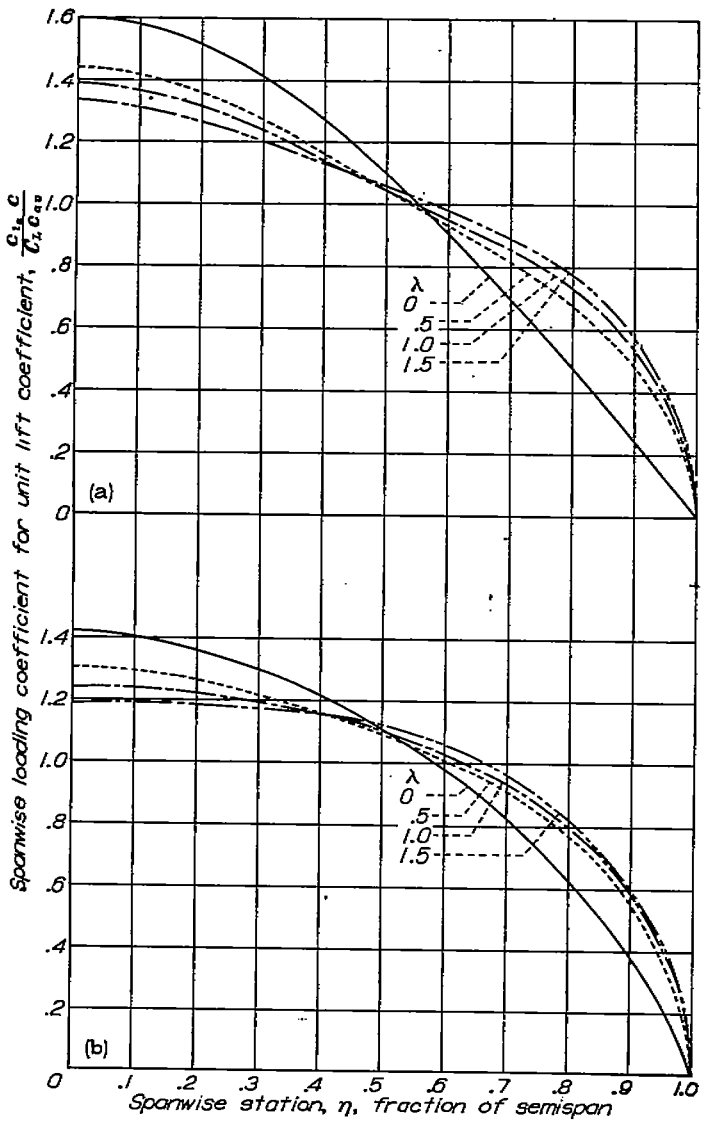

(a) $\Lambda = -45°$.

(b) $\Lambda = 0°$.

FIGURE 20.—The effect of taper ratio on the additional loading of wings having an aspect ratio of 3.0 and various values of sweep.

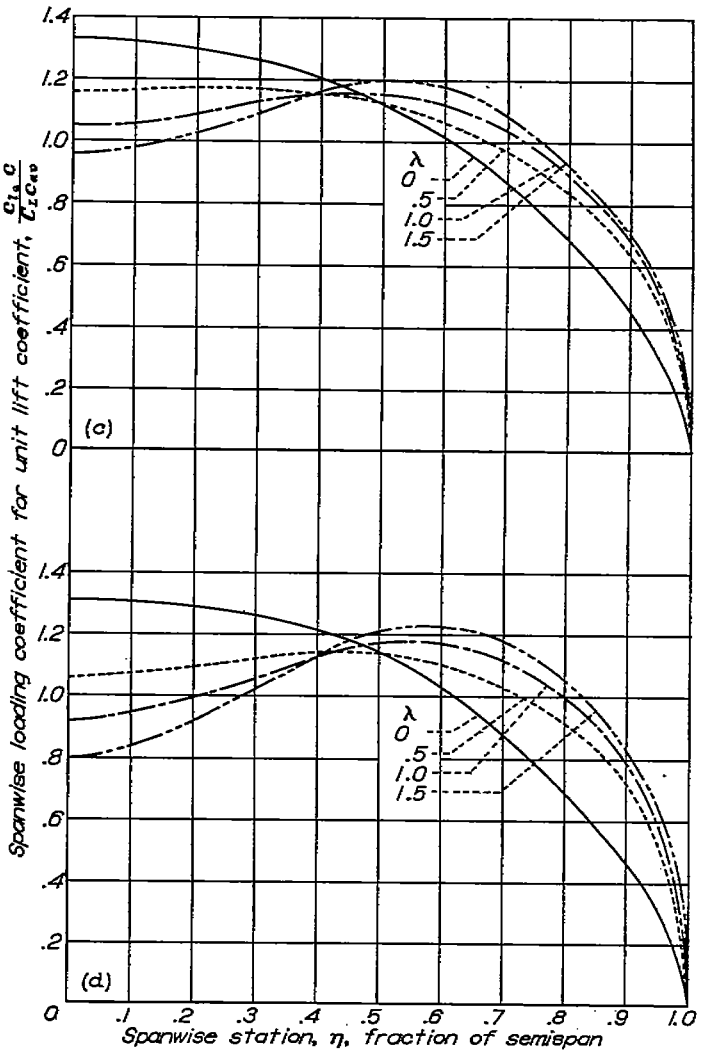

(c) $\Lambda = 45°$.

(d) $\Lambda = 60°$.

FIGURE 20.—Concluded.

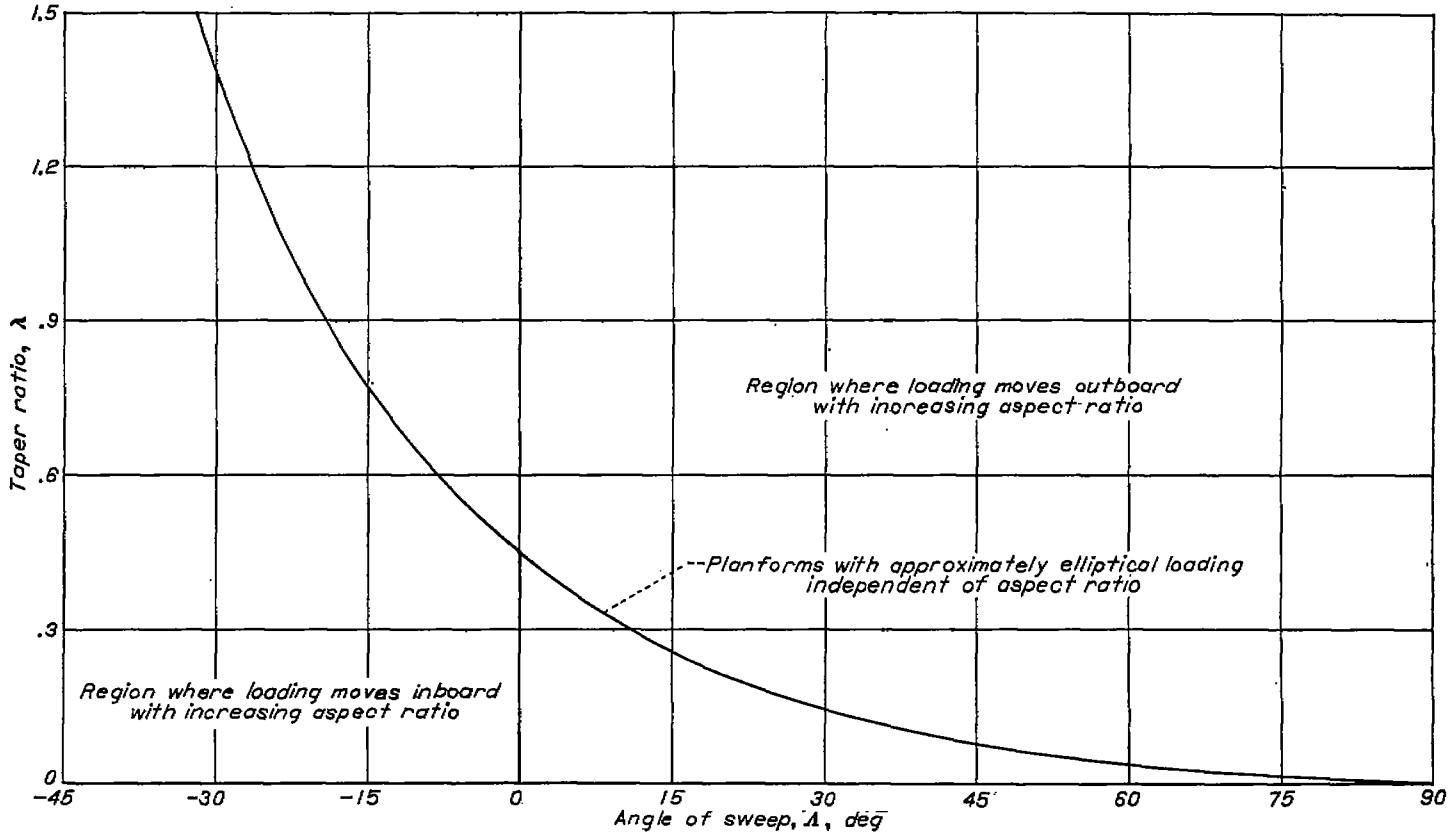

FIGURE 21.—Relation of taper ratio to sweep angle required for approximately elliptical loading.

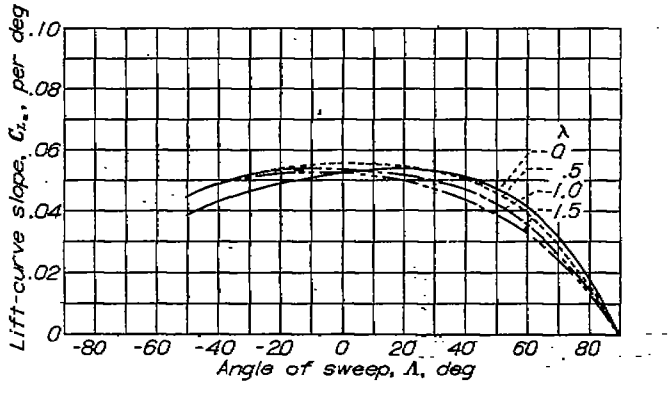

FIGURE 22.—Variation of lift-curve slope with sweep for constant aspect ratio of 3.0 and various values of taper ratio.

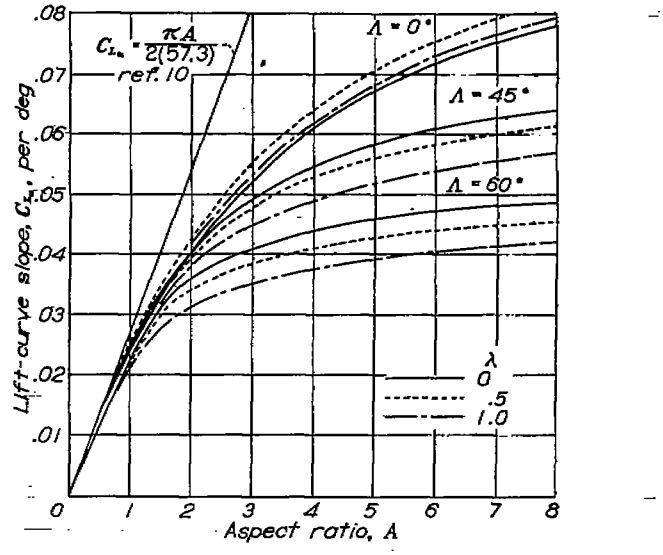

FIGURE 23.—Variation of lift-curve slope with aspect ratio for various values of sweep and taper ratio.

U. S. GOVERNMENT PRINTING OFFICE, 1950